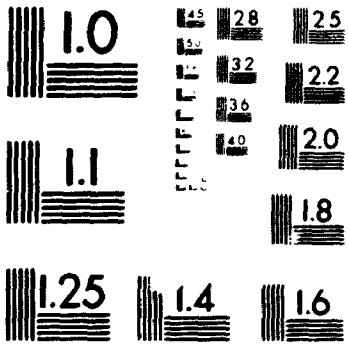

MICROCOPY RESOLUTION TEST CHART
NATIONAL BUREAU OF STANDARDS
STANDARD REFERENCE MATERIAL 1010a
(ANSI and ISO TEST CHART No. 2)

STRUCTURE AND GEOCHRONOLOGY OF THE GREATER HIMALAYA, KALI GANDAKI REGION, WEST-CENTRAL NEPAL

By

Jeffrey H. Nazarchuk, B.Sc.

A thesis submitted to the Faculty of Graduate Studies and Research in partial fulfilment of the requirements for the degree of Master of Science, Department of Earth Sciences

Carleton University
Ottawa, Ontario
May 19, 1993

ISBN 0-315-89748-1

Name Jeff Nazarchuk

Dissertation Abstracts International is arranged by broad, general subject categories. Please select the one subject which most nearly describes the content of your dissertation. Enter the corresponding four-digit code in the spaces provided.

Earth Science, Geology — SUBJECT TERM

0372 — SUBJECT CODE

U·M·I

Subject Categories

THE HUMANITIES AND SOCIAL SCIENCES

COMMUNICATIONS AND THE ARTS
Architecture 0729
Art History 0377
Cinema 0900
Dance 0378
Fine Arts 0357
Information Science 0723
Journalism 0391
Library Science 0399
Mass Communications 0708
Music 0413
Speech Communication 0459
Theater 0465

EDUCATION
General 0515
Administration 0514
Adult and Continuing 0516
Agricultural 0517
Art 0273
Bilingual and Multicultural 0282
Business 0688
Community College 0275
Curriculum and Instruction 0727
Early Childhood 0518
Elementary 0524
Finance 0277
Guidance and Counseling 0519
Health 0680
Higher 0745
History of 0520
Home Economics 0278
Industrial 0521
Language and Literature 0279
Mathematics 0280
Music 0522
Philosophy of 0998
Physical 0523
Psychology 0525
Reading 0535
Religious 0527
Sciences 0714
Secondary 0533
Social Sciences 0534
Sociology of 0340
Special 0529
Teacher Training 0530
Technology 0710
Tests and Measurements 0288
Vocational 0747

LANGUAGE, LITERATURE AND LINGUISTICS
Language
- General 0679
- Ancient 0289
- Linguistics 0290
- Modern 0291

Literature
- General 0401
- Classical 0294
- Comparative 0295
- Medieval 0297
- Modern 0298
- African 0316
- American 0591
- Asian 0305
- Canadian (English) 0352
- Canadian (French) 0355
- English 0593
- Germanic 0311
- Latin American 0312
- Middle Eastern 0315
- Romance 0313
- Slavic and East European 0314

PHILOSOPHY, RELIGION AND THEOLOGY
Philosophy 0422
Religion
- General 0318
- Biblical Studies 0321
- Clergy 0319
- History of 0320
- Philosophy of 0322

Theology 0469

SOCIAL SCIENCES
American Studies 0323
Anthropology
- Archaeology 0324
- Cultural 0326
- Physical 0327

Business Administration
- General 0310
- Accounting 0272
- Banking 0770
- Management 0454
- Marketing 0338

Canadian Studies 0385
Economics
- General 0501
- Agricultural 0503
- Commerce Business 0505
- Finance 0508
- History 0509
- Labor 0510
- Theory 0511

Folklore 0358
Geography 0366
Gerontology 0351
History
- General 0578
- Ancient 0579
- Medieval 0581
- Modern 0582
- Black 0328
- African 0331
- Asia, Australia and Oceania 0332
- Canadian 0334
- European 0335
- Latin American 0336
- Middle Eastern 0333
- United States 0337

History of Science 0585
Law 0398
Political Science
- General 0615
- International Law and Relations 0616
- Public Administration 0617

Recreation 0814
Social Work 0452
Sociology
- General 0626
- Criminology and Penology 0627
- Demography 0938
- Ethnic and Racial Studies 0631
- Individual and Family Studies 0628
- Industrial and Labor Relations 0629
- Public and Social Welfare 0630
- Social Structure and Development 0700
- Theory and Methods 0344

Transportation 0709
Urban and Regional Planning 0999
Women's Studies 0453

THE SCIENCES AND ENGINEERING

BIOLOGICAL SCIENCES
Agriculture
- General 0473
- Agronomy 0285
- Animal Culture and Nutrition 0475
- Animal Pathology 0476
- Food Science and Technology 0359
- Forestry and Wildlife 0478
- Plant Culture 0479
- Plant Pathology 0480
- Plant Physiology 0817
- Range Management 0777
- Wood Technology 0746

Biology
- General 0306
- Anatomy 0287
- Biostatistics 0308
- Botany 0309
- Cell 0379
- Ecology 0329
- Entomology 0353
- Genetics 0369
- Limnology 0793
- Microbiology 0410
- Molecular 0307
- Neuroscience 0317
- Oceanography 0416
- Physiology 0433
- Radiation 0821
- Veterinary Science 0778
- Zoology 0472

Biophysics
- General 0786
- Medical 0760

EARTH SCIENCES
Biogeochemistry 0425
Geochemistry 0996
Geodesy 0370
Geology 0372
Geophysics 0373
Hydrology 0388
Mineralogy 0411
Paleobotany 0345
Paleoecology 0426
Paleontology 0418
Paleozoology 0985
Palynology 0427
Physical Geography 0368
Physical Oceanography 0415

HEALTH AND ENVIRONMENTAL SCIENCES
Environmental Sciences 0768
Health Sciences
- General 0566
- Audiology 0300
- Chemotherapy 0992
- Dentistry 0567
- Education 0350
- Hospital Management 0769
- Human Development 0758
- Immunology 0982
- Medicine and Surgery 0564
- Mental Health 0347
- Nursing 0569
- Nutrition 0570
- Obstetrics and Gynecology 0380
- Occupational Health and Therapy 0354
- Ophthalmology 0381
- Pathology 0571
- Pharmacology 0419
- Pharmacy 0572
- Physical Therapy 0382
- Public Health 0573
- Radiology 0574
- Recreation 0575
- Speech Pathology 0460
- Toxicology 0383

Home Economics 0386

PHYSICAL SCIENCES
Pure Sciences

Chemistry
- General 0485
- Agricultural 0749
- Analytical 0486
- Biochemistry 0487
- Inorganic 0488
- Nuclear 0738
- Organic 0490
- Pharmaceutical 0491
- Physical 0494
- Polymer 0495
- Radiation 0754

Mathematics 0405
Physics
- General 0605
- Acoustics 0986
- Astronomy and Astrophysics 0606
- Atmospheric Science 0608
- Atomic 0748
- Electronics and Electricity 0607
- Elementary Particles and High Energy 0798
- Fluid and Plasma 0759
- Molecular 0609
- Nuclear 0610
- Optics 0752
- Radiation 0756
- Solid State 0611

Statistics 0463

Applied Sciences

Applied Mechanics 0346
Computer Science 0984
Engineering
- General 0537
- Aerospace 0538
- Agricultural 0539
- Automotive 0540
- Biomedical 0541
- Chemical 0542
- Civil 0543
- Electronics and Electrical 0544
- Heat and Thermodynamics 0348
- Hydraulic 0545
- Industrial 0546
- Marine 0547
- Materials Science 0794
- Mechanical 0548
- Metallurgy 0743
- Mining 0551
- Nuclear 0552
- Packaging 0549
- Petroleum 0765
- Sanitary and Municipal 0554
- System Science 0790

Geotechnology 0428
Operations Research 0796
Plastics Technology 0795
Textile Technology 0994

PSYCHOLOGY
General 0621
Behavioral 0384
Clinical 0622
Developmental 0620
Experimental 0623
Industrial 0624
Personality 0625
Physiological 0989
Psychobiology 0349
Psychometrics 0632
Social 0451

The undersigned hereby recommend to the Faculty of Graduate Studies and Research acceptance of the thesis,

STRUCTURE AND GEOCHRONOLOGY OF THE GREATER HIMALAYA, KALI GANDAKI REGION, WEST-CENTRAL NEPAL

Submitted by Jeffrey H. Nazarchuk, B.Sc., in partial fulfilment of the requirements for the degree of Master of Science

Thesis Supervisor

Chairman, Department of Earth Science

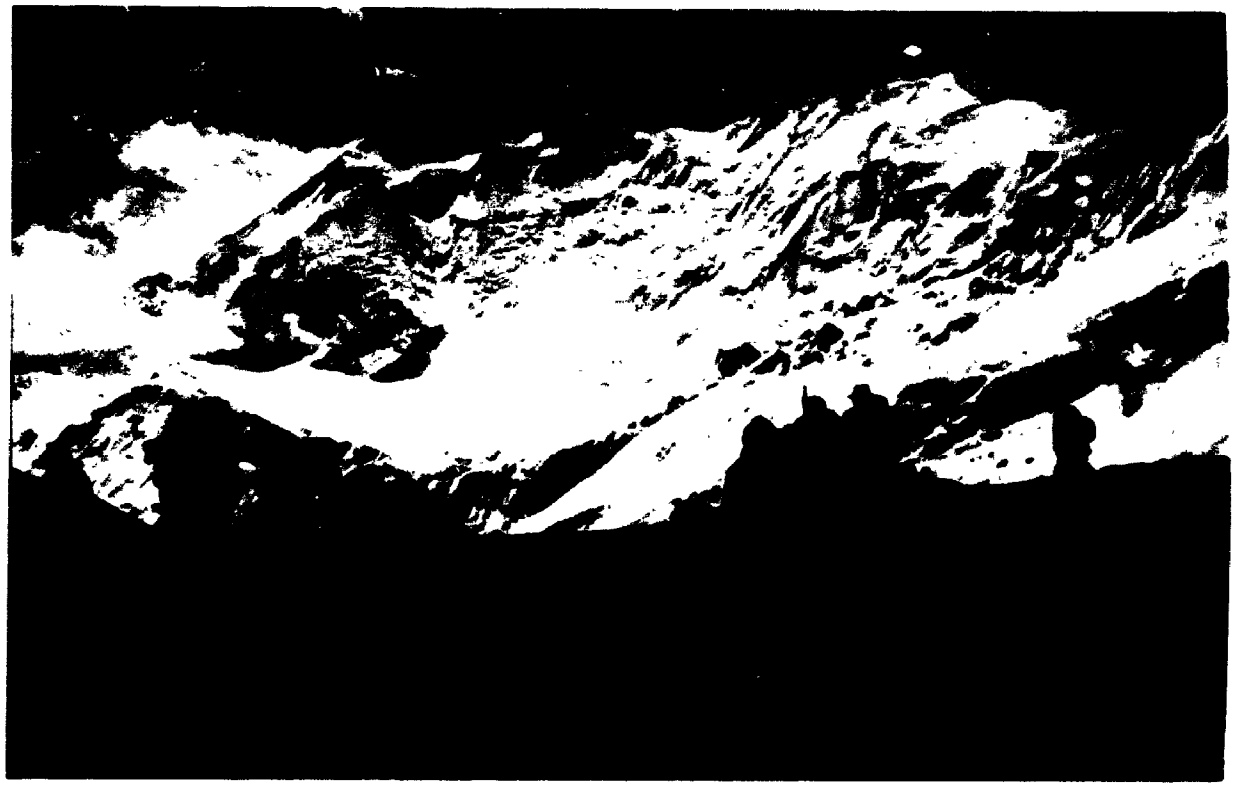

FRONTISPIECE

In the vicinity of the village of Letdar, on descent from the Thorong La (La = pass; 5415 m) down the Marsyandi River valley. View is to the south of the north faces of Annapurna II (left; 7937 m) and Annapurna IV (right; 7525 m). The summits of the two peaks are composed of the low-grade Nilgiri and Sombre formations of the Tibetan sedimentary sequence.

ABSTRACT

Field work in the Kali Gandaki region in the spring of 1991 transected three tectonostratigraphic units: 1) the Lesser Himalayan sedimentary sequence (Lesser Himalaya); 2) the Greater Himalayan metamorphic sequence (Greater Himalaya); and 3) the Tibetan sedimentary sequence. The Lesser Himalaya comprises biotite-grade quartzite and pelitic and calcareous schist and garnet-grade carbonate rocks. The Greater Himalaya is ~6 km thick and consists of kyanite-grade quartzo-feldspathic and pelitic gneiss and migmatite, garnet-hornblende-diopside-bearing calc-silicate gneiss, and discordant sheets of foliated garnet-tourmaline-bearing two-mica leucogranite. The oldest rocks of the Greater Himalaya are thought to be Precambrian. The Tibetan sedimentary sequence is ~11 km thick and consists of Cambro-Ordovician to Eocene passive-margin sedimentary rocks that locally reach biotite-grade in the structurally lowest levels; Mesozoic rocks have Gondwana and Tethyan affinities.

The two main tectonic boundaries in this region are the Main Central Thrust (MCT) and the Annapurna detachment fault (ADF). The MCT is a moderately northeast dipping (38°) crustal-scale, ductile-brittle shear zone that has displaced the Greater Himalaya southwestward over the Lesser Himalaya. The ADF is a moderately northeast dipping (30-40°) ductile-brittle normal fault that juxtaposes the Tibetan sedimentary sequence of the hanging wall with the Greater Himalaya.

Structural and metamorphic relationships indicate a two-stage normal faulting history on the ADF: the first stage occurred at middle crustal levels, followed by static recrystallization; the second stage occurred at upper crustal levels forming a discrete zone of brittle deformation. The ADF is interpreted as a segment of the South Tibetan detachment system.

The MCT has undergone three phases of motion: the dominant phase of deformation (D_{1MCT}) occurred at kyanite-grade conditions, followed by static recrystallization; D_{2MCT} locally formed chlorite-grade mylonites; D_{3MCT} was a brittle event.

Single- and multi-grain fractions of monazite and thorite from two samples in the Greater Himalaya have been dated using the U-Pb system. An undeformed, coarse-grained pegmatite that crosscuts the prominent foliation in the MCT shear zone has an interpreted crystallization age of 21.8 ± 0.5 Ma. Above the high strain portion of the MCT shear zone, a multiply deformed leucogranite body that contains the prominent foliation has an interpreted minimum crystallization age of 22.5 ± 0.1 Ma.

These new data indicate that the prominent fabrics and structures preserved in the Kali Gandaki region formed during the first phase of ductile deformation on the MCT over a time span that ranges from 0.1 to 1.3 Ma. Ductile deformation on the MCT was completed by 21.8 ± 0.5 Ma. Following static recrystallization at middle crustal levels, the Greater Himalaya was rapidly uplifted with little motion on the MCT and tectonically denuded by the Annapurna detachment fault.

ACKNOWLEDGEMENTS

This project was made possible through NSERC Research Grant A2693 awarded to Richard L. Brown, the "Lost Ocean Expedition, '91" organized by Felix Gradstein, field support from the Sherpa Society, assistance from the Jesuit School of Kathmandu to R.L.B. in 1992, use of the geochronology lab at the Geological Survey of Canada in Ottawa and advice from Kip Hodges at MIT in the early stages of planning.

I would like to thank Dick Brown for taking me on as a student of Himalayan geology and for being enthusiastic and involved with the project and Randy Parrish with whom I did my geochronological work. The final version of this thesis benefited greatly from the critical reading and comments by Dick and Randy and from the extremely thorough editing and proof reading of Lois Hardy.

For the numerous hours spent getting computers to do what you want them to, I thank Lisel Currie, Jim Crowley, Lois Hardy and Eric de Kemp for their experience and help and Dick Brown for supplying state-of-the-art equipment.

Thank you to Brad Johnson, David Corrigan, Eric de Kemp, Veronica Irigoyen, Sharon Carr, Shelia Thayer, Sally Hill and everyone else in the department who helped me through the ropes of writing a thesis and Carleton.

Special thanks to Lisel Currie for her friendship and dependable cheery personality with whom I spent many hours discussing geology, the meaning of life and our similar interests. I also thank Lisel for introducing me to field geology and for being like my second advisor at times.

Special thanks to Leslie Reid for her companionship and for helping me through the good times and bad and listening when I needed to talk. I also thank the Reid's for having an open door and being like a second family for me here in Ottawa.

Special thanks to my parents Harry and Verna for their full support and encouragement of my passion for the mountains and geology.

ORIGINAL CONTRIBUTION

Field mapping and sample collection was carried out by the author between March 23 and April 17, 1991, in the Kali Gandaki-Annapurna region of west-central Nepal with the accompaniment of Richard Brown. Petrography, map compilation and geochronology sample preparation were all performed by the author. Sample preparation of three rock samples included crushing and mineral separation using a "Rodger's Table", heavy liquids and "Frantz" magnetic separator. Mineral fractions for analyses were chosen from only two of the samples. Chemistry and mass spectrometry were performed by technicians at the Geological Survey of Canada geochronology laboratory in Ottawa. The integration of structural and geochronological data contained in this thesis is the first of its kind for the Kali Gandaki-Annapurna region.

TABLE OF CONTENTS

CHAPTER 3

GEOLOGY, U-Pb AGE CONSTRAINTS AND TECTONIC HISTORY OF THE KALI GANDAKI REGION, ANNAPURNA HIMAL, WEST CENTRAL NEPAL

LIST OF FIGURES AND MAPS

LIST OF TABLES

LIST OF PLATES

LIST OF APPENDICES

CHAPTER 1

GENERAL INTRODUCTION

INTRODUCTION

I was invited as a student to join Richard Brown and nine other geoscientists on a geological excursion to west-central Nepal called the "Lost Ocean Expedition, '91" in the spring of 1991. This thesis is written on the basis of samples and field data collected from along the Kali Gandaki (Kali = a Hindu Goddess; Gandaki = Sanskrit for river), Ghaleti Khola (Khola = Nepalese for river) and subsidiary drainages during this expedition, as well as samples and data collected by Richard Brown from the same region in the spring of 1992; published literature on the Kali Gandaki and adjacent regions is also considered (see Figs. 2.1 and 2.2 in Chapter 2 for locations of geographic and geologic names).

The expedition was led and organized by Felix Gradstein of the Atlantic Geoscience Centre in Nova Scotia and included members from Canada, the United States, England, Italy, Germany, Japan and Norway. It was 31 days long and followed the famous Annapurna circuit.

Starting at 900 m in the subtropical town of Pokhara with approximately fifty Gurung porters and ten Sherpa guides, we began the 200 mile trek which circumnavigates the 6000-8000 m peaks of the Annapurna Himal and crosses the 5415 m Thorong La (La = mountain pass). After five days trekking, small groups were formed and work began in the specific areas of interest.

The main goal of the "Lost Ocean Expedition '91" was to follow up on sedimentological and paleomagnetic work performed on Mesozoic sedimentary rocks of Tethyan affinity in the Thakkhola region during the "Lost Ocean Expedition '88". Note: Thakkhola or Thak Khola (Thak = red in local Nepalese) is commonly used as the name for the upper Kali Gandaki, where many sedimentary rocks, especially the Plio-Pleistocene Tetang and Thakkhola formations, are bright red in colour; it is also home to the Thakali people. Richard Brown and I were invited on the trip to contribute to the understanding of the structure and tectonic significance of the abundant high-grade metamorphic rocks, as well the low-grade sedimentary rocks which all other members of the expedition were studying.

Of the three chapters comprised in this thesis, Chapter 1 serves as a preamble, and Chapters 2 and 3 are in the form of independent papers to help facilitate publication in journals. The author apologizes for any redundancy (e.g., regional geology, references, figures).

Chapter 2 documents the previously unrecognized, although postulated (K. V. Hodges, unpublished), Annapurna detachment fault, a normal fault in the Thakkhola region. A paper concerning this fault (Brown and Nazarchuk, 1993) has already been accepted for publication.

Chapter 3 documents the structural geology of the Main Central Thrust and Greater Himalaya metamorphic sequence and presents two new U-Pb monazite, thorite and zircon age determinations which bracket the dominant phase of deformation. The tectonic implications of structures, faults and age constraints are also discussed.

At the end of the thesis are appendices of mineral abbreviations and hand sample and thin section descriptions and locations, a geological map (compiled from Colchen et al., 1986) and a station location map, all of which are common to both papers.

Previous work

The Tibetan sedimentary sequence is well exposed and accessible in the Thakkhola region of the upper Kali Gandaki valley. This region underwent five separate geological studies during the 1950's and early 1960's, which are discussed in Gansser (1964). Following this preliminary work, a more detailed structural and sedimentological study of the Thakkhola region resulted in a 1:75,000 scale map (Bordet et al., 1968) and an extensive regional report (written in French; Bordet et al., 1971). More recently, the paleogeography has been studied using paleomagnetic, sedimentological and macro- and micro-fossil data (Gradstein et al., 1992).

The Lesser Himalayan sedimentary sequence and the Greater Himalayan metamorphic sequence have been studied along the Kali Gandaki (Le Fort, 1975) and the Modi Khola south of the Annapurna Sanctuary (Hashimoto et al., 1973; Arita, 1983). Field mapping by Colchen et al. (1986) in the Annapurna - Manaslu - Ganesh Himal between 1966 and 1978 led to a geological report written in French and English and a 1:200,000 scale map, which included the Tibetan sedimentary sequence, Greater Himalayan metamorphic sequence and Lesser Himalayan sedimentary sequence of the Kali Gandaki region. Incorporated in the Colchen et al. (1986) study

is A. Pecher's Ph. D. thesis on the geology of the Main Central Thrust and Greater Himalayan metamorphic sequence (see Pecher, 1977). Geothermobarometry of samples from the Greater Himalayan metamorphic sequence between the Kali Gandaki and the Ministi Khola was performed by Le Fort et al. (1987a). Previous to this study, no U-Pb age determinations had been performed in the Kali Gandaki region.

References

See Chapters 2 and 3 for references cited.

CHAPTER 2

THE ANNAPURNA DETACHMENT FAULT, THAKKHOLA REGION, WEST-CENTRAL NEPAL: A SEGMENT OF THE SOUTH TIBETAN DETACHMENT SYSTEM

ABSTRACT

Field observations from the Thakkhola region of the upper Kali Gandaki valley indicate that the contact between the Greater Himalayan metamorphic sequence (Greater Himalaya) and Tibetan sedimentary sequence is a moderately northeast dipping (30-40°), crustal-scale, ductile-brittle normal fault. The footwall contains kyanite-grade quartzo-feldspathic gneiss and garnet-tourmaline-bearing two-mica leucogranite with normal-sense ductile shearing fabrics. The hanging wall contains biotite-grade schist and phyllite and is separated from the footwall by a 5-10 m thick crushed zone.

Structural and metamorphic relationships indicate a two-stage normal faulting history: the first stage occurred at middle crustal levels and was followed by static recrystallization; the second stage occurred at upper crustal levels forming a discrete zone of brittle deformation and may have been accompanied by orogen-parallel extension. This fault is interpreted as a segment of the South Tibetan detachment system and is named the Annapurna detachment fault.

In the hanging wall of the Annapurna detachment fault, five phases of deformation are recognized: first-phase meso- to megascopic southwest-verging isoclines and an associated layer-parallel foliation; second-phase northeast-verging, tight to open megascopic folds (Nilgiri nappe) with an axial planar biotite foliation; third-phase post-metamorphic, southwest-verging micro- to mesoscopic folds, thrust faults and an associated suite of boudinaged felsic dikes; fourth-phase northwest-southeast striking upright, gentle folds; and fifth-phase northeast-southwest striking brittle fractures and faults.

The third-phase southwest-verging folds in the hanging wall of the Annapurna detachment fault are the youngest structures truncated by the crushed zone; these structures indicate that a period of southwest-directed thrusting may have predated the most recent normal faulting. The origin of the second-phase, northeast-verging Nilgiri nappe is unclear. It may have formed during crustal thickening or in a broad zone of normal-sense shear related to the South Tibetan detachment system.

INTRODUCTION

Extensional faulting and the generation of normal-sense ductile shear zones are recognized as important features of convergent orogens; low angle normal-sense shear zones give rise to rapid exhumation of high-grade rocks (Coney, 1980; Armstrong, 1972). More recently it has been shown that in tectonically active regions such as Tibet, normal faulting is contemporaneous with contractional deformation but perpendicular to the overall compressive direction of the Himalayan orogen (Molnar and Tapponnier, 1978; Armijo et al., 1986). In the Andes, orogen-parallel normal faulting and thrust faulting are occurring simultaneously (Dalmayrac and Molnar, 1981). Numeric models indicate that in high standing regions such as the Tibetan plateau or high Andes of Peru gravitational potentials are large enough to change the orientation of the principal stress axis. When gravitational stresses exceed the strength of the rocks, orogen-parallel extension of the upper crust occurs (Burchfiel and Royden, 1985; Dalmayrac and Molnar, 1981).

The metamorphic core of the Himalayan orogen, the Greater Himalayan metamorphic sequence (Greater Himalaya), is bound at the base by the Main Central Thrust, a crustal-scale, ductile-brittle shear zone that dips moderately to the northeast. In southern Tibet, the Greater Himalaya is separated from the overlying Tibetan sedimentary sequence by orogen-parallel, crustal-scale, ductile-brittle normal faults that dip gently to the northeast (the South Tibetan detachment system) (Burg et al., 1984; Herren, 1987; Burchfiel et al., 1992). Integrated structural, petrological and geochronological studies indicate that in the Qomolangma region (Everest), the Greater

Himalaya was extruded southward and exhumed during simultaneous movement on the Main Central Thrust and South Tibetan detachment system during the Miocene (Burchfiel et al., 1992 and references therein).

In the Kali Gandaki region of central Nepal, the contact between the Greater Himalaya and Tibetan sedimentary sequence was originally believed to correspond to a metamorphic and structural transition from superstructure to infrastructure; with a lack of evidence for discordance, the Greater Himalaya was considered to be the Precambrian basement to the Tibetan sedimentary sequence (Gansser, 1964; Le Fort, 1975). This contact was later interpreted as a recrystallized zone of gravity-driven ductile deformation that formed when the Tibetan sedimentary sequence detached from the underlying Greater Himalaya (Caby et al., 1983; Colchen et al., 1986). The crustal-scale nappe seen in the peaks of Nilgiri and Annapurna (I) was interpreted as a gravity collapse structure that formed during this detachment (Caby et al., 1983; Colchen et al., 1986). It is now believed that the Nilgiri nappe and a similar north-verging structure in the Gyirong region east of Manaslu formed in response to a broad zone of normal-sense shear related to the South Tibetan detachment system (Burchfiel et al., 1992).

Observations from field mapping in the Kali Gandaki region (Figs. 2.1 & 2.2) in the spring of 1991 indicate that the contact between the Greater Himalaya and Tibetan sedimentary sequence is a crustal-scale, ductile-brittle normal fault. This paper will: 1) document the presence of the Annapurna detachment fault, a segment of the South Tibetan detachment system; 2) describe the structure and metamorphism in the

Tibetan sedimentary sequence, which forms the hanging wall of the Annapurna detachment fault; and 3) discuss the significance of structures in the Tibetan sedimentary sequence and the origin of the Nilgiri nappe.

REGIONAL GEOLOGY

In central Nepal, the three main tectonostratigraphic units are the Lesser Himalayan sedimentary sequence, the Greater Himalayan metamorphic sequence and the Tibetan sedimentary sequence (Fig. 2.1). For brevity the Lesser Himalayan sedimentary sequence and Greater Himalayan metamorphic sequence are referred to throughout the text as the Lesser Himalaya and Greater Himalaya. The Greater Himalaya is comprised of 4-10 km of coarse-grained gneiss and leucogranite believed to represent a sliver of the Indian craton displaced southwestward by more than 100 km on the Main Central Thrust; it now overlies the lower-grade Lesser Himalaya (Figs. 2.2 & 2.3) (Gansser, 1964; Molnar and Tapponnier, 1975; Molnar, 1984). The Greater Himalaya has undergone polyphase metamorphism and preserves an inverted sequence of isograds (sillimanite above kyanite) in the middle to uppermost structural levels (Swapp and Hollister, 1991 and references therein). This apparent metamorphic inversion may be the result of a Miocene moderate-pressure, high-temperature Buchan metamorphic event superposed on an Eocene high-pressure, high-temperature Barrovian metamorphic event, not a continuous increase in metamorphic grade (Brunel and Kienast, 1986; Hodges and Silverberg, 1988; Hodges et al., 1988 and references therein; Swapp and Hollister, 1991).

The Tibetan sedimentary sequence consists of polydeformed, weakly metamorphosed to nonmetamorphosed calcareous and siliciclastic miogeoclinal rocks (Gansser, 1964). In the Thakkhola region (Figs. 2.1 & 2.2), the Tibetan sedimentary sequence has a stratigraphic thickness of ~11 km and is folded in the spectacular Nilgiri nappe (Fig. 2.4) (Gansser, 1964; Bordet et al., 1968 & 1971; Le Fort, 1975; Colchen et al., 1986). The oldest rocks dated with paleontological certainty are the Ordovician Nilgiri limestones (Colchen et al., 1986) (Map 1). Stratigraphically below the Nilgiri limestones are the Pi, Annapurna and Sanctuary formations. The oldest of these, the Sanctuary Formation, contains no fossils. The Annapurna Formation, however, contains poorly preserved, unidentified trace fossils and trilobites(?), indicating a possible Cambro?-Ordovician age (Colchen et al., 1986). Above the Nilgiri limestones the stratigraphic section is nearly continuous through to the Eocene. Plate reconstructions indicate that in the Early Cretaceous, the Thakkhola region was situated on the south side of the Tethys Ocean on the northern margin of Gondwana (Gradstein et al., 1992).

FIELD RELATIONS

The Annapurna detachment fault

In the Thakkhola region, the contact between the Greater Himalaya and the Tibetan sedimentary sequence is well exposed in a narrow stream gully on the west bank of the Kali Gandaki, west of the village of Dhumpu (Fig. 2.2). The contact dips moderately to the northeast (30-40°) with the distinctively layered and yellow

weathering Annapurna Formation of the Tibetan sedimentary sequence (Colchen et al., 1986) forming the north side of the gully and Formation III of the Greater Himalaya forming the south side of the gully (Plate 2.1a).

The footwall of the Annapurna detachment fault consists of coarse-grained kyanite-bearing quartzo-feldspathic migmatite and minor calc-silicate gneiss that are intruded by m-scale sheets of garnet-tourmaline-bearing two-mica leucogranite and cm- to dm-scale coarse-grained granitic intrusions. Leucogranite sheets are discordant but are sheared and have a well developed foliation (Plate 2.1b) that is subparallel to the foliation in the gneisses and the contact between the Greater Himalaya and Tibetan sedimentary sequence. The coarse-grained lenses are not foliated and crosscut the larger leucogranite bodies (Plate 2.1c). In thin section, shearing fabrics are statically annealed (Plate 2.1d).

Stretching lineations are not well developed, but where observed they are down the dip of the foliation. In thin section, kinematic indicators are absent but in outcrop they include asymmetric folds with horizontal hinge lines, C-S fabrics, shear bands and dike arrays that have been either extended or shortened depending on their orientation with the shear plane; all indicate top-down-to-the-northeast sense of shear (Plate 2.2a, b & c; Fig. 2.5). These ductile fabrics are observed from ~100 m below to within 10 m of the contact with the overlying Annapurna Formation. The contact is a 5-10 m thick zone of crushed and brecciated felsic material (Fig. 2.5).

Within the footwall of the Annapurna detachment fault there has been no metamorphic retrogression of the peak mineral assemblage. Kyanite-garnet-bearing

pelitic layers indicate middle amphibolite facies metamorphism with pressure and temperature ranges of 6-8 kbars and 600-670°C, respectively (Barker, 1990). In the crush zone, however, minor pelitic layers contain chlorite. For a complete description of the structures and metamorphism in the Greater Himalaya, see Chapter 3.

Directly above the crush zone are fine- to medium-grained, biotite-grade calcareous psammite and semi-pelitic schist and phyllite of the Annapurna Formation. Top-down-to-the-northeast shear-sense indicators are not observed adjacent to the contact with the Greater Himalaya, although the rocks are ductilely sheared and very planar (Plate 2.2d). The compositional layering and parallel foliation is truncated by the crush zone of the Annapurna detachment fault.

Structure and metamorphism in the Tibetan sedimentary sequence

In this section, the structural and metamorphic relationships observed in the Tibetan sedimentary sequence directly above the Annapurna detachment fault, to about the structural level of the village of Marpha (Figs. 2.2 & 2.4), will be described. The structures (F_{1-n}), surfaces (S_{1-n}) and metamorphic events (M_{1-n}) are assigned to deformation events (D_{1-n}) throughout the text and are summarized in Table 2.1.

In the Thakkhola region, five phases of deformation are observed. D_1 is represented by a layer-parallel S_1 mica foliation and rootless F_1 isoclinal fold closures. Locally, S_1 cuts the hinges of F_1 isoclinal folds (Plate 2.3a). F_1 closures are shown on a crustal scale in cross sections through the Annapurna massif (Fig. 2.4) (Colchen et al., 1986) and are visible in the west face of Annapurna (I). In Figure 2.4 a large

refolded F_1 closure is shown in the summit of Fang. On the basis of stratigraphic superposition, this fold probably originated as a southwest-verging anticline (Brown and Nazarchuk, 1993); therefore, D_1 was presumably a southwest-directed phase of shearing.

D_2 is represented by the prominent S_2 foliation and northeast-verging, tight to open megascopic folds that are parasitic to the recumbent, crustal-scale Nilgiri nappe (Plate 2.3b & c) (see also the fold-out plate and photograph #1 in Colchen et al. (1986) for excellent views of the Nilgiri nappe). S_2 is defined by the preferred orientation of mica in semi-pelitic to pelitic rocks and as a spaced cleavage in more arenaceous rocks (Plate 2.3d). In cross sections by Colchen et al. (1986), there is a truncation of the lower limb of the Nilgiri nappe at the proposed level of the Annapurna detachment fault (Fig. 2.4).

D_3 is represented by well developed southwest-verging micro- to mesoscopic, post-metamorphic crenulations and folds (Plate 2.4a & b) that refold all other structures (Plate 2.4 c). The axial planes of these structures are subhorizontal to moderately northeast dipping. Associated with D_3 folding is a suite of tourmaline-bearing quartz-plagioclase dikes that are oriented parallel to the axial planes of F_3 folds (Plate 2.4d). Above the Annapurna detachment fault, these dikes form high angles with S_2 and are extended and boudinaged, indicating that D_3 was a phase of southwest-directed shearing, possibly coeval with southwest-directed thrusts observed higher in the Tibetan sedimentary sequence. Adjacent to the Annapurna detachment fault, these dikes become subparallel to layering (S_{0+1+2}) and are progressively more

boudinaged and eventually truncated at the brittle zone.

D_4 represents a period of km-scale-amplitude, upright, gentle folding. The axial planes of the D_2 Nilgiri nappe (Fig. 2.4) and its parasitic F_2 folds (Plate 2.3c) outline F_4 folds. Upright flower structures seen at a few localities may also be related to D_4 (Plate 2.5a).

D_5 consists of northeast-southwest striking brittle fractures and normal faults that are related to the Thakkhola normal fault (Fig. 2.2). The Thakkhola normal fault has ~4000 m of vertical displacement and gives the region its characteristic half-graben geometry (Colchen et al., 1986). D_5 brittle deformation was not observed in the Greater Himalaya, although a northeast-southwest striking normal fault is shown extending well into the Greater Himalaya on the map by Colchen et al. (1986) (Fig. 2.2; Map 1).

In the Tibetan sedimentary sequence, three metamorphic events are recognized. M_1 occurred during D_1 and produced the S_1 mica foliation that cuts the hinges of F_1 folds. M_2 occurred during D_2 and produced the prominent S_2 biotite-muscovite foliation. M_2 has a normal upwards decrease in metamorphic grade. At the Annapurna detachment fault, the Tibetan sedimentary sequence is at biotite grade; near Jomosom rocks are nonmetamorphosed (Fig. 2.2). Directly above the Annapurna detachment fault, all rock types have a well developed, planar S_{0+1+2} biotite-muscovite foliation (Plate 2.2d). Biotite also forms blocky, medium-grained porphyroblasts that overgrow the dominant foliation indicating that M_2 outlasted D_2 deformation (Plate 2.5b). The blocky biotite is partially or completely replaced by chlorite.

Overprinting all fabrics are medium-grained porphyroblasts of randomly oriented muscovite (Plate 2.5c), anomalous blue and brown chlorite, and inclusion-filled albite (Plate 2.5d). Epidote is also present as small spheres, altered clots, and tabular or anhedral crystals, some having zoned birefringence or an anomalous blue colour. The textural relationships and mineral assemblage muscovite + chlorite + epidote + albite clearly document a post-tectonic greenschist facies metamorphism (M_3) (Hyndman, 1985) overprinting an earlier biotite-grade metamorphism (Table 2.1).

INTERPRETATION

The Annapurna detachment fault

On the basis of metamorphic juxtaposition and footwall rocks that preserve ductile normal-sense shearing fabrics formed at middle crustal levels, the Annapurna detachment fault is interpreted as a crustal-scale normal fault. On the basis of regional mapping by Burchfiel et al. (1992), the Annapurna detachment fault is correlated with the South Tibetan detachment system. The structural evolution of the Annapurna detachment fault differs, however, from other detachment faults in the South Tibetan detachment system.

Along the South Tibetan detachment system, the footwall typically preserves mylonitic fabrics that show evidence of progressively more brittle deformation with associated metamorphic retrogression as the structure evolved (Herren, 1987; Burchfiel et al., 1992). The hanging wall contains south-verging structures refolded by large upright to overturned north-verging folds, interpreted as drag structures related to

normal faulting (Burchfiel et al., 1992). Therefore, the youngest fabrics truncated in the footwall and hanging wall of the South Tibetan system indicate normal-sense shearing.

In the Thakkhola region, the footwall of the Annapurna detachment fault does not mylonites, but instead rocks that were ductilely sheared with a top-to-the-northeast normal-sense of motion and subsequently annealed at middle crustal levels. Also, other than the crush zone that separates the Greater Himalaya and Tibetan sedimentary sequence, neither brittle fabrics nor retrogressive metamorphism are recorded in the footwall. In the hanging wall of the Annapurna detachment fault, the youngest structures demonstrably cut by the crush zone are the southwest-verging, thrust-related D_3 folds and associated suite of dikes. This gives the Annapurna detachment fault an incompatible juxtaposition of northeast-verging normal-sense fabrics in the footwall with southwest-verging thrust-sense fabrics in the hanging wall. In the hanging wall, although not directly observed, the decrease in angles between F_3 axial planes and S_2 as well as an increase in the intensity of D_3 boudinage towards the south suggests that brittle motion on the Annapurna detachment fault has reactivated or formed near a previously existing thrust fault.

As indicated, brittle motion on the Annapurna detachment fault is at least younger than D_3 southwest-directed shearing. An attempt at dating one of the quartz-plagioclase dikes associated with D_3 thrusting using the U-Pb system has been unsuccessful due to a lack of suitable minerals; only a few crystals of titanite and zircon were recovered from a 10 kg sample. Successful geochronometry work on this

suite of dikes or the S_2 biotite foliation would place important timing constraints on structures in the Tibetan sedimentary sequence. It is unclear if any of the brittle motion on the Annapurna detachment fault post-dates D_4 or D_5 in the Tibetan sedimentary sequence; therefore, Quaternary motion cannot be ruled out.

In contrast with other segments of the South Tibetan detachment system, the Annapurna detachment fault has a two-stage history of normal faulting. The first stage occurred entirely at middle crustal levels and may have had little vertical throw as transitional ductile-brittle fabrics are not preserved. The second stage was dominantly brittle and juxtaposed rocks with different metamorphic and structural histories. The truncation of the lower limb of the Nilgiri nappe and the presence of minor chlorite-grade shearing preserved in the crush zone of the Annapurna detachment fault suggest that mylonites may have formed but were faulted out during the second stage of brittle motion on the Annapurna detachment fault.

D_3 structures and the Nilgiri nappe

In the Tibetan sedimentary sequence, the dominant structures are the D_2 Nilgiri nappe and its associated F_2 parasitic folds. The immense scale of the nappe (tight to isoclinal folding of an ~2500 m thick stratigraphic section; Fig. 2.4) and northeast vergence that contrasts with the southwest vergence of the structurally lower Greater Himalaya have led to much speculation about its origin. Although key relationships such as the age of D_2 or M_2 are unknown, the formation of the Nilgiri nappe has been attributed to gravitational sliding (Caby et al., 1983; Colchen et al., 1986) and to

northeast normal-sense shearing associated with the South Tibetan detachment system (Burchfiel et al., 1992).

In the hanging wall of the Annapurna detachment fault there are no biotite-grade extensional structures correlative with D_2, and the geometry of the Nilgiri nappe tends to thicken rather than thin the crust. Also, the D_2 folds and associated S_2 biotite foliation are overprinted by a chlorite-grade metamorphism and folded by post-metamorphic D_3 folds, indicating that D_2 was not the culminating event. Therefore, it is equally plausible that D_1, D_2 and D_3 represent phases of regional metamorphism and crustal thickening that occurred during the initial Eocene collision between India and Eurasia (Gansser, 1964; Molnar and Tapponnier, 1975) and that D_2 structures have no genetic relationship to the Annapurna detachment fault. If it is accepted that the Nilgiri nappe formed during the initial stages of normal faulting, the two-stage history of motion on the Annapurna detachment fault requires an intervening period of thrusting (D_3).

In the hanging wall of the Annapurna detachment fault, upright D_4 "flower-structures" that fold S_2 were observed in cliff faces (Plate 2.5a). In the Gyirong region, upright structures in the hanging wall of the Bhote Kosi detachment fold an older metamorphic foliation (see Fig. 6 in Burchfiel et al., 1992). In the Padam region of India, the hanging wall of the Zanskar normal fault contains upright folds interpreted as gravity collapse structures (see Figs. 7 & 10a in Searle, 1986). It is proposed here that the products of normal faulting along segments of the South Tibetan detachment system are these less dominant, smaller scale upright structures, not the north-verging.

recumbent, crustal-scale structures such as the Nilgiri nappe. Because the D_5 brittle structures associated with the Thakkhola normal fault are not found in Greater Himalaya, they appear to have been concentrated in upper crustal levels and may be kinematically related to D_4 and the Annapurna detachment fault.

As proposed above, the Nilgiri nappe may be the result of early crustal thickening and regional metamorphism. If so, then the F3 contractional structures and suite of granitic dikes in the Tibetan sedimentary sequence are documenting a post-metamorphic, southwest-directed thrusting event that occurred prior to movement on the Annapurna detachment fault. Elsewhere in the Himalaya, field relations as well as pressure-temperature paths from garnet-bearing pelitic rocks in the Greater Himalaya indicate that the Buchan metamorphism overprinting the earlier Barrovian metamorphic event was associated with the generation of leucogranites and a tectonic reburial of 5-7 km (Hodges and Silverberg 1988; Hodges et al., 1988). This reburial was found to be widespread, but the lack of appropriate structures from detailed mapping in the Tibetan sedimentary sequence hindered explanation. It is suggested here that the D_3 contractional structures and suite of granitic dykes in the hanging wall of the Annapurna detachment fault may be documenting the event that caused the post-Barrovian tectonic reburial observed in pressure-temperature paths and are possibly related to the Buchan metamorphism and leucogranite generation. Further structural mapping in the hanging wall of the Annapurna detachment fault is necessary to understand the regional implications of D_3 structures.

CONCLUSIONS

The Annapurna detachment fault is a moderately northeast dipping, crustal-scale normal fault. Structural and metamorphic data indicate that the Annapurna detachment fault had a two-stage normal faulting history: 1) an early stage of middle crustal shearing followed by static recrystallization; and 2) a dominantly brittle stage that produced the discrete crushed and brecciated zone separating the Greater Himalaya and the Tibetan sedimentary sequence.

Five phases of deformation are recognized in the Tibetan sedimentary sequence. Southwest-verging D_3 structures are the youngest phase of deformation cut by the most recent movement on the Annapurna detachment fault. The kinematic significance of the D_2 Nilgiri nappe is unclear. It may have formed during initial crustal thickening in response to convergence between India and Eurasia or as the result of a broad zone of normal-sense shear related to the South Tibetan detachment system.

Figure 2.1. Geological map of central Nepal modified after Colchen et al. (1986). Inset in upper left hand corner shows location of field area; box shows location of detail map in Figure 2.2; A-A' locates line of cross section in Figure 2.4; MCT = Main Central Thrust; ADF = Annapurna detachment fault; TNF = Thakkhola normal fault.

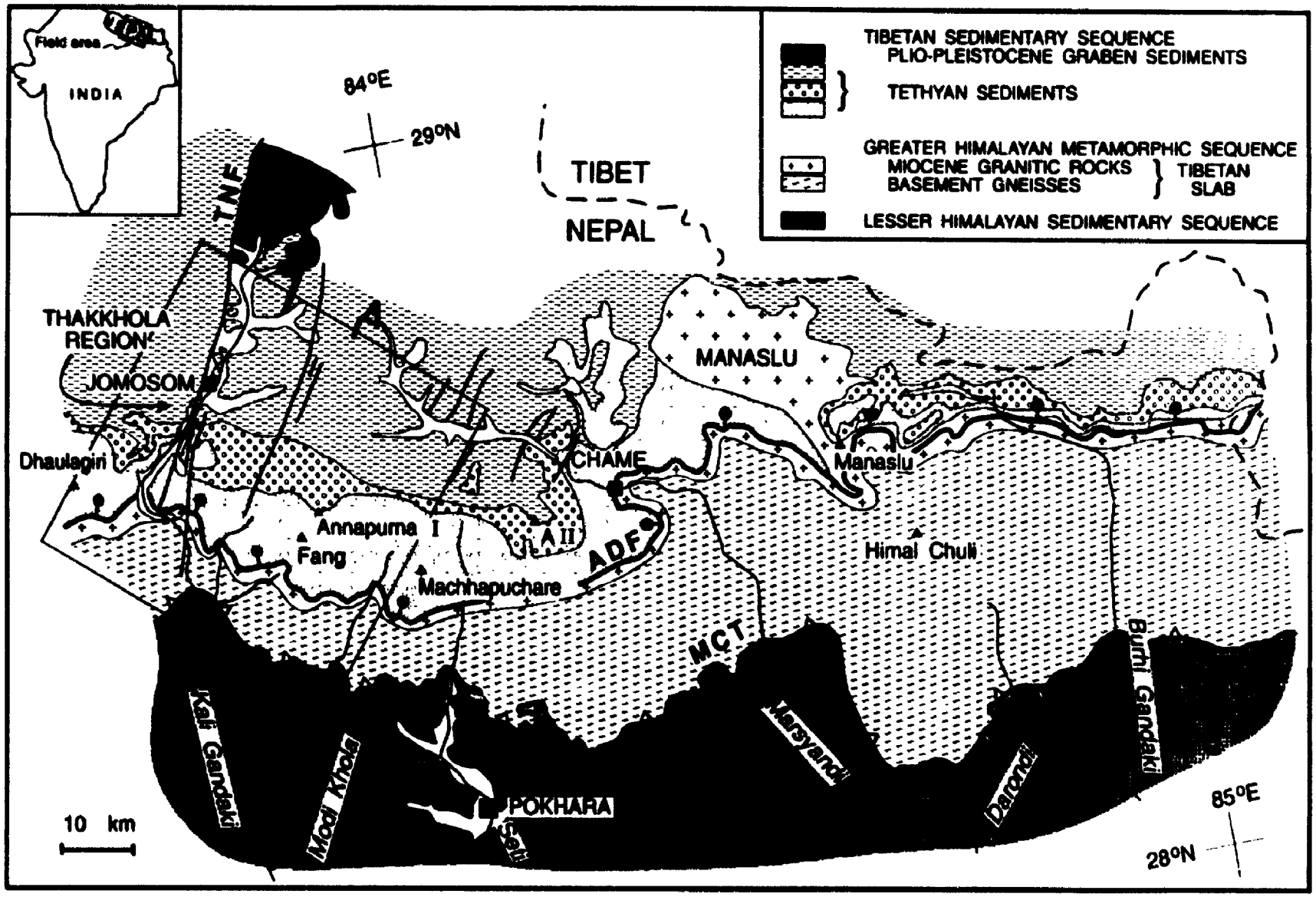
Field area
INDIA
84°E
29°N
TIBET
NEPAL
TNF
THAKKHOLA REGION
JOMOSOM
Dhaulagiri
MANASLU
CHAME
Manaslu
Annapurna I
Fang
II
ADF
Machhapuchare
Himal Chuli
MCT
Kali Gandaki
Modi Khola
POKHARA
Marsyandi
Darondi
Burhi Gandaki
10 km
85°E
28°N
TIBETAN SEDIMENTARY SEQUENCE
PLIO-PLEISTOCENE GRABEN SEDIMENTS
TETHYAN SEDIMENTS
GREATER HIMALAYAN METAMORPHIC SEQUENCE
MIOCENE GRANITIC ROCKS
BASEMENT GNEISSES
TIBETAN SLAB
LESSER HIMALAYAN SEDIMENTARY SEQUENCE

Figure 2.2. Detail of the field area: shaded dashed line follows route of traverses; A-A' locates line of cross section in Figure 2.4; MCT = Main Central Thrust; ADF = Annapurna detachment fault; TNF = Thakkhola normal fault; see Figure 2.1 for legend.

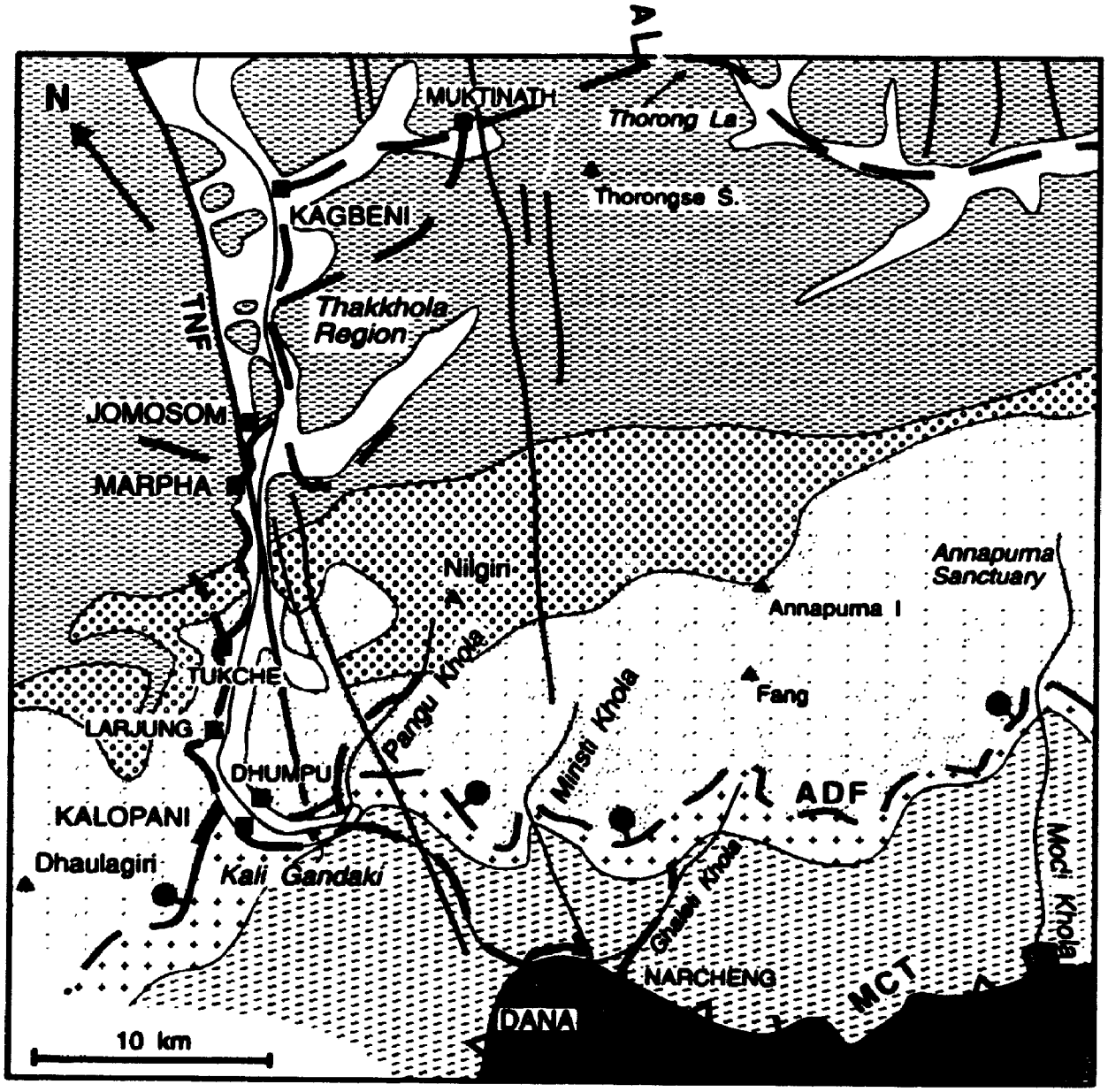
N
MUKTINATH
Thorong La
Thorongse S.
KAGBENI
Thakkhola Region
TNF
JOMOSOM
MARPHA
Nilgiri
Annapurna Sanctuary
Annapurna I
TUKCHE
Pangu Khola
Fang
LARJUNG
Miristi Khola
DHUMPU
ADF
KALOPANI
Dhaulagiri
Kali Gandaki
Ghale Khola
Modi Khola
NARCHENG
MCT
DANA
10 km

Figure 2.3. (a) balanced and (b) restored cross sections of the eastern Nepal Himalaya through the Greater Himalaya north of Melung-Tse and the Ganges Plain south of Sindhuli Bazaar (from Schelling, 1992). Rocks above the MCT belong to the Greater Himalaya. Only the Lesser and Sub-Himalaya beneath and south of the MCT have been restored. Main Central Thrust, MCT; Sun Kosi Thrust, SKT; Main Boundary Thrust, MBT; Main Detachment Fault, MDF; Kamala Thrust, KT; Main Frontal Thrust, MFT.

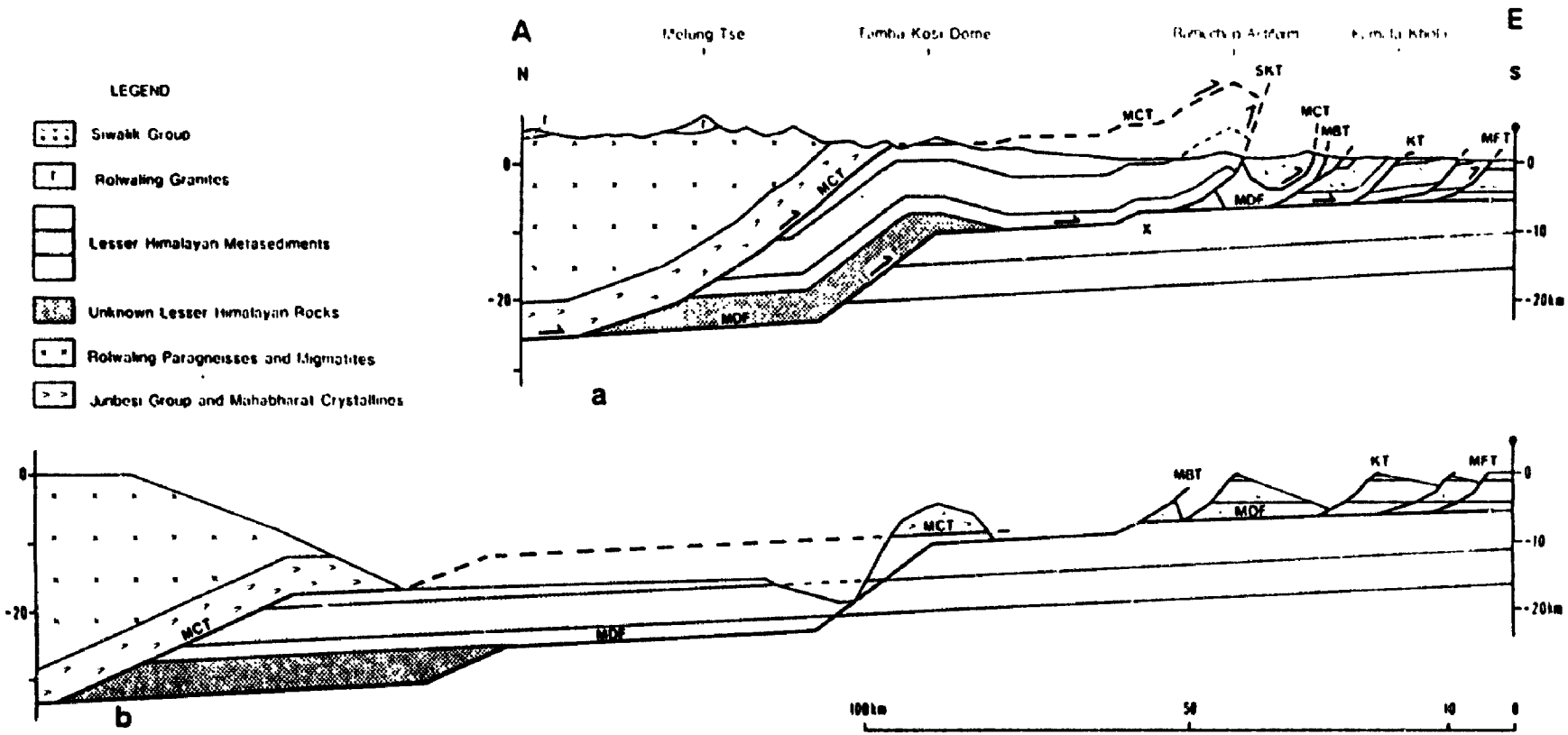
LEGEND
Siwalik Group
Rolwaling Granites
Lesser Himalayan Metasediments
Unknown Lesser Himalayan Rocks
Rolwaling Paragneisses and Migmatites
Junbesi Group and Mahabharat Crystallines
A
E
N
S
Melung Tse
Tumba Kosi Dome
SKT
MCT
MBT
KT
MFT
MDF
X
0
-10
-20km
-20
a
b
100km
50
10
0

Figure 2.4. Cross section modified after Colchen et al. (1986). MCT = Main Central Thrust; ADF = Annapurna detachment fault (located as per Caby et al., 1983).

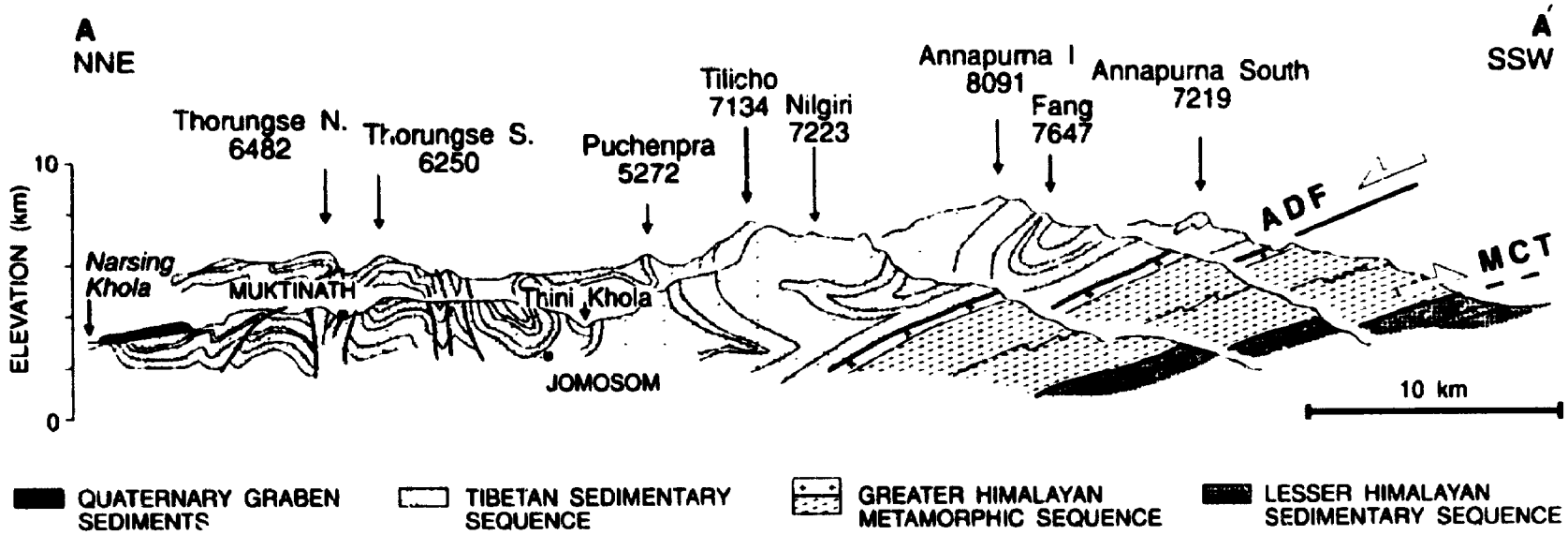
A
NNE
A'
SSW
Thorungse N.
6482
Thorungse S.
6250
Puchenpra
5272
Tilicho
7134
Nilgiri
7223
Annapurna I
8091
Fang
7647
Annapurna South
7219
ADF
MCT
Narsing
Khola
MUKTINATH
Thini Khola
JOMOSOM
ELEVATION (km)
10
0
10 km
QUATERNARY GRABEN SEDIMENTS
TIBETAN SEDIMENTARY SEQUENCE
GREATER HIMALAYAN METAMORPHIC SEQUENCE
LESSER HIMALAYAN SEDIMENTARY SEQUENCE

Figure 2.5. Illustration of view looking west in the Dhumpu region west of the Kali Gandaki: ADF = Annapurna detachment fault; arrows indicate sense of shear within footwall rocks; lightly shaded bands in footwall schematically illustrate sheared leucogranite; two orientations of lines within leucogranites illustrate C-S fabric; magnifying glass schematically illustrates pressure shadows on rotated and unrotated porphyroclasts; S0 = orientation of bedding; S1, S2, and S3 = first-, second-, and third-phase foliations; F2 and F3 = second- and third-phase folds; darkly shaded lenses in upper plate illustrate boudinaged quartz-feldspar dikes. See text for explanation. Diagram not to scale.

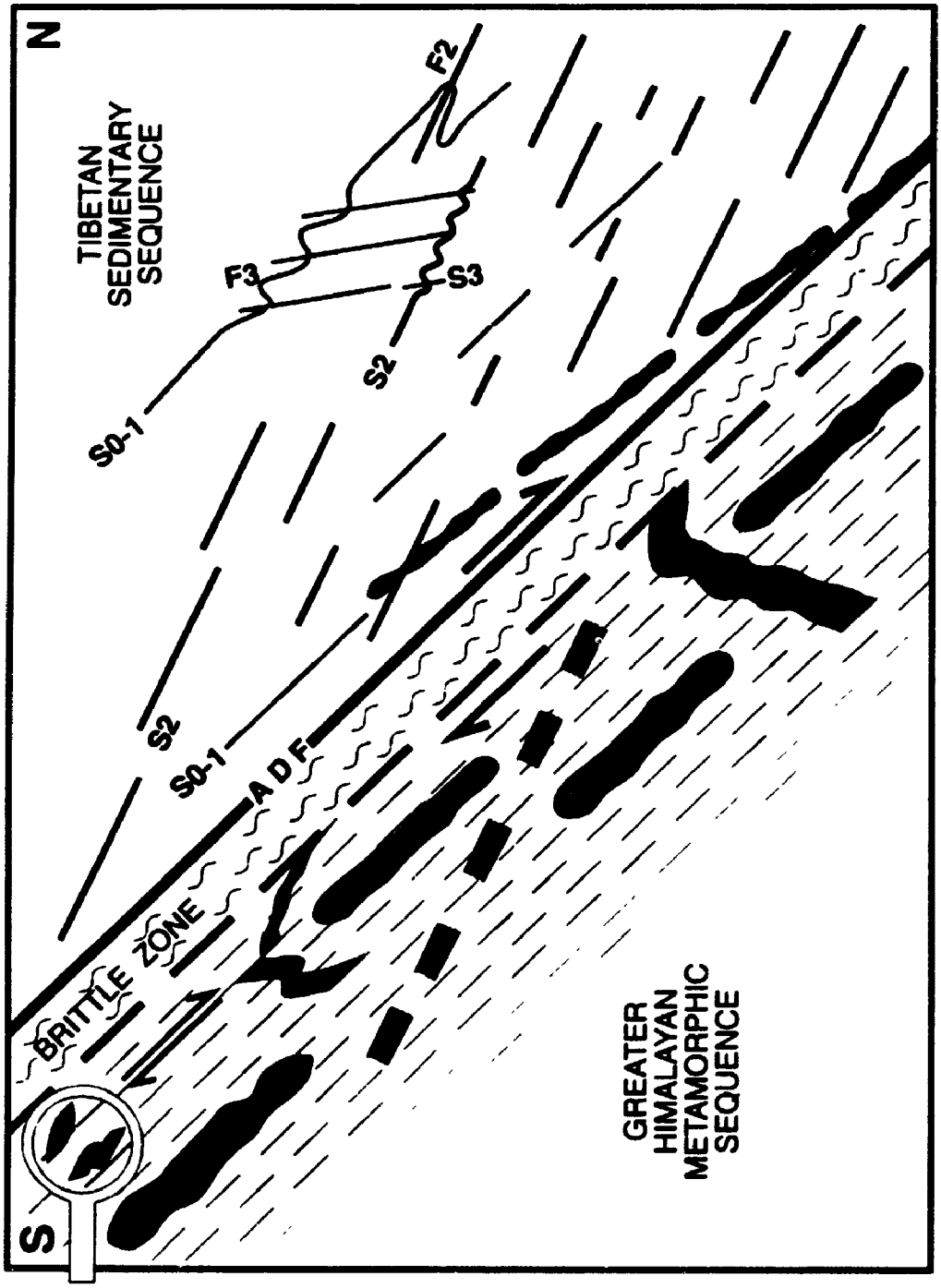
N
S
TIBETAN
SEDIMENTARY
SEQUENCE
F2
F3
S3
S2
S0-1
S2
S0-1
A D F
BRITTLE ZONE
GREATER
HIMALAYAN
METAMORPHIC
SEQUENCE

Table 2.1. Structures and metamorphism recognized in the Tibetan sedimentary sequence

	TSS	
	Structure	**Metamorphism**
D1	- isoclines in compositional layering parallel to S1 and S2 foliations	- biotite-grade? - **M1**
D2	- megascopic northeast-verging folds (Nilgiri nappe) and prominent S2 foliation	- biotite-grade - **M2**
D3	- micro- to mesoscopic southwest-verging crenulations and folds in S2 and compositional layering - southwest-verging thrusts and northeast dipping boudinaged dikes	- post-tectonic greenschist-facies metamorphism
D4	- northwest-southeast striking, km-scale-amplitude upright folds - upright flower structures	- **M3**
D5	- northeast-southwest striking brittle fractures and faults - Thakkhola normal fault	

Tibetan sedimentary sequence (TSS) forms the hanging wall of the Annapurna detachment fault. D(1-n), deformation events; S(1-n), surfaces; M(1-n), metamorphic events.

Plate 2.1

A) View to the west of the Annapurna detachment fault. Solid line is the contact between kyanite-grade migmatite and leucogranite of the Greater Himalaya in the footwall and biotite-grade psammite and micaceous schist of the Tibetan sedimentary sequence in the hanging wall. See Figure 2.5 for details of the contact relations.

B) Sheared and foliated two-mica leucogranite with cm-scale quartz-feldspar segregations; garnet (g); tourmaline (t).

C) Undeformed, coarse-grained tourmaline-bearing granitic dike intruded into foliated leucogranite.

D) Photomicrograph of sheared and recrystallized leucogranite; biotite (b), plagioclase (p), k-feldspar (k), quartz (q).

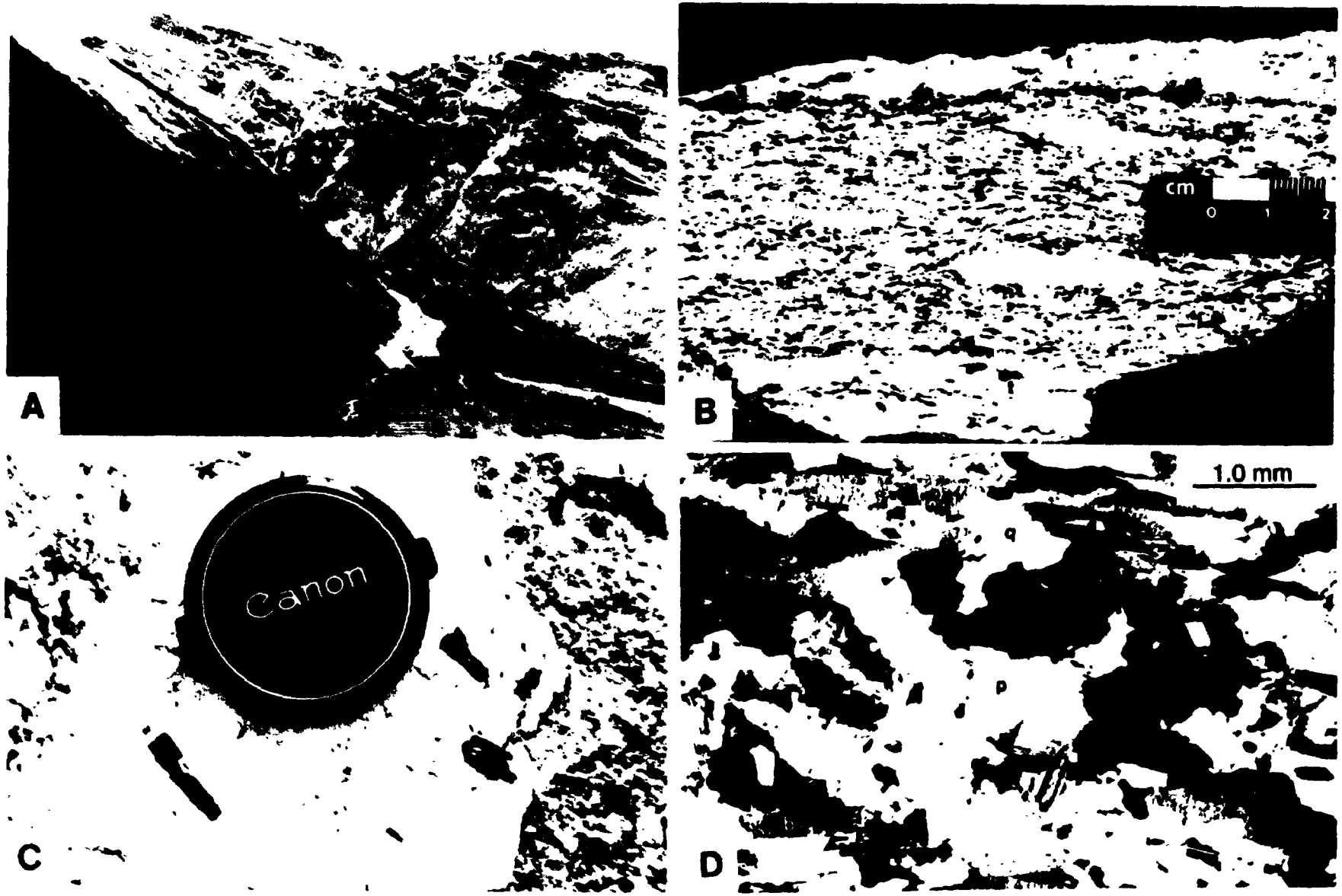
A
B
cm
0
1
2
C
Canon
D
1.0 mm
q
p

Plate 2.2

A) View to the southeast in the footwall of the Annapurna detachment fault. "S"-fold in sheared quartzofeldspathic gneiss indicates top-down-to-the-northeast sense of shear.

B) View to the southeast in the footwall of the Annapurna detachment fault. Granitic dike dips more steeply than the shear plane and has been compressed and folded, indicating top-down-to-the-northeast sense of shear.

C) View to the northwest of C-S fabrics in the footwall of the Annapurna detachment fault. The flattening fabric (S-plane) in leucogranite layers dips less steeply than the shear foliation (C-plane), indicating top-down-to-the-northeast sense of shear.

D) Very planar calcareous psammite from the hanging wall of the Annapurna detachment fault, ~10 m above the brittle contact with the Greater Himalaya. Biotite and muscovite form the foliation; the large porphyroclast is made of quartz.

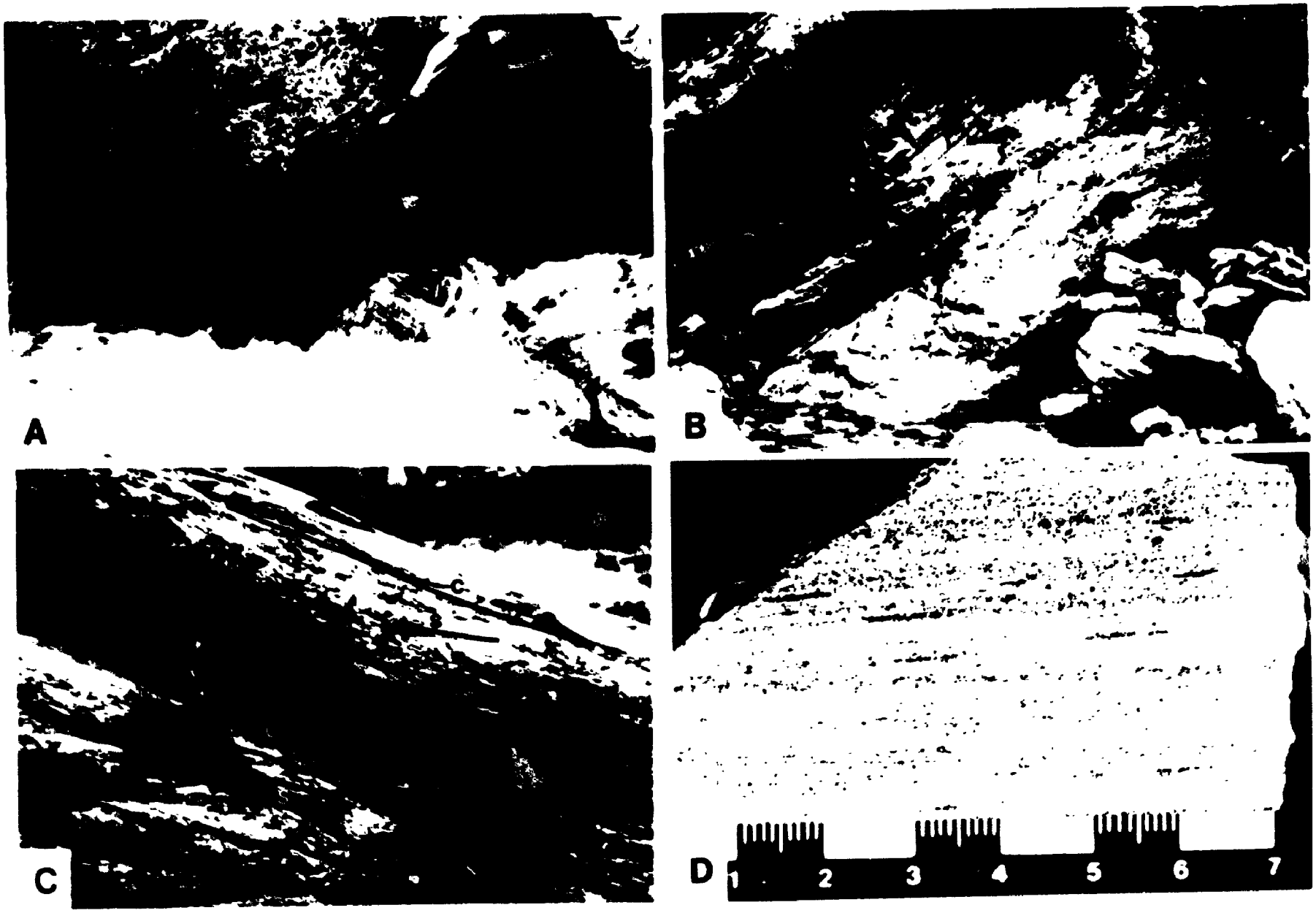
A
B
C
c
D
1
2
3
4
5
6
7

Plate 2.3

A) F_1 isocline outlined by original layering (S_0) in the hanging wall of the Annapurna detachment fault. At this location (south of Larjung), S_0, S_1, and S_2 are all sub-parallel.

B) Looking east from Marpha at a megascopic northeast-verging F_2 fold closure.

C) View to the east of a megascopic F_2 fold closure that is parasitic to the northeast-verging Nilgiri nappe (Jomosom and the Kali Gandaki in the foreground). Photograph shows a lower right-way-up long limb and an upper overturned short limb. The axial plane of this fold is refolded by broad, upright F_4 folds.

D) Decimeter-scale layered sandstone and pelite with a well developed spaced axial-plane cleavage in the core of a northeast-verging F_2 fold (in the vicinity of Marpha).

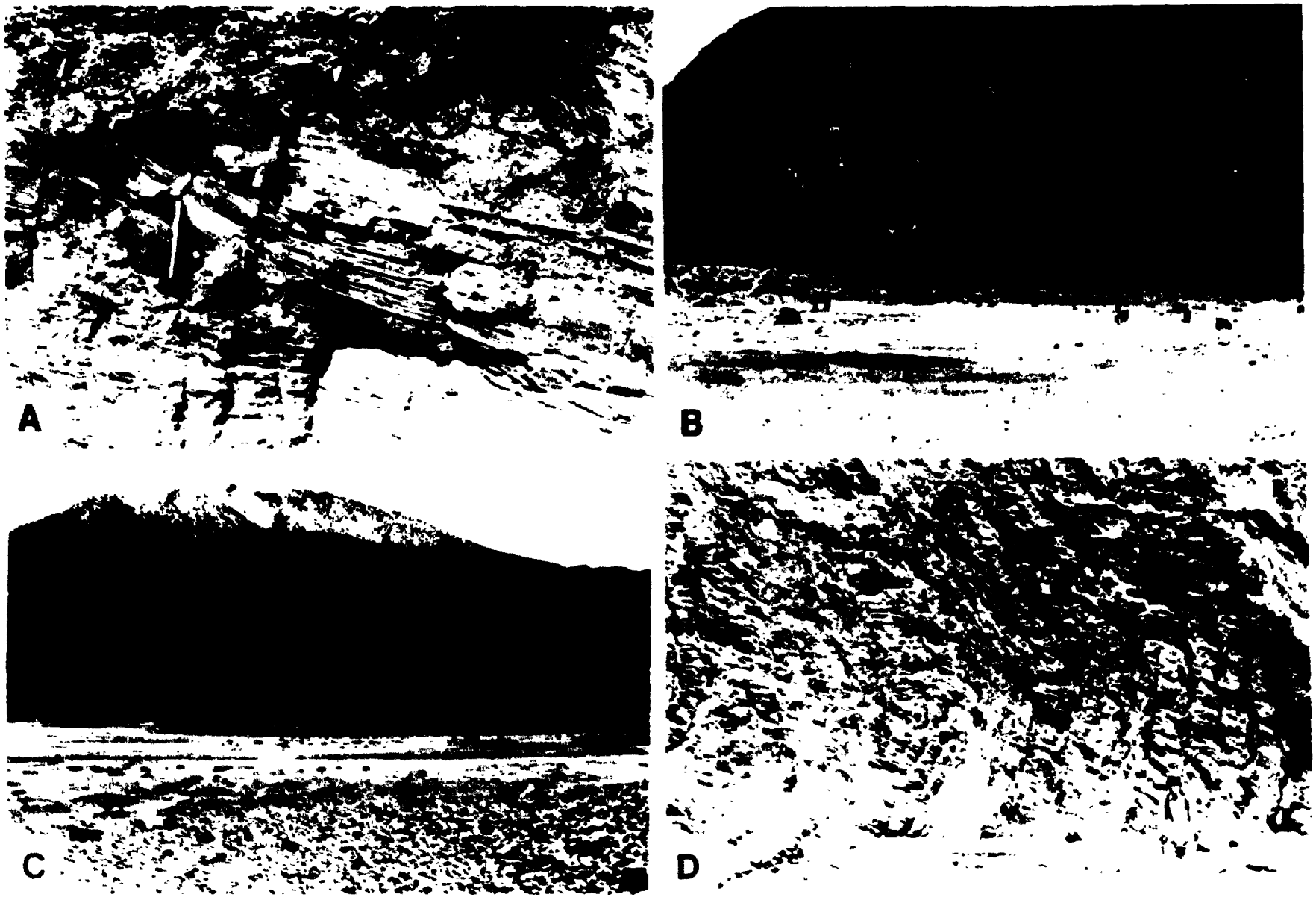
A
B
C
D

Plate 2.4

A) F_3 folds with a shallow northeast dipping axial plane (south of Larjung).

B) View is to the north from Marpha. A strong subhorizontal lineation is outlined by the hinge lines of F_3 folds in sandstone. The enveloping surface defines a southwest dipping overturned limb on a northeast-verging F_2 fold. The triangular white region is a Buddhist temple built into the cliff.

C) Looking east at an overturned limb on a northeast-verging F_2 fold along the east bank of the Kali Gandaki across from Marpha. Photograph shows F1 isoclinal hooks (S_0 + S_1) sub-parallel to S_2 and subsequent refolding by southwest-verging F_3 folds. This photograph is a close-up of the overturned limb on the fold in Plate 2.3b.

D) View to the west of a boudinaged, tourmaline-rich, quartz-plagioclase pegmatite dike in biotite-grade psammite in the hanging wall of the Annapurna detachment fault. The extended dike dips more steeply than the prominent S_2 cleavage and is sub-parallel to the axial planes of F_3 folds, indicating southwest-directed thrusting.

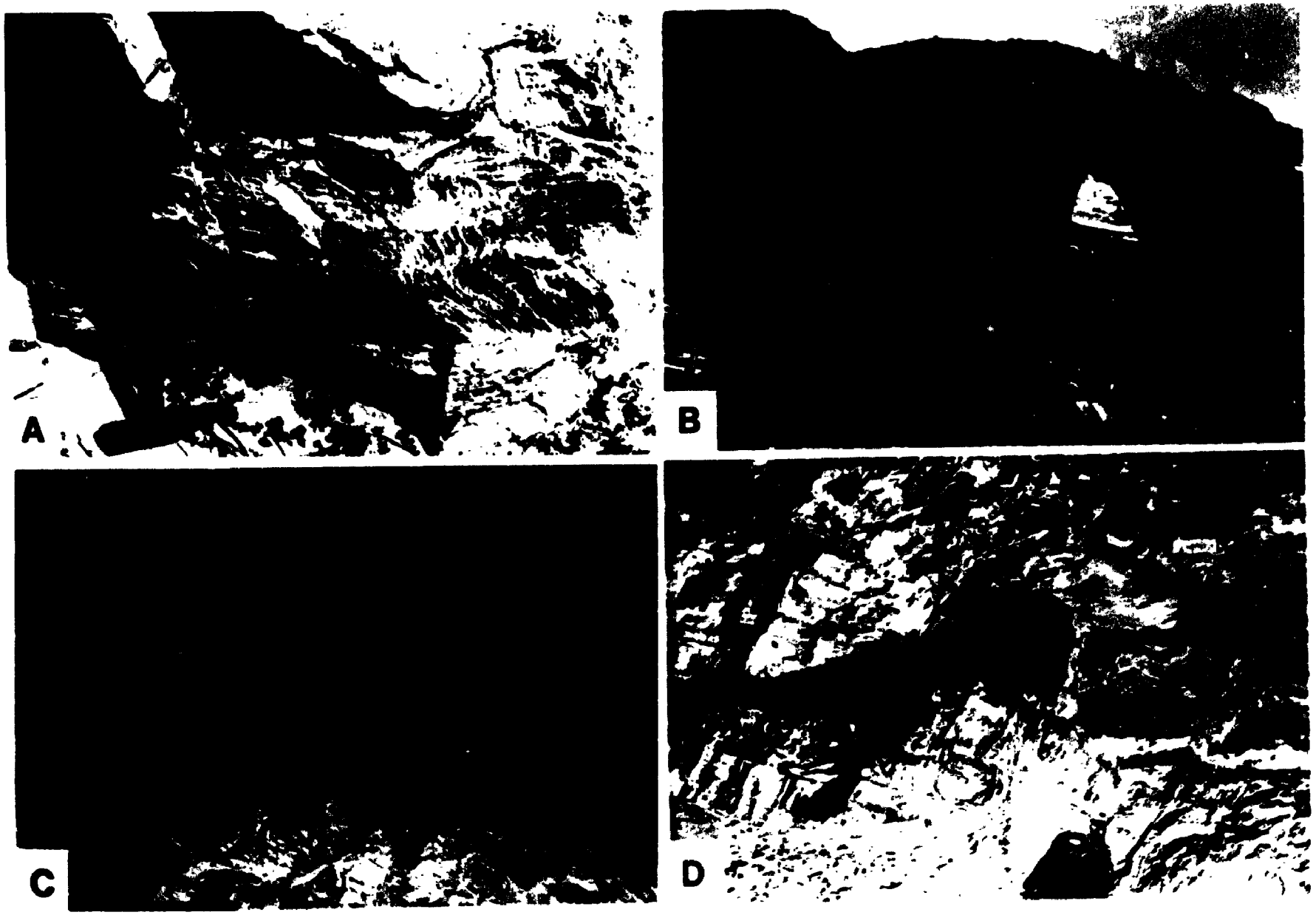
A
B
C
D

Plate 2.5

A) View to the west of upright F_4 folds in the hanging wall of the Annapurna detachment fault (in the vicinity of Tukche).

B) Calcareous schist with blocky, randomly oriented biotite porphyroblasts.

C) Photomicrograph of blocky, randomly oriented muscovite porphyroblasts overprinting the S_2 foliation.

D) Photomicrograph of randomly oriented albite porphyroblasts overprinting the S_2 foliation.

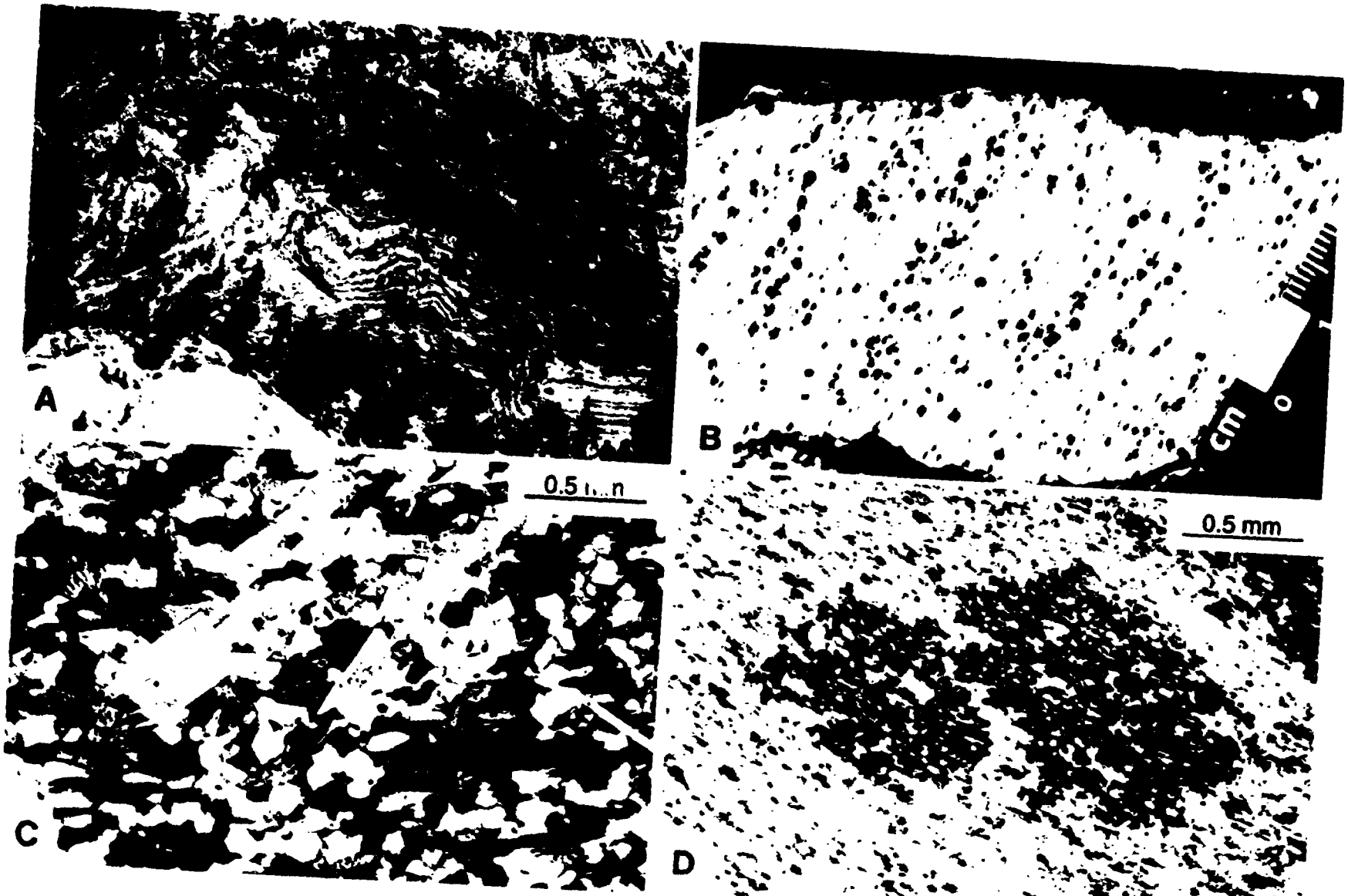
A
B
C
D
0.5 mm
0.5 mm

REFERENCES

Armijo, R., Tapponnier, P., Mercier, J. L. and Han, T., 1986. Quaternary extension in southern Tibet: field observations and tectonic implications. Journal of Geophysical Research, **91(B14)**:13803-13872.

Armstrong, R. L., 1972. Low-angle (denudation) faults, hinterland of the Sevier orogenic belt, eastern Nevada and western Utah. Geological Society of America Bulletin, **83**: 1729-1754.

Barker, A. J., 1990. Introduction to metamorphic textures and microstructures. Chapman and Hall, New York, 161 p.

Bordet, P., Colchen, M., Krummenacher. D., Le Fort, P., Mouterde, R. and Remy, M., 1968. Esquisses geologiques de la Thakkhola (Nepal Central). Editions du Centre National de la Recherche Scientifique, Paris, France, 1/75 000.

Bordet, P., Colchen, M., Krummenacher, D., Le Fort, P., Mouterde, R. and Remy, M., 1971. Recherches geologiques dans L'Himalaya du Nepal, region de la Thakkhola. Editions du Centre National de la Recherche Scientifique, Paris, France, 279 p.

Brown, R. L. and Nazarchuk, J. H., 1993. Annapurna detachment fault in the Greater Himalaya of central Nepal. **In** Himalayan Tectonics. **Edited by** P. J. Treloar and M. P. Searle, Geological Society Special Publication, in press.

Brunel, M. and Kienast, J. R., 1986. Etude petro-structurale des chevauchements ductiles himalayens sur la transversale de l'Everest-Makulu (Nepal oriental). Canadian Journal of Earth Sciences, **23**: 1117-1137.

Burchfiel, B. C. and Royden, L. H., 1985. North-south extension within the convergent Himalayan region. Geology, **13**: 679-682.

Burchfiel, B. C., Chen, Z., Hodges, K. V., Liu, Y., Royden, L. H., Deng, C. and Xu, J., 1992. The south Tibetan detachment system, Himalayan orogen: extension contemporaneous with and parallel to shortening in a collisional mountain belt. Geological Society of America, Special Paper 269, 41 p.

Burg, J. P., Brunel, M., Gapais, D., Chen, G. M. and Liu, G. H., 1984. Deformation of leucogranites of the crystalline Main Central Sheet in southern Tibet (China). Journal of Structural Geology, **6**: 535-542.

Caby, R., Pêcher, A. and Le Fort, P., 1983. Le grand chevauchement central himalayen: nouvelles données sur le métamorphisme inverse à la base de la

Dalle du Tibet. Revue de géologie dynamique et de géographie physique, **24**: 89-100.

Colchen, M., Le Fort, P. and Pecher, A., 1986. Geological researches in the Nepal's Himalaya: Annapurna - Manaslu - Ganesh Himal. Editions du Centre National de la Recherche Scientifique, Paris, France, 136 p., 1 geologic map, 1:200,000 scale.

Coney, P. J., 1980. Cordilleran metamorphic core complexes: An overview. **In** Cordilleran metamorphic core complexes. **Edited by** M. D. Crittenden, Geological Society of America, Memoir 153, p. 7-31.

Dalmayrac, B. and Molnar, P., 1981. Parallel thrust and normal faulting in Peru and constraints on the state of stress. Earth and Planetary Science Letters, **55**: 473-481.

Gansser, A., 1964. Geology of the Himalayas. Interscience Publishers, London, England, 289 p.

Gradstein, F. M., von Rad, U., Gibling, M. R., Jansa, L. F., Kaminski, M. A., Kristiansen, I. L., Ogg, J. G., Rohl, U., Sarti, M., Thurow, J. W., Westerman, G. E. G. and Weidmann, J., 1992. Stratigraphy and depositional history of the Mesozoic continental margin of central Nepal. Geologisches Jahrbuch, Bundesanstalt fur Geowissenschaften und Rohstoffe, Reihe B, Heft 77, 140 p.

Herren, E., 1987. Zanskar shear zone: northeast-southwest extension within the Higher Himalayas (Ladakh, India). Geology, **15**: 409-413.

Hodges, K. V., and Silverberg, D. S., 1988. Thermal evolution of the Greater Himalaya, Garhwal, India. Tectonics, **7**: 583-600.

Hodges, K. V., Hubbard, M. S. and Silverberg, D. S., 1988. Metamorphic constraints on the thermal evolution of the central Himalayan Orogen. Philosophical Transactions of the Royal Society of London, **A326**: 257-280.

Hyndman, D. W., 1985. Petrology of igneous and metamorphic rocks, second edition. McGraw-Hill, 767 p.

Le Fort, P., 1975. Himalayas: the collided range. Present knowledge of the continental arc. American Journal of Science, **275-A**: 1-44.

Molnar, P., 1984. Structure and tectonics of the Himalaya: constraints and implications of geophysical data. Annual Review of Earth and Planetary

Science, 12: 489-518.

Molnar, P. and Tapponnier, P., 1975. Cenozoic tectonics of Asia: Effects of a continental collision. Science, 189: 419-426.

Molnar, P. and Tapponnier, P., 1978. Active tectonics of Tibet. Journal of Geophysical Research, 83: 5361-5375.

Searle, M. P., 1986. Structural evolution and sequence of thrusting in the High Himalayan, Tibetan-Tethys and Indus suture zones of Zanskar and Ladakh, Western Himalaya. Journal of Structural Geology, 8: 923-936.

Swapp, S. M. and Hollister, L. S., 1991. Inverted metamorphism within the Tibetan Slab of Bhutan: Evidence for a tectonically transported heat source. Canadian Mineralogist, 29: 1019-1041.

CHAPTER 3

GEOLOGY, U-Pb AGE CONSTRAINTS AND TECTONIC HISTORY OF THE KALI GANDAKI REGION, ANNAPURNA HIMAL, WEST CENTRAL NEPAL

ABSTRACT

The Main Central Thrust (MCT) is a crustal-scale, ductile-brittle shear zone that spans the contact between the Greater Himalayan metamorphic sequence (Greater Himalaya) and Lesser Himalayan sedimentary sequence (Lesser Himalaya). The MCT and Greater Himalaya have been studied in detail along the Kali Gandaki and Ghaleti Khola. Two intrusive rocks from the Greater Himalaya have been dated using the U-Pb system.

In the Kali Gandaki region, the Greater Himalaya is approximately 6 km thick and consists of three lithotectonic units: 1) kyanite-grade quartzo-feldspathic and pelitic gneiss in the lowest structural level (Formation I); 2) garnet-diopside-bearing calc-silicate gneiss in the middle portion (Formation II); and 3) garnet-tourmaline-bearing two-mica leucogranite and quartzo-feldspathic migmatite in the highest structural level (Formation III). Beneath the Greater Himalaya, the Lesser Himalayan is at biotite grade and consists of quartzite and pelitic and calcareous schist and phyllite. The Greater Himalaya is separated from the overlying Tibetan sedimentary sequence by the Annapurna detachment fault.

In the portion of the MCT shear zone that contains the Greater Himalaya, three phases of ductile deformation are recognized. First-phase (D_1) structures include layer-parallel isoclinal folds outlined by compositional layering and a foliation (S_1) preserved as inclusion trails in garnet. Second-phase (D_2) structures are the product of southwest-directed progressive deformation that occurred at kyanite-grade conditions and consist of a pervasive foliation (S_2), a down-dip stretching lineation, tight to isoclinal folds and shearing fabrics, all of which have been subsequently deformed by southwest-verging folds and crenulations. Third-phase (D_3) structures locally form chlorite-grade mylonite shears near the base of the Greater Himalaya. In the Lesser Himalaya four ductile deformation events, with characteristics similar to those in the Greater Himalaya, are overprinted by a fifth phase of brittle deformation. Two phases of ductile deformation and one phase of brittle deformation related to movement on the MCT are recognized.

The effects of ductile shearing on the MCT are most pronounced in Formation I of the Greater Himalaya where the dominant fabric is very planar, gneisses are medium-grained, and the hinge lines of D_1 and D_2 folds are oriented parallel to down-dip stretching lineations. Associated with ductile shearing is a strain gradient. This is demonstrated by the rotation of D_1 and D_2 hinge lines from a down dip orientation near the base of Formation I to subhorizontal near the top. There is also an upwards coarsening of gneisses, fabrics are less planar, and the angle between S_1 and S_2

increases. Abundant top-to-the-southwest shear sense indicators related to movement on the MCT are observed, but well developed mylonites either did not form or are obscured by the extensive kyanite-grade static recrystallization.

Single- and multi-grain fractions of monazite and thorite from two samples have been dated. An undeformed, coarse-grained pegmatite that crosscuts S_2 in the high strain portion of the MCT shear zone has an interpreted crystallization age of 21.8 ± 0.5 Ma. Above the high strain zone, a deformed leucogranite body in the calc-silicate gneiss unit that exhibits interference patterns between D_1 and D_2 folds and contains the S_2 foliation has an interpreted minimum crystallization age of 22.5 ± 0.1 Ma.

The new structural and U-Pb data indicate that the prominent fabric and structures preserved in the Kali Gandaki region formed during the first phase of ductile deformation along the MCT, which perhaps began after 22.5 ± 0.1 Ma and had ceased by 21.8 ± 0.5 Ma. Following static recrystallization at middle crustal levels, the Greater Himalaya was rapidly uplifted and tectonically denuded by the Annapurna detachment fault. The exhumed MCT was reactivated at upper crustal levels generating brittle fabrics of uncertain age.

INTRODUCTION

In central Nepal and throughout most of the Himalaya, the metamorphic core of the Himalayan orogen (i.e., the Greater Himalayan metamorphic sequence) is a laterally continuous belt of kyanite- to sillimanite-grade gneisses and syntectonic leucogranites. These rocks underwent intense ductile shearing and metamorphism during southwestward displacement on the Main Central Thrust (MCT), which in part occurred simultaneously with northeast-directed normal faulting resulting in exhumation during the Miocene (Hodges et al., 1988; Burchfiel et al., 1992). Although there have been many regional-scale mapping projects, as well as studies focusing on the petrological evolution and geochemical nature of the Greater Himalaya, very few detailed structural studies integrated with precise geochronometry have been done to place tight age constraints on the high-grade ductile deformation associated with the MCT.

Field mapping in the spring of 1991 along the Kali Gandaki and its subsidiary drainages formed a transect through the Lesser Himalayan sedimentary sequence, Greater Himalayan metamorphic sequence and Tibetan sedimentary sequence (Figs. 3.1 & 3.2; the Lesser Himalayan sedimentary sequence and Greater Himalayan metamorphic sequence will be referred to as the Lesser and Greater Himalaya, respectively, from here on). The main objectives of this work were to cross the MCT and gain an understanding of its structural and metamorphic history, locate and sample outcrops that had rock types suitable for U-Pb geochronology as well as clear structural relationships, and investigate the contact between the Greater Himalaya and

the Tibetan sedimentary sequence with knowledge that elsewhere this contact is an extensional normal fault.

This paper will: 1) document the detailed geology of the Greater Himalaya and MCT in the Kali Gandaki region; 2) bracket the age of the dominant phase of ductile deformation and metamorphism associated with shearing on the MCT using U-Pb geochronology; and 3) provide a tectonic model for the Kali Gandaki region based on the field relations and timing constraints.

TECTONIC SETTING

The present day configuration of the Himalayan orogen is a direct result of the collision between India and Eurasia. Although not tightly constrained, several indirect lines of evidence suggest that continental collision between India and Eurasia probably began in the Eocene: Marine sedimentation in the northern Himalaya terminated in the Eocene (Gansser, 1964). Fossils of large terrestrial animals common to Asia are found in India after the beginning of the Middle Eocene, implying a land bridge at that time (Sahni and Kumar, 1974). Between 50 and 40 Ma (Middle to Late Eocene) the convergence rate of India and Eurasia slowed from ~100-180 to ~50 mm/yr, suggesting that collision had affected relative plate motions (Molnar and Tapponnier, 1975). The Transhimalayan batholith, interpreted as a continental magmatic arc that formed during subduction of the Tethys Ocean, ranges in age from from 101 to 41 Ma; therefore, collision must have been post Middle to Late Eocene (Scharer et al., 1984).

In response to convergence between India and Eurasia, the Indian shield was initially thrust under and subducted beneath Asia. This was followed by thickening and shortening of the Indian shield by crustal-scale intracontinental subduction and deformation on the Main Central and Main Boundary thrusts, ultimately forming the Himalayan mountain chain (Fig. 3.3) (Molnar, 1984; Mattauer, 1986). Just north of the Himalaya lies the uniformly elevated Tibetan plateau with an average elevation of ~5 km. Between 1000 and 2000 km north of the Himalaya, Tertiary to present-day deformation is also related to the Indian-Eurasian continental collision (Molnar and Tapponnier, 1975). In addition, geophysical evidence indicates that the Indian-Eurasian collision has caused a near doubling in the thickness of continental crust; the Moho is located at ~38 km under stable Indian craton, ~55 km under the Himalaya and on average at ~70 km under the Tibetan plateau (Chen and Molnar, 1981; Molnar, 1988).

The exact amount of shortening that the northern margin of India has undergone since collision is not well constrained. From the displacement on major thrust faults and from a calculated shortening using the width of the deformation zone and the interpreted thickness of the crust, a minimum of 300 km of shortening must have taken place (Molnar and Tapponnier, 1975). Paleomagnetic data indicate 300-500 km of crustal shortening (Besse et al., 1984). In addition, during the initial collision it is likely that 100-200 km of Indian crust was subducted beneath Tibet (Molnar and Tapponnier, 1975), making the total shortening ~700 km. Although the present-day convergence rate between India and Eurasia is ~50 mm/yr (Minster and Jordan, 1978), a wide zone of distributed deformation extending well into Asia suggests that not all

of the convergence is taken up in the Himalaya (Molnar and Tapponnier, 1975). On the basis of thrust displacement, shortening rates in the Himalayan are believed to have been and presently still are, ~10-20 mm/yr (Molnar, 1984).

The Himalayan mountain chain from the Indus River in Pakistan to the Brahmaputra River east of Bhutan extends for a length of over 2500 km, is between 200 and 250 km wide (Le Fort, 1975), and has the highest summits and the deepest valleys on earth (14 peaks are over 8000 m; the Kali Gandaki and Karnali River gorges are ~6 km deep). The orogen can be divided into five main subdivisions (Fig. 3.4) (Gansser, 1964; Molnar, 1984). From north to south they are: 1) the Transhimalayan batholith; 2) the Indus-Tsangpo suture zone; 3) the Tibetan sedimentary sequence; 4) the Greater Himalayan metamorphic sequence; 5) the Lesser Himalayan sedimentary sequence; and 6) the Sub-Himalaya. (See figure caption 3.4 for other commonly used names).

The Transhimalaya, as mentioned previously, is a laterally continuous chain of mid-Cretaceous to Eocene batholiths (Honegger et al., 1982; Scharer et al., 1984). The Indus-Tsangpo suture zone, just south of the Transhimalaya, is a discontinuous belt of ophiolites and arc volcanic rocks that marks the collision zone between the Indian and Eurasian continents (Gansser, 1964 & 1980; Honegger et al., 1982); south of the Indus-Tsangpo suture zone virtually all of the rocks belong to India or its continental margin (Molnar, 1984). The Tibetan sedimentary sequence is ~11 km thick and consists of passive-margin sedimentary rocks that are nearly continuous from the Cambro?-Ordovician to Eocene (Gansser, 1964; Bordet et al., 1968 & 1971; Le Fort,

1975; Colchen et al., 1986). Combined paleolatitude analysis, paleontology and sedimentology indicate that Early Cretaceous strata of the Tibetan sedimentary sequence in the Thakkhola region of Nepal were deposited on the south side of the Tethys Ocean on the northern margin of Gondwana and are correlative with rocks on the Exmouth-Wombat Plateaus off of northwest Australia (Gradstein et al., 1992).

The Greater Himalaya forms the high-grade metamorphic core of the orogen and probably represents a sliver of the Indian craton that has been displaced by the MCT and now overlies the Lesser Himalaya (Fig. 3.5) (Gansser, 1964; Molnar and Tapponnier, 1975; Molnar, 1984). In eastern Nepal, structural projection of klippen that lie south of the Greater Himalaya indicate that the cumulative displacement on the MCT is at least 140 km and possibly as much as 210 km (Fig. 3.5) (Schelling, 1992). The Greater Himalaya was originally believed to be the metamorphic basement on which the Tibetan sedimentary sequence was unconformably deposited (Gansser, 1964). In many places the contact between the Greater Himalaya and the Tibetan sedimentary sequence is now recognized as a normal fault (Burchfiel et al., 1992 and references therein; Brown and Nazarchuk, 1993; Chapter 2).

Crystalline rocks of the Greater Himalaya also occur as klippen in the hanging wall of the MCT within the physiographic Lesser Himalaya. The Lesser Himalaya consists of ~20 km of siliciclastic, carbonate and volcanogenic sedimentary rocks that are generally weakly metamorphosed, but locally attain kyanite grade in the footwall of the MCT (Le Fort, 1975; Stocklin, 1980; Colchen et al., 1986). Due to poor exposure, sparse fossil control and a general lack of understanding of the Lesser

Himalaya, it is unclear if the apparent thickness is related to structural duplication (Stocklin, 1980). The fossils documented in the Lesser Himalaya indicate a predominance of Precambrian-Paleozoic and Permo-Carboniferous ages, minor Mesozoic-Tertiary ages and a large gap of mid-Paleozoic ages (Stocklin, 1980 and references therein). The Sub-Himalaya consists of Middle Miocene to Pleistocene Siwalik molasse, which was derived by erosion of the Himalaya (Gansser, 1964). The Lesser Himalaya is separated from the underlying Sub-Himalaya by the Main Boundary Thrust, which probably has more than 100 km of displacement (Molnar, 1984).

TECTONIC BOUNDARIES AND ROCK TYPES IN THE KALI GANDAKI REGION

In the study area (Figs. 3.1 & 3.2) the two main tectonic boundaries are the MCT and the newly recognized Annapurna detachment fault (Brown and Nazarchuk, 1993; see also Chapter 2). The MCT is a crustal scale, ductile-brittle shear zone that spans the contact between the Greater Himalayan metamorphic sequence and the underlying Lesser Himalayan sedimentary sequence (Figs. 3.6, 3.7 & 3.8). The Annapurna detachment fault is a normal-sense ductile-brittle shear zone that separates the Greater Himalaya from the overlying Tibetan sedimentary sequence (Figs. 3.6 & 3.7). The MCT and Annapurna detachment fault have been studied in detail along the Kali Gandaki and Ghaleti Khola near Dana and in a drainage west of Dhumpu, respectively. The nature of these contacts and the rock types within the three bounding

tectonostratigraphic packages are discussed here.

The Main Central Thrust

The MCT is usually referred to as a distinct fault and is represented as a line on a map separating the Lesser Himalaya from the overlying Greater Himalaya. In some regions, such as along the Kali Gandaki, this is roughly valid as there is a lithologic and metamorphic break between the Midland formations of the Lesser Himalaya and Formation I of the Greater Himalaya. In other areas though, such as along the Marsyandi, a metamorphic break does not correspond with the lithologic break between the Lesser Himalaya and the Greater Himalaya (Colchen et al., 1986). Also, imbricate zones of kyanite-bearing gneiss may be intercalated with biotite-grade phyllites and schists (i.e., near Dana; this study, Fig. 3.2), further complicating the location of the MCT. Due to the variable nature of this contact the MCT is best described as a shear zone, defined not only by lithology and metamorphic grade, but by structure and fabric as well (Pecher, 1977). In the Kali Gandaki region (Figs. 3.1 & 3.2) the MCT shear zone spans the Lesser Himalaya-Greater Himalaya contact and is delimited by: 1) the metamorphic and lithologic break between biotite-grade quartzites and pelitic rocks of the Lesser Himalaya and kyanite-grade quartzo-feldspathic and pelitic gneisses of the Greater Himalaya; 2) a zone of intense ductile deformation and fabric reorientation which extends approximately 1.5 km up into the Greater Himalaya and about the same distance down into the Midland formations of the Lesser Himalaya; and 3) minor chlorite-grade mylonitic shears in the Greater Himalaya and

brittle fabrics superimposed on ductile fabrics in the Lesser Himalaya. The details of the MCT are presented and discussed later in the text.

The Annapurna detachment fault

The contact between the Greater Himalaya and the Tibetan sedimentary sequence was originally believed to correspond to a metamorphic and structural transition between superstructure and infrastructure, with no discordance, requiring the Greater Himalaya to be Precambrian basement to the Tibetan sedimentary sequence (Gansser, 1964; Le Fort, 1975). The contact was later interpreted as a highly recrystallized zone of ductile deformation that formed when the Tibetan sedimentary sequence detached from the underlying Greater Himalaya in response to gravity sliding and formation of the Nilgiri nappe (Caby et al., 1983; Colchen et al., 1986). The contact is now recognized as the Annapurna detachment fault, a segment of the South Tibetan detachment system (Burchfiel et al., 1992). (A full description of the Annapurna detachment fault can be found in Chapter 2 and Brown and Nazarchuk, 1993).

The Lesser Himalayan sedimentary sequence

In the region between the Modi Khola and the Burhi Gandaki (Fig. 3.1), the Lesser Himalaya has been folded in the Pokhara-Kunchha-Gurkha anticlinorium (Pecher, 1977). The northern limb of the anticlinorium is composed of the Upper Midland formations (Hashimoto et al., 1973; Arita, 1983; Le Fort, 1975; Colchen et

al., 1986), which are found beneath and within the MCT shear zone in the Kali Gandaki region (Figs. 3.7 & 3.8).

South of the Modi Khola (Fig. 3.1), exposures are limited to large erosional slumps and isolated trail or stream cuts. Observed in this area are outcrops of chlorite-grade phyllite, quartzite with preserved trough cross-beds indicating right way up, the Ulleri augen gneiss (Pecher and Le Fort, 1977) and minor gabbroic intrusions.

Near Dana, in the Kali Gandaki gorge, exposure is good and rock types include clean quartzite (Plate 3.1a), quartz-rich micaceous carbonate, dolomitic carbonate (Plate 3.1b) and pelitic phyllite and schist (Table 3.1). The distribution of units on the map by Colchen et al. (1986) appears to be quite accurate in places, but the location of the lithologic break between the Lesser Himalaya and Greater Himalaya east of the Kali Gandaki has been modified slightly (Map 1). Also, in this study, the composition of both the Singla quartzite (Sq) and the Barpak-Benignat schists (BB) (Map 1) are much more carbonate rich than described by Colchen et al. (1986).

The Greater Himalayan metamorphic sequence

In the Kali Gandaki valley, the Greater Himalaya is approximately 6 km thick and is divided into three lithologic packages: Formation I (1.5 km thick), Formation II (3.5 km thick) and Formation III (1.0 km thick) (Le Fort, 1975; Colchen et al., 1986) (Fig. 3.7). Formation I contains kyanite-garnet-bearing quartzo-feldspathic and pelitic paragneiss that becomes coarse grained and migmatitic up section (Table 3.1). The migmatitic layers are formed by mm- to cm-scale quartz-feldspar sweats (Plate 3.1c)

and transposition of cm- to dm-scale granitic leucosome (Plate 3.1d; Fig. 3.9). The gross cm-to m-scale gneissic banding is formed by quartzo-feldspathic and pelitic layers, which probably represents the intercalation of originally arenaceous and argillaceous sedimentary beds (Plate 3.1d; Fig. 3.9).

The appearance of thick marbles and increasingly more carbonate-rich rocks marks the gradation into Formation II (Fig. 3.7). Formation II is a diopside-garnet-amphibole-bearing calc-silicate gneiss package with typically planar mm- to cm-scale light green layers (Table 3.1) (Plate 3.2a). Near the top of the unit, very coarse grained (cm-scale) migmatitic layers are abundant, and pods of insitu anatectic melt become apparent (Plate 3.2b). The top-most portion also contains small multiply deformed leucogranite bodies.

Formation III (Fig. 3.7) is marked by the gradation from dominantly calc-silicate gneiss into highly migmatitic quartzo-feldspathic and calc-silicate gneiss with discordant lenses of variably strained and foliated garnet-tourmaline-bearing two-mica leucogranite (Table 3.1). At high elevations Formation III generally forms steep inaccessible cliffs such as in the upper reaches of the Ghaleti Khola, but lower down in the Kali Gandaki it is poorly exposed. Where observed in the Kali Gandaki region, Formation III appears to differ from descriptions and photographs (Colchen et al., 1986; Le Fort, 1975) of the same unit in the Marsyandi and Burhi Gandaki regions; it is lacking the very coarse grained and homogeneous augen gneisses. These coarse augen gneisses may represent the sheared equivalent of a more porphyritic phase of leucogranite or a lateral variation in the protolith of Formation III.

The Tibetan sedimentary sequence

In the vicinity of Larjung (Fig. 3.2), the lowest portion of the Tibetan sedimentary sequence that is preserved is the Cambro?-Ordovician (Colchen et al. 1986) Annapurna Formation; it is separated from the underlying Formation III by the Annapurna detachment fault (Fig. 3.7). The Annapurna Formation is typically yellow weathering and is composed of biotite-grade psammitic and semi-pelitic schists and phyllites, all of which contain a large component of carbonate (Table 3.1) (see Chapter 2 for a full description of the Tibetan sedimentary sequence).

STRUCTURE AND METAMORPHISM

In this section are presented the structural and metamorphic relationships observed within the MCT shear zone, and in the portion of the Greater Himalaya that lies above the MCT and is truncated by the Annapurna detachment fault. The structures (F_{1-n}), surfaces (S_{1-n}) and metamorphic events (M_{1-n}) are assigned to deformation events (D_{1-n}) throughout the text and are summarized in Table 3.2. Additional subscripts, ($_{LH}$), ($_{GH}$) and ($_{MCT}$) refer to the Lesser Himalaya, Greater Himalaya and MCT specifically. No correlation of events is implied here as this will be discussed later in the text.

The Main Central Thrust shear zone

The MCT shear zone spans the contact between the Lesser Himalaya and the Greater Himalaya; therefore, both units have structures that are genetically related

(Fig. 3.8), but since the Lesser Himalaya and the Greater Himalaya have differing lithology and metamorphic histories, they are described separately.

In the Lesser Himalaya five phases of deformation have been identified (Table 3.2). In less competent layers such as dolomite or calcareous rocks the deformation is most intense and best preserved resulting in complex interference patterns. In competent quartz-rich rocks only a single planar fabric may be present.

In carbonate-rich and pelitic rocks D_{1LH} is represented by isoclinal fold closures in compositional layering (F_{1LH}) and by the remnants of an S_{1LH} muscovite foliation that has been almost completely transposed into the S_{2LH} foliation (Plate 3.2c). D_{2LH} is defined by the prominent S_{2LH} layer-parallel biotite-muscovite foliation that dips 46° to the northeast (Fig. 3.10), a well developed down-dip stretching lineation (Fig. 3.11), sheath folds and steeply dipping hinge lines. D_{3LH} consists of isolated north-verging folds and crenulations (F_{3LH}) formed in the S_{2LH} foliation with no new cleavage developed. The S_{2LH} foliation and F_{3LH} folds have been overprinted by D_{4LH} southwest-verging folds (F_{4LH}) and an associated S_{4LH} biotite crenulation cleavage that dips in the same direction as, but slightly steeper than $S_{0+1+2LH}$ (Plates 3.2d and 3.1b).

In quartzite, the prominent S_{2LH} fabric is generally parallel to the S_{1LH} foliation, although at some localities a top-to-the-southwest C-S fabric is defined by the preferred orientation of quartz and S_{2LH} biotite dipping more steeply than S_{0+1LH} (Plates 3.3a and 3.1a). Although all rock types are highly recrystallized, evidence for relict mylonitic shearing is seen in thin section as zones of more finely grained quartz relative to the surrounding matrix. Southwest-verging F_{2LH} folds have also developed

(Fig. 3.8). D_{3LH} and D_{4LH} folds, crenulations and cleavage are not observed in quartzites. D_{5LH} is a brittle event represented by shattered quartzites, extensive calcite veining in carbonate-rich rocks and rigid-body back rotation of cm-scale lithons in pelite that indicate top-to-the-southwest thrusting (Fig. 3.8).

Three metamorphic events have occurred in the Lesser Himalaya (Table 3.2). M_{1LH} occurred during D_{1LH} and forms the S_{1LH} foliation that is preserved as rare crenulation hinges (Plate 3.2c). M_{1LH} has been overprinted by M_{2LH}, which occurred during D_{2LH} and forms the prominent S_{2LH} foliation. From Pokhara to Dana (Fig. 3.1) the grade of the M_{2LH} event increases up-section structurally from chlorite grade through to the biotite isograd and locally attains garnet grade within the MCT shear zone; near Dana, grossular garnets were observed in micaceous carbonates only. In the study area, all rock types contain the M_{2LH} muscovite +/- biotite foliation. M_{2LH} is the peak metamorphic mineral assemblage and has no indication of metamorphic retrogression. M_{3LH} occurred during D_{4LH} to form the S_{4LH} biotite foliation that overprints all other fabrics. Quartz and calcite are highly recrystallized indicating that metamorphism outlasted ductile deformation.

Within the portion of the Greater Himalaya that is incorporated in the MCT shear zone, three phases of deformation are recognized (Table 3.2). D_{1GH} is defined by isoclinal fold closures in compositional layering (F_{1GH}) (Plate 3.3b) and a transposed layer-parallel biotite-muscovite foliation (S_{1GH}) (Fig. 3.9). S_{1GH} is also preserved as inclusion trails in syn- to post-D_{1GH} garnets (Plate 3.3c). The structures defining the second event are subdivided into D_{2aGH} and D_{2bGH} (Table 3.2). D_{2aGH} is defined by a

very planar biotite-muscovite foliation (S_{2GH}) (Fig. 3.8) dipping 38° to the northeast (Fig. 3.12), a well defined but poorly preserved down-dip stretching and kyanite mineral lineation (Fig. 3.11) and ductile folds and crenulations (F_{2GH}) to which S_{2GH} is axial planar (Plate 3.3d; Fig. 3.8). The orientations of S_{2GH} and the stretching lineation is a pervasive feature of the Greater Himalaya in central Nepal that has been documented by other workers (Pecher, 1977; Colchen et al., 1986; Macfarlane et al., 1992). D_{2bGH} is prominent near the base of Formation I and is represented by southwest-verging folds and crenulations with variably plunging hinge lines that have formed in the prominent $S_{0+1+2GH}$ foliation and by migmatitic layering (Plates 3.3d and 3.4b). The axial planes of F_{2bGH} crenulations are often subhorizontal with S_{2GH}.

Associated with D_{2GH} is a strain gradient (Fig. 3.13). Typically, in the highest strain zones near the base of Formation I, the following fabric relations are observed: all surfaces are very planar and parallel (Plate 3.1d); F_{1GH} and F_{2GH} hinge lines are parallel to the stretching lineation (Figs. 3.9 & 3.13); sheath folds have developed (Plate 3.1c) (excellent photograph of sheath folds in Colchen et al., 1986); gneisses are medium-grained (Plate 3.4a); and in thin section all fabrics are annealed, although some layers are more finely grained than the surrounding material suggesting that dynamic recrystallization and grain size reduction had occurred (i.e., relict mylonite). Structurally above the planar gneisses, the following fabric relations are observed: D_{2bGH} forms a strong crenulation in S_{2GH} (Plate 3.4b), as well as meso- to megascopic folds inferred from dip reversals in S_{2GH} (Map 1); F_{2GH} hinge lines and S_1-S_2 intersection lineations are subhorizontal (Map 1); and above, gneisses are coarse

grained, planar and more migmatitic (Plate 3.4c). This strain gradient and rotation of S_2 hinge lines has also been documented by Pecher (1977). The top of the MCT shear zone is marked by more migmatitic gneisses, where the dominant fabric is composed of S_{1GH} and S_{2GH}, which are roughly subparallel but occasionally form an intersection lineation.

Within the MCT shear zone, kinematic indicators such as C-S fabric, asymmetric folds, pressure shadows around garnet, and extended or compressed leucosome all indicate top-to-the-southwest thrusting (Plates 3.4d and 3.5a). Although the base of the Greater Himalaya has been highly strained in the MCT shear zone, as evidenced by the very planar structure, ductile shearing fabrics and apparent reduction in grain size, there is a conspicuous lack of mylonitic textures in outcrop and thin section due to extensive post-D_{2GH} static annealing.

The third deformation event in the MCT shear zone (D_{4GH} for the Greater Himalaya as a whole; Table 3.2) is localized at the base of the Greater Himalaya and is represented by folds in the S_{2GH} foliation, sparse chlorite-grade mylonites and C-S fabrics indicating top-to-the-southwest thrusting (Plate 3.5b; Fig. 3.8). Chlorite-grade mylonitization is not extensive, and thin layers (mm- to cm-scale) of quartz and feldspar that have undergone grain size reduction due to dynamic recrystallization are surrounded by recrystallized D_{2GH} fabrics. Higher in Formation I, e-lamellae and wavy extinction in previously recrystallized quartz are observed (Plate 3.5c).

Formation I in the MCT shear zone has undergone three metamorphic events. The first metamorphic event (M_{1GH}) occurred prior to D_{2GH} ductile shearing (Table 3.2)

and produced kyanite?, garnet and the S_{1GH} biotite-muscovite foliation. It is unclear if kyanite grew during this event as it is not observed wrapping around the hinges of F_{1GH} folds. M_{1GH} garnets are up to 10 mm across, are ductilely deformed (Plate 3.5d) and highly fractured, have inclusion-rich cores and were probably syn- to post-D_{1GH} as evidenced by straight and sigmoidal inclusion trails outlined by opaques (Plate 3.3c). The outer rims of M_{1GH} garnets are usually inclusion free.

The second metamorphic event (M_{2GH}) occurred synchronously with, but outlasted, D_{2GH} shearing on the MCT (Table 3.2) to produce syn- to post-D_{2GH} kyanite and garnet, as well as the S_{2GH} biotite-muscovite foliation which wraps M_{1GH} garnets. Some samples near the base of Formation I contain syn-kinematic staurolite, epidote and zoisite. M_{2GH} kyanite is oriented parallel to the stretching lineation within the strong S_{2GH} foliation near the base of Formation I and is folded or broken by D_{2bGH} folds and crenulations near the top of the MCT shear zone (Plate 3.4b). M_{2GH} kyanite is also observed in quartzo-feldspathic sweats where it is cm-scale in length and are either oriented or random; the kyanite commonly exhibits undulose extinction, and has pull-aparts filled with white mica (Plate 3.6a). M_{2GH} garnets are mm-scale in size, euhedral with few or no inclusions, and relatively pristine with few fractures (Plate 3.6b). Other evidence for metamorphism outlasting deformation also exists: muscovite occurs as a coarse blocky overprint (Plate 3.6c) and Formation I has a strongly annealed texture. The M_{2GH} metamorphic mineral assemblage in Formation I paragneisses (Table 3.1) and the presence of anatectic melt are typical of middle amphibolite facies metamorphism with pressure and temperature ranges of about 6-8

kbar and 600-670°C, respectively (Barker, 1990). M_{3GH} occurred during the formation of D_{4GH} mylonites and has locally overprinted the S_{2GH} biotite foliation with chlorite (Plate 3.5b) and variably replaced and filled fractures in garnet and kyanite with muscovite and chlorite (Plates 3.6d and 3.7a).

Overall, there has been little metamorphic retrogression of the M_{1GH} and M_{2GH} mineral assemblages, except near the base of Formation I.

The Greater Himalayan metamorphic sequence

The MCT shear zone only penetrates to about the top of Formation I (Fig. 3.13), where the effects of ductile shearing and reorientation are less pronounced. In Formation II the fabric relationships between F_{1GH} and F_{2GH} folds and S_{1GH} and S_{2GH} foliations are clearly visible. At station JN91-15 in the upper reaches of the Ghaleti Khola (Maps 1 & 2), a small leucogranite body and the S_{1GH} foliation in calc-silicate gneisses have been folded by a shallow plunging (10° toward 340°) F_{2GH} fold to which S_{2GH} is axial planar (Plate 3.7b) (this leucogranite has been dated using the U-Pb system and is presented later in the text). The parasitic minor folds on the limbs of the F_{2GH} structure appear to be interfering with an earlier set of structures (F_{1GH} folds) to create a "type-2 mushroom" geometry (Ramsay, 1967) (Plate 3.7b & c). There is also a well defined "type-2 mushroom" in a leucosome layer visible adjacent to the F_{2GH} fold (Plate 3.7c). In addition, complex interference patterns are observed in surrounding gneisses, and the intersection of axial planes of isoclinal folds outlined by S_{1GH} and the S_{2GH} foliation is oblique with roughly perpendicular strikes (Map 1),

which would create a "type-2 mushroom".

Higher in formations II and III, S_{1GH} and S_{2GH} are generally parallel and can only be distinguished as subhorizontal intersection or crenulation-hinge-line lineations (Map 1). In leucogranite, S_{2GH} is a well developed biotite-muscovite foliation.

The third deformation event (D_{3GH} for the Greater Himalaya as a whole; Table 3.2) involved top-down-to-the-northeast ductile shearing on the Annapurna detachment fault in the top-most preserved portion of Formation III. Kinematic indicators include asymmetric folds, C-S fabrics and extended or shortened dikes (see plates 2.2a, b & c). D_{3GH} was followed by a period of static recrystallization at kyanite-grade conditions. A fifth deformation event (D_{5aGH}) involved the formation of broad open warps in the Greater Himalaya and brittle faulting on the Annapurna detachment fault (D_{5bGH}), the relative ages of which are unknown (Table 3.2).

The bulk composition of the calc-silicate gneisses in Formation II does not allow the growth of index minerals such as kyanite, but the assemblage garnet-diopside-hornblende (Table 3.1) indicates amphibolite facies metamorphism (Hyndman, 1985). In Formation III, approximately 100 m beneath the contact with the Tibetan sedimentary sequence, kyanite is observed in quartzo-feldspathic sweats from pelitic rocks. Overall, the entire Greater Himalaya in the Kali Gandaki region, from the lower portion of Formation I to the top of Formation III, is at middle amphibolite facies with stable kyanite and muscovite throughout. No sillimanite has been observed.

CORRELATION AND INTERPRETATION OF THE STRUCTURES AND METAMORPHISM IN THE KALI GANDAKI REGION

The characteristics of deformation and metamorphism observed in the Lesser Himalaya and the Greater Himalaya were previously described and listed in Table 3.2. In this section correlations and interpretations of the structural and metamorphic events within and between the Lesser Himalaya and the Greater Himalaya are made.

In the Lesser Himalaya, the S_{1LH} muscovite foliation has been almost completely transposed into the S_{2LH} foliation and is therefore older. Since both of these foliations are associated with metamorphic events, M_{1LH} is older than M_{2LH}. Similarly, in the Greater Himalaya, D_{1GH} structures and metamorphism are clearly older than and overprinted by the D_{2GH} structures and metamorphism. Therefore, in both the Lesser Himalaya and the Greater Himalaya, D_1 structures and metamorphism are the oldest recognizable events. It is unclear if D_{1LH} and D_{1GH} are genetically related and therefore have not been correlated.

D_2 forms the prominent fabrics in both the Lesser Himalaya and the Greater Himalaya. In the Greater Himalaya, D_{2aGH} and D_{2bGH} are correlated and considered to be end members of a single progressive ductile event, where D_{2aGH} structures and fabrics formed during the bulk of the D_2 shearing and D_{2bGH} occurred at the very end of D_2, forming folds in the slightly older D_{2aGH} structures. D_{2GH} is interpreted as the first phase of deformation related to movement on the MCT (D_{1MCT}; Table 3.2). In the Lesser Himalaya, D_{2LH} also contains southwest-verging structures and shearing fabrics. The D_{2LH} structures have been refolded by D_{3LH} north-verging folds that do not have

an associated foliation. D_{4LH} consists of southwest-verging structures and a strong crenulation cleavage that have overprinted and refolded all other fabrics. Since D_{2LH} and D_{4LH} structures have the same vergence and metamorphic grade (both have biotite-muscovite foliations), D_{2LH}, D_{3LH} and D_{4LH} are considered together as a single progressive ductile event, similar to D_2 in the Greater Himalaya (Table 3.2). Based on their similar fabrics and kinematics, D_{2LH}, D_{3LH}, D_{4LH}, D_{2aGH} and D_{2bGH} are all correlated and interpreted as the first phase of ductile movement on the MCT (D_{1MCT}; Table 3.2).

M_{1GH} and M_{2GH} in the Kali Gandaki region are difficult to differentiate. M_{2GH} produced abundant syn- to post-D_{2GH} kyanite. If kyanite grew during M_{1GH} it is now oriented parallel to the stretching lineation and is indistinguishable from M_{2GH} kyanite. Therefore, it is inconclusive as to whether or not M_{1GH} is higher than garnet grade.

M_{1GH} garnets are large with inclusion-rich cores and clear rims. M_{2GH} garnets are smaller and inclusion free and are possibly the same generation as the garnet forming the rims on M_{1GH} garnets. Geothermometry performed on M_{1GH} garnet-bearing Formation I pelitic rocks from the Ministi Khola (Fig. 3.2) have apparent temperatures that increase with depth towards the MCT and abruptly drop adjacent to the contact with the Lesser Himalaya; approximate temperatures and distances above the MCT are 620°C at 3 km, 710°C at 1 km and 672°C at 0.2 km (Le Fort et al., 1987a). M_{1GH} garnets from the Ministi and Modi Kholas (Figs. 3.1 & 3.2) have "reverse" compositional zoning with pyrope-rich cores and almandine-rich rims indicating a decrease in temperature (Arita, 1983; Le Fort et al., 1987a; Pecher, 1989). Also, white mica compositions from the Modi Khola region suggest that muscovite at the base of

the Greater Himalaya is not in equilibrium with the M_{1GH} mineral assemblage and must have re-equilibrated at a lower temperature (Plate 3.6c) (Arita, 1983). Therefore, in the Kali Gandaki region, M_{2GH} appears to be a lower-temperature overprint of M_{1GH}, although at kyanite grade.

M_{2LH} in the Kali Gandaki region is an inverted prograde event as evidenced by the map pattern of isograds and by the metamorphic textures in thin section. In the Modi Khola region 20 km east of the Kali Gandaki (Fig. 3.1), garnets from the Lesser Himalaya have a "normal" compositional zoning pattern with spessartine-rich cores and almandine-rich rims (Arita, 1983), which indicates prograde metamorphism. The inverted metamorphism seen in the Kali Gandaki region is found throughout the Himalaya and believed to be the result of a sigmoidal inversion of isograds (similar geometry to a "drag" fold) related to movement on the MCT (Le Fort, 1975 & 1981; Pecher, 1989). As the "hot" Greater Himalaya was thrust over the "cold" Lesser Himalaya, conductive heating caused prograde metamorphism in the Lesser Himalaya (Arita, 1983) and a temperature drop at the base of the Greater Himalaya (Le Fort, 1981; Le Fort et al., 1987b). Based on the data from the Kali Gandaki region, M_{2LH} and M_{2GH} fit the model of Le Fort (1975 & 1981) and are probably related to ductile movement on the MCT (i.e., D_{1MCT}; Table 3.2).

Associated with D_{1MCT} deformation and metamorphism in the Kali Gandaki region are pre- to post-tectonic melts that form migmatites and leucogranite bodies. Field relations and geochemical studies show that the leucogranites are anatectic melts that were probably derived from Formation I gneisses (Vidal et al., 1982; Deniel et al.,

1987; Gariepy et al., 1985). One of the proposed models for leucogranite generation and emplacement is directly related to the hot-over-cold superposition caused by the MCT (Le Fort, 1981 & 1986; Le Fort et al., 1987b; Vidal et al., 1982). During prograde metamorphism in the Lesser Himalaya, dehydration and decarbonation reactions released large volumes of metamorphic fluids. These fluids then rose above the MCT shear zone into the Greater Himalaya. Where temperatures in the Greater Himalaya were above the solidus for a muscovite granite, anatectic melts were produced with the volume of granite being dependant on the volume of fluid. These melts then migrated upwards concentrating at or near the disharmonic break between the Tibetan slab and the overlying Tethyan sediments (Le Fort et al., 1987b).

The Greater Himalaya exposed in the Kali Gandaki region differs from its structural and lithologic equivalent elsewhere in the Himalaya. In many regions, the metamorphic grade in the Greater Himalaya increases structurally up-section to produce an apparent inversion of isograds (sillimanite above kyanite) (Swapp and Hollister, 1991 and references therein) and the relative abundance of migmatite and leucogranite is high; the Manaslu pluton and the sillimanite isograd are roughly 70 km east of the Kali Gandaki. It has been shown that this is not a true inversion but rather a low-pressure, high-temperature Buchan overprint (M_2) of an earlier high-pressure, high-temperature Barrovian event (M_1) (Brunel and Kienast, 1986; Hodges and Silverberg, 1988; Hodges et al., 1988 and references therein; Swapp and Hollister, 1991). Also, at the base of the MCT in some locations (the Marsyandi valley for example) there is no metamorphic break across the MCT and both the footwall and

hanging wall of the shear zone reach kyanite grade. In contrast with this is the Kali Gandaki region, where: 1) no sillimanite has been observed, in either hand sample or thin section; 2) migmatization is less intense and leucogranites form only small lenses; 3) metamorphism in the footwall of the MCT shear zone is of lower grade than the hanging wall; and 4) the total thickness of the Greater Himalaya is relatively thin. Many of these differences have been explained in terms of a "thick slab" (Manaslu section) and a "thin slab" (Annapurna section) and their relative distance from the tip of the MCT (Pecher, 1989). Far from the tip of the MCT, the Manaslu section is thick and contained enough heat to bring the footwall of the MCT (Lesser Himalaya) to the same temperature (i.e., metamorphic grade) as the hanging wall (Greater Himalaya) and to cause extensive anatectic melting. Closer to the tip of the MCT, the Annapurna section is thinner and contained less heat for metamorphism of the Lesser Himalaya and for anatectic melting in the Greater Himalaya. Near the tip of the MCT, the high-grade Lesser Himalayan nappes had lost all their heat and are separated from essentially nonmetamorphosed rocks by a brittle fault. This explanation is satisfactory for observations near the tip and far from the tip, but the Annapurna section is roughly the same distance from the tip of the MCT as the Manaslu section. In a comparison of lithologic sections through the Greater Himalaya (figure 7, p. 95, in Colchen et al., 1986), Formation I in the Kali Gandaki is about one quarter to one third as thick as it is in the Modi Khola, Marsyandi valley and Burhi Gandaki. Therefore, the Greater Himalaya is thinner and probably did contain less heat than thicker sections, but this is more likely a function of the MCT riding at various structural levels within Formation

I, not a function of the distance from the tip of the thrust.

In the Kali Gandaki region, M_{2GH} is prominent in the lower portions of the Greater Himalaya and is probably not a prograde event. As previously mentioned, M_2 elsewhere is a high-temperature overprint. The heat source of this high-temperature metamorphism is unresolved, but explanations include frictional heating, delamination of the lithosphere and upwelling of asthenosphere, heat focusing due to thermal conductivity contrasts and heterogeneities in the concentration of minerals that contain radioactive elements (see Hodges et al., 1988 and references therein).

D_3 in the Greater Himalaya is localized at the top of Formation III and represents a phase of kyanite-grade normal-sense ductile shearing that occurred on the Annapurna detachment fault; D_{3GH} is not necessarily older than D_{1MCT} as deformation and static recrystallization during both events occurred while in the kyanite field (Table 3.2). The shear foliation in leucogranites that underwent ductile deformation on the Annapurna detachment fault is roughly parallel to the regional S_{2GH} foliation and probably only penetrates the top of Formation III to a depth of about 100 m (as deep as normal-sense shear fabrics are observed; see Chapter 2): therefore, D_{3GH} fabrics are local. D_{3LH} also has a northward vergence and may overlap in time with D_{3GH}, but these are not correlative events.

D_{4GH} formed chlorite-grade mylonite with a top-to-the-southwest shear sense that is clearly retrogressive and post-dates the earlier D_{1MCT} related fabrics (Table 3.2). In the Lesser Himalaya there are no post-D_{1MCT} mylonites or retrogressive fabrics that can be correlated with D_{4GH}, and it appears that ductile shearing was partitioned within

the Greater Himalaya. Throughout Formation I the localization of secondary muscovite along fractures in kyanite as well as variably chloritized garnet, biotite and kyanite are probably the result of D_{4GH} metamorphism (M_{3GH}; Table 3.2), although mylonitization was not extensive. The D_{4GH} structures and metamorphism are interpreted as a second phase of ductile movement on the MCT (D_{2MCT}; Table 3.2).

D_5 in the Lesser Himalaya and D_5 in the Greater Himalaya are brittle events that overprint ductile fabrics, but they are not correlative. D_{5GH} is a phase of brittle faulting related to the Annapurna detachment fault that has juxtaposed kyanite-grade rocks with biotite-grade rocks. D_{5LH} is a phase of brittle deformation with evidence for southwest-directed thrusting. Although no metamorphic or stratigraphic offsets related to D_{5LH} have been recognized, near the contact between the Lesser Himalaya and the Greater Himalaya north of Dana (Fig. 3.2) there is an imbrication of kyanite-garnet-bearing gneisses and lower-grade pelite and quartzite. This imbrication is probably not related to D_{1MCT} as either a metamorphic retrogression of the gneisses or an equivalent kyanite-grade metamorphism in the pelitic rocks would be expected, and since the gneisses do not contain chlorite-grade mylonites, imbrication is not related to D_{2MCT}. D_{5LH} fabrics and brittle imbrication along the contact between the Lesser and Greater Himalaya are interpreted as a third phase of movement on the MCT (D_{3MCT}; Table 3.2). Other than imbrication, there are no correlative brittle fabrics in the Greater Himalaya.

GEOCHRONOLOGY

Samples and field relations

Two igneous rocks were collected from the Greater Himalaya to constrain the age of D_{1MCT} deformation and metamorphism using U-Pb geochronometry. Sample JN91-7b (Maps 1 & 2) was collected from a coarse-grained post-tectonic pegmatite that crosscuts the S_{2GH} foliation in Formation I (Plates 3.7d and 3.8a). The pegmatite is not foliated but its margins are slightly strained, and in thin section some quartz grains have sub-grain boundaries. This mild strain probably occurred during D_{2MCT} (Table 3.2), which was concentrated near the base of the Greater Himalaya but strained previously recrystallized quartz throughout Formation I. The sample weighed 3 kg and was predominantly cm-scale plagioclase with quartz, biotite, muscovite, rutile, tourmaline, zircon and monazite (Plate 3.8b & c).

Sample JN91-15 (Maps 1 & 2) is from the small deformed leucogranite body in the upper portion of Formation II described earlier in the structure of the Greater Himalaya (see page 62). The intrusion is multiply deformed and outlines a shallow plunging (10° towards 340°) F_{2GH} fold that contains an axial planar S_{2GH} foliation. Although the interference patterns observed suggest that the leucogranite has been folded twice (Plate 3.7b & c), the leucogranite only contains the S_{2GH} foliation. The lack of S_{1GH} in the leucogranite is problematic but can be explained in several ways: 1) the S_{1GH} foliation has recrystallized as S_{2GH}; 2) the leucogranite was emplaced or injected parallel to a folded metamorphic layering and is only mimicking an earlier phase of folding (i.e., F_{1GH}); 3) the leucogranite was emplaced after D_{2GH} started and is

only mimicking the F_{1GH}-F_{2GH} interference pattern; or 4) the leucogranite was emplaced and deformed near the end of D_{1GH} after S_{1GH} had formed, but before D_{2GH} began. Explanation (1) is difficult to prove but could have occurred. Explanations (2), (3) are possible, but unlikely as adjacent granitic layers have similar interference patterns (Plate 3.7c), near by S_{1GH} and S_{2GH} foliations have the correct orientations for the observed interference pattern (Map 1) and similar interference patterns are observed lower down in the Greater Himalaya (Plate 3.1c). Therefore, the last explanation (4) is favoured.

The sample collected weighed 10 kg and contained quartz, plagioclase, K-feldspar, biotite, muscovite, apatite, tourmaline, rutile, garnet, zircon and thorite (Plate 3.8d).

Analytical procedures

Heavy mineral separates were obtained from the crushed samples using a standard "Rodger's Table" and heavy liquids at Carleton University. Zircon, monazite and thorite were obtained by "Frantz" magnetic separation and picked in alcohol under reflected and plane polarized light at the Geological Survey of Canada geochronology laboratory in Ottawa. Mineral fractions were chosen based on size, morphology, fractures, inclusions, clarity and visible inheritance seen as cores. Some of the zircon and monazite analyses were air abraded (Table 3.3) following Krogh (1982), and U-Pb analytical methods are those of Parrish et al. (1987). The respective U and Pb blanks measured in picograms wereas follows: zircon, <1 and 10-15; monazite, $\leq$1 and 20-25;

and thorite, ≤1-3 and 5-15.

Analytical results

The U-Pb analytical data for the two samples are given in Table 3.3 and presented on concordia plots in Figs. 3.14, 3.15 and 3.16. Error ellipses are shown at the 2 sigma level.

Abundant euhedral igneous zircon was recovered from samples JN91-15 and JN91-7b. The zircons are generally tabular (2:1 length to width ratio) to equant ranging from 40 to 360 microns in length, are clear yellow (probably due to the extremely high U content; see Table 3.3) and unfractured and have minor inclusions (Plate 3.8b). Under reflected light most zircons have cloudy partially resorbed irregular cores that are overgrown by an outer rim of clear zircon. Many of the crystals that appear to be core free under reflected light reveal ghosts of internal, euhedral cores under plane polarized light. The largest, clearest crystals with no visible cores were chosen for analysis; of these the largest were lightly abraded for 2-3 hours to remove crystal faces. Multigrain fractions from 2 to 20 crystals yielded highly discordant ages (Table 3.3; Figs. 3.14 & 3.15).

Monazite from sample JN91-7b has two morphologies: 1) a thin, clear yellow (minor inclusions) octahedral form that ranges from 50 to 200 microns in diameter (Plate 3.8c); and 2) more abundant, large (200-400 microns) clear to frosty-yellow fragments with some crystal faces (Plate 3.8c). The fragments are probably the remains of much larger crystals (although not visible in the area of a single thin

section) that were broken up during sample crushing. Single- and multi-grain fractions from both morphologies, some with strong abrasion, were analyzed (Table 3.3). Five of the seven fractions form a tight, but reverse discordant cluster (Fig. 3.16).

Thorite crystals recovered from sample JN91-15 are clear, dark green and euhedral with two crystal morphologies: a tabular form 50-100 microns in length; and prisms 100 microns in length (4:1 length to width ratio) (Plate 3.8d). Most crystals have broken edges and minor inclusions. Single- and multi-grain fractions with no abrasion were analyzed (Table 3.3) yielding slightly reverse discordant ages from about 9 to 22.5 Ma (Fig. 3.16).

Interpretation

The highly discordant and non-linear pattern of the zircon data from both samples (Table 3.3; Figs. 3.14 & 3.15) indicates that more than two components of inherited radiogenic ^{206}Pb have been involved in mixing, probably in the form of invisible cores. The two fractions from JN91-7b had 17 and 22 crystals each (JN91-7b fractions contained 2 to 3 crystals); therefore, a single analysis may be the average of several different ages of zircon. Because of the non-linearity in the data set and the possibility of age averaging in a single fraction, the zircon data can only be used to make a rough estimate of the age of inheritance. The upper intercepts of regression lines through ~22 Ma and the zircon data indicate that the possible ages of components of inherited zircon range from Devonian to Proterozoic: 755-1333 Ma and 407-797 Ma for samples JN91-7b and JN91-15, respectively (Figs. 3.14 & 3.15). The

inheritance in zircon also helps confirm that the leucogranites are anatectic in nature and were probably derived from partial melting of Formation I gneisses (Vidal et al., 1982; Deniel et al., 1987; Gariepy et al., 1985).

Although the zircon data do not give precise inheritance ages, a strong Proterozoic component can be inferred from sample JN91-7b and possibly a younger Paleozoic-Precambrian component from JN91-15; similar findings elsewhere in the Himalaya indicate that the age of zircon inheritance ranges from roughly 500 to 2300 Ma (Copeland et al., 1988; Parrish and Tirrul, 1989; Scharer et al., 1986 & 1990). The youngest component of the zircon inheritance may be related to a Paleozoic metamorphic and/or igneous event interpreted from inheritance in monazite; the approximate ages of monazite inheritance are 252 and 355 Ma in the Karakorum region (Scharer et al., 1990) and 471 Ma in the Everest region (Copeland et al., 1988). It has been suggested that there is also monazite inheritance in the Manaslu leucogranite (Copeland et al., 1990). A Paleozoic metamorphic event that gave rise to anatectic melting is inferred for the origin of several other granite-orthogneiss bodies in the Himalaya. One of these, the Palung granite (470 +/- 4 Ma), is interpreted to have intruded the Greater Himalaya prior to Himalayan thrusting and is now preserved in a klippe south of Kathmandu (Scharer and Allegre, 1983). The Palung granite is largely undeformed, contains sillimanite-rich inclusions and locally becomes a sheared orthogneiss with a foliation that is concordant with the prominent fabric in the country rocks. This granite is thought to be an anatectic melt that formed in response to regional metamorphism in the Middle Ordovician (Scharer and Allegre, 1983). They

too found a strong Proterozoic inheritance in zircon with minimum ages ranging from 800 to 1700 Ma. Other Paleozoic ages interpreted as metamorphic and melting events come from the Kangmar granite-gneiss northeast of Everest (562 +/- 4 Ma; Scharer et al., 1986) and from a country rock gneiss in the Lhasa block of the Tibetan Plateau (531 +13/-14 Ma; Xu et al., 1985).

On the basis of regional data, it appears that the inheritance observed in the two samples analyzed from the Kali Gandaki is in part due to the partial melting of a sedimentary protolith (probably Formation I) with a strong Proterozoic zircon component and a weaker Paleozoic zircon component. Although Formation I of the Greater Himalaya has been identified as the probable source of the leucogranites, its depositional age is still unclear. Using the zircon data, two simple extreme end-member possibilities exist: 1) Formation I is Proterozoic in age and is composed of Proterozoic components that were metamorphosed in the Paleozoic and again during the Himalayan orogeny, which seems to be the case for the Palung granite; or 2) Formation I is as young as Tertiary in age and was derived from a source area containing Proterozoic igneous rocks and Paleozoic metamorphic and/or igneous rocks, followed by metamorphism during the Himalayan orogeny.

Five of the seven monazite fractions from sample JN91-7b form a tight cluster (Fig. 3.16); the cluster of five had the same morphology, were abraded and except for fraction R, were single-grain analyses (Table 3.3). Fraction K differs from the cluster of five in that it is slightly younger, had a different morphology and was not abraded. Three possible explanations for the slightly younger age of fraction K are: 1) it has

suffered Pb-loss due to high-temperature diffusion; 2) it contains metamorphic crystals that grew after intrusion of the pegmatite; or 3) it has suffered minor Pb-loss due to surface phenomena. Empirical observations indicate that monazite has a closure temperature of about 725 $\pm$ 25°C (Parrish, 1990). In the Baltoro region of the Karakorum, high-temperature Pb-loss is thought to have occurred where leucogranites were intruded into metamorphic rocks that had temperatures near the closure of monazite (i.e., sillimanite-grade); monazite ages are about 2-4 Ma younger than the crystallization ages from zircon and thorite (Parrish and Tirrul, 1989). In the Kali Gandaki region, the temperature estimates for Formation I based on the mineral assemblage and geothermometry (Le Fort, 1986) are about 600-700°C. Because the pegmatite sample (JN91-7b) was intruded into rocks which were probably never above the closure temperature of monazite, the younger age of fraction K is probably not due to high-temperature Pb-loss, and, because the pegmatite cuts S_2 (the peak metamorphic fabric) the monazite in fraction K is probably not metamorphic. Therefore, fraction K is probably the same age as the fractions in the cluster, but because it was not abraded the effects of minor Pb-loss caused by surface phenomena are apparent.

Fraction J differs from the cluster of five in that it is just slightly older, had four crystals and was not abraded. Although fraction J contained monazite with fresh, broken surfaces, large crystal faces still remained. If fraction J had been abraded, Pb-loss caused by surface phenomena would have been removed, and the analysis may have plotted even further to the right of the cluster. This suggests that there may be a minor component of inherited monazite from the metamorphosed country rock that the

pegmatite intrudes (i.e., M_{2GH} monazite in Formation I would be slightly older) or that there may be inheritance from the source of the melt. Monazite inheritance has been recognized in other Himalayan leucogranites (Scharer et al., 1990; Copeland et al., 1988; Copeland et al., 1990) and was discussed earlier with the zircon interpretation.

Reverse discordance is a common occurrence in monazite (Parrish, 1990), which has been attributed to an initial excess of ^{230}Th (Scharer, 1984). A correction for the initial excess ^{230}Th can be applied to the $^{206}Pb/^{238}U$ ratio whereby monazite data are made concordant (Scharer, 1984). The two underlying assumptions of this correction are that: 1) the magma was in radioactive equilibrium before crystallization; and 2) the whole rock Th/U ratio still reflects the Th/U ratio of the magma from which the monazite crystallized. The correction has not been applied in this study because the Th/U ratio of the melt is not accurately known, and for a variety of reasons outlined by Parrish (1990), monazite data commonly do not become concordant after correction. Multi-mineralic studies with zircon, xenotime and monazite have shown that although the $^{206}Pb/^{238}U$ ratio may be influenced by an excess of ^{230}Th, the $^{207}Pb/^{235}U$ ages from monazite still give the correct crystallization age (Scharer, 1984; Scharer et al., 1986; Parrish, 1990). Therefore, in light of the above discussion, the interpreted crystallization age of sample JN91-7b is based on the $^{207}Pb/^{235}U$ ages of the five monazite fractions in the cluster only.

In Figure 3.16 and Table 3.3, the maximum and minimum $^{207}Pb/^{235}U$ ages in the cluster are 21.3 ± 0.1 and 22.2 ± 0.2 Ma from fractions P and Q, respectively. Fractions N, O and R all have the same age of about 21.8 Ma, which is the average

between fractions P and Q. Therefore, the interpreted crystallization age for the crosscutting pegmatite dike (sample JN91-7b) is 21.8 ± 0.5 Ma.

The thorite data from sample JN91-15 are slightly reverse discordant and spread along concordia from ~9 to 22.5 Ma (Figs. 3.15 & 13.16), although the concentration of data is above 20 Ma with fractions H and I having identical $^{207}Pb/^{235}U$ ages of 22.5 Ma (Table 3.3). Thorite is not a commonly used mineral for U-Pb geochronometry. The cause of the reverse discordance has not been identified, although it may be related to an initial excess of ^{230}Th, which causes excess radiogenic ^{206}Pb, similar to that observed in monazite. In a geochronological study of the Baltoro granite of northern Pakistan, monazite interpreted to have undergone high-temperature Pb-loss gives ages younger than the interpreted crystallization age determined from thorite and zircon (Parrish and Tirrul, 1989). This indicates that thorite has a closure temperature higher than monazite; therefore, the interpreted age of sample JN91-15 would be that of crystallization, not cooling.

By using air abrasion on zircon it has been shown that there is a positive correlation between U content and discordance caused by leaching and radiation damage near the surface of a crystal (Krogh, 1982; Parrish et al., 1992). Thorite has a Th-U content of 60-80% by weight (from 250,000 to 550,000 ppm U per fraction; Table 3.3) and can undergo extensive alteration caused by alpha-particle bombardment from the radioactive decay of U and Th (Frondel, 1958). Pb-loss of this type is usually used to explain a linear discordance of points along a chord from the interpreted age to zero. In young rocks (i.e., less than ~50 Ma), however, concordia has virtually no

curvature; therefore, a linear Pb-loss chord will be almost parallel producing several "apparently" concordant ages.

The thorite crystals analyzed were too small to abrade without loss or destruction; therefore, the array of thorite ages presented here is interpreted to be the result of Pb-loss caused by surface phenomena in the same manner as zircon. Thorite fractions H and I have identical $^{207}Pb/^{235}U$ ages (Table 3.3) and represent the oldest crystals analyzed, but because abrasion was not done and Pb-loss may have occurred, they may be giving ages slightly younger than the true crystallization age. Based on this, the interpreted minimum age of crystallization for the leucogranite sample JN91-15 is 22.5 ± 0.1 Ma. It is stressed here that the error of ± 0.1 Ma given to this age is an analytical error based on the precision of the technique. Assigning this age as a minimum is an interpretation of the accuracy based on knowledge of U-Pb systematics.

Discussion

Many different types of geochronological studies have been done on Himalayan leucogranites, but with variable success. The Rb-Sr, K-Ar and ^{40}Ar-^{39}Ar systems have been used to determine whole-rock and mineral ages for leucogranites in all regions of the Himalaya (Le Fort et al., 1987b; Searle and Fryer, 1986; Searle et al., 1989; see Hubbard and Harrison, 1989 for a review), although there are problems that limit their use and reliability. In the Rb-Sr system, the closure temperatures for commonly dated minerals such as muscovite and biotite are 500°C (Purdy and Jager, 1976) and 300-

350°C (Dodson, 1973), respectively. In the K-Ar system, the closure temperatures of hornblende, muscovite and biotite are 530 ± 40°C (Harrison, 1981), 350°C (Purdy and Jager, 1976) and 280 ± 40°C (Harrison et al., 1985), respectively. This means that all Rb-Sr, K-Ar and 40Ar-39Ar age determinations on primary igneous minerals are strictly cooling ages (Hanes, 1991) and do not reflect the much higher temperature emplacement age, unless it is demonstrable or assumed that the pluton cooled quickly. This problem is accentuated in regions such as the Himalaya where leucogranites were emplaced in high-temperature gneisses (i.e., kyanite to sillimanite grade).

Due to the mobility of Rb it is difficult to determine if minerals have remained closed (Shirey, 1991). Also, heterogeneities in the Sr isotopic composition have been described in the Transhimalaya (Scharer et al., 1984) and in the Manaslu leucogranite (Vidal et al., 1982). Such problems can lead to incorrect age determinations due to accidental linear arrays (Scharer et al., 1986), such as in the Everest-Makalu region, where leucogranites have an interpreted whole-rock Rb-Sr emplacement age of 52 Ma (Ferrara et al., 1983), as well as U-Pb monazite ages of 21 and 24 Ma (Scharer, 1984). Similarly, the Bhagirathi leucogranite has an Rb-Sr whole rock age of 64 ± 11 Ma and Rb-Sr and K-Ar cooling ages of 19-21 Ma from biotite and muscovite, respectively (Stern et al., 1989). Since no U-Pb data have been obtained it is difficult to determine if this whole-rock age is significant. It is these systematic problems that make the Rb-Sr and K-Ar systems less useful than U-Pb for determining crystallization ages. The current practice is not to rely on Rb-Sr for crystallization ages unless they can be confirmed with a more precise system such as U-Pb (Shirey, 1991).

Very few U-Pb studies exist in the published literature for the Greater Himalayan leucogranites (Table 3.4; Fig. 3.4). The rocks dated in these studies are similar in mineralogy and tectonic setting; garnet-tourmaline-bearing two-mica leucogranites generally intruded along and adjacent to the contact between the Greater Himalaya and the Tibetan sedimentary sequence (i.e., the South Tibetan detachment system; Burchfiel et al., 1992). In Table 3.4 there is a conspicuous grouping of leucogranite ages from about 20 to 25 Ma with errors in the order of less than 1 Ma. Two of the studies suggest that there are two pulses of magmatism, one at about 21-22 Ma and another at about 24-25 Ma (Scharer, 1984; Scharer et al., 1990). Within the 20-25 Ma age range, the leucogranites studied vary from sheared and metamorphosed to undeformed; undeformed leucogranites post-date MCT ductile shearing or are intruded high enough into the Tibetan sedimentary sequence to have escaped ductile normal faulting on the South Tibetan detachment system. On the basis of the regional U-Pb data, all the Greater Himalayan leucogranites were emplaced between ~20 and 25 Ma.

TIMING CONSTRAINTS IN THE KALI GANDAKI REGION

Since M_{ILH} in the Kali Gandaki region has not been dated, its relationship, if any, to the Himalayan orogen is unclear. An illite crystallinity study in the Kumaon Himalaya has shown that the regional metamorphic fabric in the Lesser Himalaya (possibly M_{ILH} in the Kali Gandaki region) is Paleozoic-Mesozoic in age and unrelated to the Himalayan orogeny (Johnson and Oliver, 1990). Alternatively, if M_{ILH} occurred

2 of/de 2

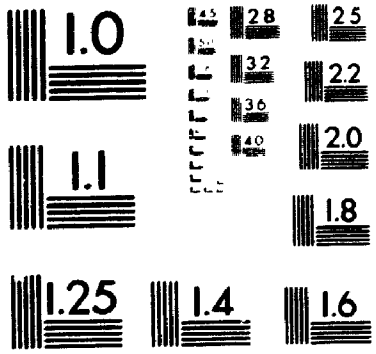

during the Himalayan orogeny, it may be part of a single continuous event, where the D_{1LH} metamorphic fabric is older than, but related to D_{2LH}.

Field relations in the Kali Gandaki region indicate that D_{1GH} and M_{1GH} have been overprinted by D_{2GH} and M_{GH} (D_{1MCT}; Table 3.2) and that the dated leucogranite sample JN91-15 was intruded into Formation II post-M_{1GH}, near the end of D_{1GH} and the onset of D_{2GH}. Since the leucogranite appears to have been folded by F_{1GH}, the very end of D_{1GH} occurred perhaps as late as 22.5 ± 0.1 Ma, outlasting M_{1GH}. The same granite is folded by F_{2GH}, therefore, D_{2GH} could be younger than 22.5 ± 0.1 Ma. The intrusion of pre- to post-D_{2GH} anatectic granites suggests that M_{2GH} began just before and outlasted D_{2GH}. D_{3GH} also involved ductile shearing of leucogranites and gneisses on the Annapurna detachment fault while at kyanite-grade conditions (see Chapter 2). On the basis of metamorphic grade, similarities in tectonic setting, mineralogy and ages of other Himalayan leucogranites, a portion of the ductile shearing of Formation III in the footwall of the Annapurna detachment fault is thought to be synchronous with D_{2GH}.

Using the age of the pegmatite sample (JN91-7b) that crosscuts the S_{2GH} foliation in Formation I of the Greater Himalaya, all D_{2GH} kyanite-grade ductile shearing associated with movement on the MCT (D_{1MCT}; Table 3.2) was completed by 21.8 ± 0.5 Ma. Similarly, D_{3GH} kyanite-grade ductile shearing on the Annapurna detachment fault may have ceased by then as well. On the basis of the correlation of structures and fabrics between the Lesser Himalaya and the Greater Himalaya (D_{1MCT}; Table 3.2) the progressive D_{2LH} to D_{4LH} event has the same age constraints as D_{2GH} and

M_{2GH}. Using the age limits presented here, the time span of D_{1MCT} ranges from 0.1 to 1.3 Ma.

At some time after 21.8 Ma, the MCT was reactivated at greenschist-facies forming southwest-verging D_{4GH} chlorite-grade mylonites in the Greater Himalaya (D_{2MCT}; Table 3.2). After D_{4GH} the MCT was reactivated at upper crustal conditions superimposing D_{5LH} brittle fabrics on the older D_{1MCT} ductile fabrics in the Lesser Himalaya. The Annapurna detachment fault was also reactivated at upper crustal conditions (D_{5GH}) juxtaposing biotite-grade rocks against kyanite-grade rocks.

In summary, based on the structural and geochronological data presented here, the following timing constraints are proposed for the Kali Gandaki region: 1) anatectic melting, leucogranite emplacement and M_{2GH} metamorphism began by at least 22.5 ± 0.1 Ma; 2) M_{1GH} is older than 22.5 ± 0.1 Ma; 3) the very end of D_{1GH} and the onset of D_{2GH} deformation occurred perhaps as late as 22.5 ± 0.1 Ma; 4) all D_{2GH} ductile shearing and kyanite-grade metamorphism associated with D_{1MCT} and possibly ductile movement on the Annapurna detachment fault was over by 21.8 ± 0.5 Ma; 5) a portion of the ductile shearing on the Annapurna detachment fault may have been synchronous with D_{1MCT}; 6) the time span in which ductile deformation fabrics formed during D_{1MCT} ranges from less than 0.1 to 1.3 Ma; 7) D_{4GH} chlorite-grade shearing (D_{2MCT}) occurred after 21.8 ± 0.5 Ma; and 8) D_{5LH} brittle faulting (D_{3MCT}) and D_{5GH} associated with brittle faulting on the Annapurna detachment fault occurred after D_{4GH} and could be as young as Quaternary.

TECTONIC IMPLICATIONS

In the Kali Gandaki region, the Greater Himalaya has undergone multi-phase deformation and metamorphism as a result of tectonic burial and subsequent tectonic exhumation related to movement on the MCT and Annapurna detachment fault. A tectonic interpretation of the area based on the structural data and timing constraints is presented here.

In the Kali Gandaki region, the field relations and interpretations imply that D_{1GH} and M_{1GH} are younger than ~50 Ma and therefore formed during the Himalayan orogeny. This interpretation supports weak evidence that elsewhere in the Himalaya M_{1GH} is Eocene in age and probably related to continental collision between India and Eurasia (Hodges and Silverberg, 1988; Searle et al., 1989; Searle and Rex, 1989; Treloar and Rex, 1990). An Eocene age would suggest that D_{1GH}/M_{1GH} and D_{1MCT} are part of a single progressive Himalayan event, where D_{1GH} involved the burial and metamorphism of sedimentary rocks (perhaps as young as Paleocene-Eocene) during India-Eurasia continental convergence and D_{1MCT} represents a younger phase of intense metamorphism, anatectic melting and southwest-directed motion on the MCT that began in Oligocene-Miocene time (~25 Ma).

Of interest is the very short apparent time span in which the D_{1MCT} event occurred. In the Kali Gandaki region, U-Pb data indicate that D_{1MCT} occurred over a 0.1-1.3 Ma time span; in the Langtang region the main deformational fabric is believed to have occurred within a few million years of 21 Ma (Parrish et al., 1992); regionally, leucogranite ages indicate that M_2 metamorphism occurred between ~20

and 25 Ma.

The very short duration of D_{1MCT} deformation determined by this study may be the result of strain partitioning and diachronous shearing within the MCT shear zone, and/or it may be possible that the oldest thorite fraction analyzed has suffered some Pb-loss and has revealed an age a few million years younger than the true crystallization age. On the basis of regional data, Greater Himalayan leucogranites are no older than ~25 Ma. Knowing that D_{1MCT} ceased by 21.8 Ma, the ductile fabrics in the Greater Himalaya probably formed over a time span of less than ~3.2 Ma.

Despite mesoscopic observations that rocks within the MCT shear zone and footwall of the Annapurna detachment fault have undergone intense ductile shearing, the entire Greater Himalaya (except near the base of Formation I) has a highly recrystallized microscopic texture due to static annealing and lacks well preserved mylonites. The static recrystallization occurred around 21.8 Ma while the Greater Himalaya was still at kyanite-grade conditions; therefore, D_{1MCT} ductile movement on the MCT as well as D_{3GH} ductile movement on the Annapurna detachment fault must have ceased or become negligible while still at middle crustal levels.

In the Kali Gandaki region, the only fabrics that overprint the recrystallized D_{1MCT} structures are coarse chlorite-grade shears in the Greater Himalaya (D_{2MCT}) and brittle fabrics in the Lesser Himalaya (D_{3MCT}); there are no rocks that indicate deformation continued through the brittle-ductile transition. Although there are no mineral cooling ages, the preservation of both a stable, annealed middle-amphibolite-facies mineral assemblage and an inverted temperature gradient directly above the

MCT in the Kali Gandaki region (Le Fort et al., 1987a) indicate that the Greater Himalaya was quenched and brought to upper crustal levels quickly. Therefore, the kyanite-grade D_{1MCT} ductile shearing fabrics preserved in Greater Himalaya presently exposed in the Kali Gandaki region were rapidly uplifted and exhumed with virtually no motion on the MCT.

Two uplift mechanisms are considered plausible for the Greater Himalaya of the Kali Gandaki region: 1) development of a ramp and/or 2) development of a duplex along the structurally lower Main Boundary Thrust. In eastern Nepal, field relations indicate that the Main Boundary Thrust post-dates the MCT and in cross sections it is drawn rooting into a crustal-scale ramp structurally beneath a ramp in the MCT (Fig. 3.5) (Schelling, 1992). A cross section through the Kumaon Himalaya also illustrates a ramp in the Main Boundary Thrust as well as a large uplifted region above the MCT (Fig. 3.3) (Lyon-Caen and Molnar, 1983). In the Langtang region, a ramp in the Main Boundary Thrust may have caused out-of-sequence thrusting and subsequent brittle duplexing of the MCT zone (Macfarlane et al., 1992).

Exhumation mechanisms include erosion and tectonic denudation. Erosion rates in parts of the Himalayan orogen are believed to have been very rapid (i.e., 1-10 mm/yr) during the Neogene (Copeland and Harrison, 1990). However, erosion in mountainous terrain may occur primarily by back-wasting, which removes material from the valleys not reduce the height of the peaks and may not be a contributing factor (R. L. Brown, pers. comm.). The contact between the Greater Himalaya and Tibetan sedimentary sequence in the Thakkhola region of the upper Kali Gandaki

valley is interpreted as a crustal-scale, ductile-brittle, normal-sense shear zone (the Annapurna detachment fault; see Chapter 2) and is correlated with the South Tibetan detachment system. As previously mentioned, the Greater Himalaya preserves textures indicating quenching and rapid exhumation. Extensional faulting and the generation of normal-sense ductile-brittle shear zones give rise to rapid exhumation of high-grade rocks (Coney, 1980; Armstrong, 1972) and are recognized as important features of convergent orogens. The Annapurna detachment fault is therefore the structure most likely responsible for the bulk of exhumation.

Of interest are the mechanisms that cause the onset of extensional faulting that lead to tectonic denudation and exhumation. Applying critical taper theory (see Dahlen, 1990 for a review; Platt, 1986; Beaumont et al., 1992) extension in the upper crust may occur if the taper of the orogenic wedge becomes supercritical. Some of the key parameters that control critical taper are: 1) internal and basal pore fluid pressures; 2) the internal and basal coefficients of friction; 3) density of the wedge and fluid; 4) the basal slope; 5) erosion rate; and 6) subduction rate. An increase in basal pore fluid pressure or a decrease in basal friction across a preexisting surface, erosion rate, or subduction rate can cause a wedge to become supercritical.

In the Kali Gandaki region, it is possible that the Annapurna detachment fault is superposed on an older thrust fault (see Chapter 2). Also, ductile shearing on the Annapurna detachment fault was accompanied by the emplacement of leucogranites and possibly the migration metamorphic fluids released from the underthrust Lesser Himalaya. Therefore, shearing could have been initiated by an increase in pore fluid

pressure and/or a lowering of the basal friction caused by the emplacement of anatectic melts (Hollister and Crawford, 1986) along a previously existing fault plane. The convergence rate between India and Eurasia has not changed since collision (Molnar and Tapponnier, 1975) and is therefore not an important factor. A simple model proposed by Burchfiel and Royden (1985) suggests that extension is the product of gravitationally induced collapse of the Miocene topographic front between the Tibetan plateau and the Indian foreland. Burchfiel et al. (1992) believe that ductile extension at depth may have been triggered by a weakening of the crust due to anatectic melting.

A model for the tectonic evolution of the Kali Gandaki region is as follows. The Greater Himalaya was buried and metamorphosed during Eocene time (D_{1GH} and M_{1GH}) in response to the continental collision between India and Eurasia. Between ~25 and 21.8 Ma, a short but intense phase of middle-crustal thrusting accompanied by metamorphism and leucogranite emplacement formed the D_{1MCT} structures and fabrics. During this time there was probably contemporaneous kyanite-grade ductile normal faulting on the Annapurna detachment fault that was induced by anatectic melting, which weakened the crust causing gravitational instability and collapse. At 21.8 Ma ductile motion on the MCT and possibly on the Annapurna detachment fault ceased at middle crustal levels; a period of static recrystallization followed. A lowering of the Miocene topographic surface and attainment of a critical taper may have terminated D_{1MCT} deformation.

Following intense deformation and subsequent recrystallization, the Greater

Himalaya was uplifted and exhumed with only minor shearing at chlorite grade (D_{2MCT}) and brittle faulting at upper crustal levels (D_{3MCT}). Uplift of the Greater Himalaya was probably achieved with a crustal-scale ramp and/or a duplex related to the structurally lower Main Boundary Thrust. Uplift and increased topography led to supercritical conditions, renewed upper crustal normal faulting on the Annapurna detachment fault and subsequent exhumation of the Greater Himalaya. Minor phases of ductile (D_{2MCT}) and brittle (D_{3MCT}) reactivation of the MCT during uplift and exhumation may have been due to readjustments in the critical taper angle, controlled by the parameters discussed earlier.

DISCUSSION

The evidence for a short but intense phase of D_{1MCT} deformation and metamorphism followed by rapid uplift and erosion in the Kali Gandaki region is similar to the findings of other structural, petrologic and geochronologic studies in the Himalaya. In the Everest region, thermobarometric profiling and textural relationships indicate that M_2 metamorphism is not disrupted and was synchronous with movement on the MCT (Hubbard, 1989). A syn-tectonic hornblende separate from the MCT shear zone in the same region has an ^{40}Ar-^{39}Ar release spectra indicating that peak-M_2 temperatures had cooled through the closure temperature for argon in hornblende by approximately 21 Ma; therefore, movement on the MCT occurred at that time (Hubbard and Harrison, 1989). In the Langtang region, U-Pb ages for monazite and zircon from pelitic schists and leucogranites suggest M_2 metamorphism occurred at

about 21 Ma (Parrish et al., 1992), and collectively, Greater Himalayan leucogranite ages indicate that anatexis occurred between ~20 and 25 Ma. These data imply that MCT deformation, metamorphism and leucogranite emplacement where all roughly coeval.

Some of the movement on a portion of the South Tibetan detachment system has been dated as well. In the Everest region, two syn-tectonic amphibole separates from the footwall of the Qomolangma detachment have release spectra indicating that peak-M2 temperatures had cooled through the closure temperature for argon in hornblende by approximately 21 Ma and that some of the movement on the Qomolangma detachment occurred at that time (Hodges et al., 1989). In the same area, the Rongbuk leucogranite crosscuts the Qomolangma detachment and has a U-Pb zircon age of approximately 20 Ma (Copeland et al., 1988). A more precise U-Pb age of 20.6 ± 0.2 Ma was interpreted from xenotime in the same sample (Parrish, 1990). This age indicates that the bulk of the movement on the Qomolangma detachment was over by 20.6 Ma (Burchfiel et al., 1992).

Rapid uplift of the Greater Himalaya has been interpreted in several studies. Thermobarometric observations from the Greater Himalaya in the central portion of the orogen, such as minimal re-equilibration of the peak metamorphic mineral assemblage during cooling and the apparent preservation of lithostatic pressure gradients and inverted temperature gradients, suggest that rapid uplift and quenching occurred in latest Oligocene to Middle Miocene (Hodges et al., 1988). In the Everest region, ^{40}Ar-^{39}Ar cooling ages from K-feldspar, muscovite and biotite are only a few

million years younger than the crystallization ages of the Greater Himalaya leucogranites from which they were recovered and are interpreted to be the result of rapid uplift in Miocene time (Copeland and Harrison, 1987; Maluski et al., 1988).

A direct result of rapid uplift and erosion of the Himalaya was the deposition of sediment in the Bengal Fan, which contains a large component of Early to Middle Miocene age sediment. Fission-track dating of detrital apatite and ^{40}Ar-^{39}Ar dating of K-feldspar and muscovite from the Bengal Fan revealed that a large portion of the detritus is essentially the same age as the sediment. The presence of zero-age detritus was interpreted to be the result of rapid uplift, erosion and transportation since ~18 Ma (Corrigan and Crowley, 1990; Copeland and Harrison, 1990; Copeland, 1993). A provenance study of the heavy mineral detritus in the Bengal Fan indicates that the Greater Himalaya was being rapidly eroded between 17.1 and 7.5 Ma (Amano and Taira, 1992, 1993a & 1993b).

CONCLUSIONS

In the Kali Gandaki region, three phases of deformation related to the MCT are recognized. The dominant phase (D_{1MCT}) took place at middle crustal levels and began perhaps after 22.5 ± 0.1 Ma, but probably not before 25 Ma. D_{1MCT} was completed by 21.8 ± 0.5 Ma, followed by static recrystallization at kyanite-grade conditions. Associated with D_{1MCT} was ductile reorientation of earlier structures (D_{1GH}; ~Eocene) within the high-strain portion of the shear zone, and a kyanite-garnet-grade metamorphic event (M_{2GH}), which overprints the earlier metamorphism (M_{1GH}). A

portion of the ductile normal faulting on the Annapurna detachment fault was probably synchronous with D_{1MCT} thrusting.

After 21.8 Ma, the Greater Himalaya was rapidly uplifted and exhumed with only minor reactivation of the MCT at chlorite-grade conditions (D_{2MCT}) and at upper crustal conditions (D_{3MCT}). The mechanisms that brought the Greater Himalaya to the surface with very little motion on the MCT were uplift above a crustal-scale ramp and/or a duplex in the structurally lower Main Boundary Thrust and tectonic denudation as a result of renewed movement on the Annapurna detachment fault.

Figure 3.1. Geological map of central Nepal modified after Colchen et al. (1986). Inset in upper left hand corner shows location of field area; box shows location of detail map in Figure 3.2; A-A' locates line of cross section in Figure 3.6; MCT = Main Central Thrust; ADF = Annapurna detachment fault; TNF = Thakkhola normal fault.

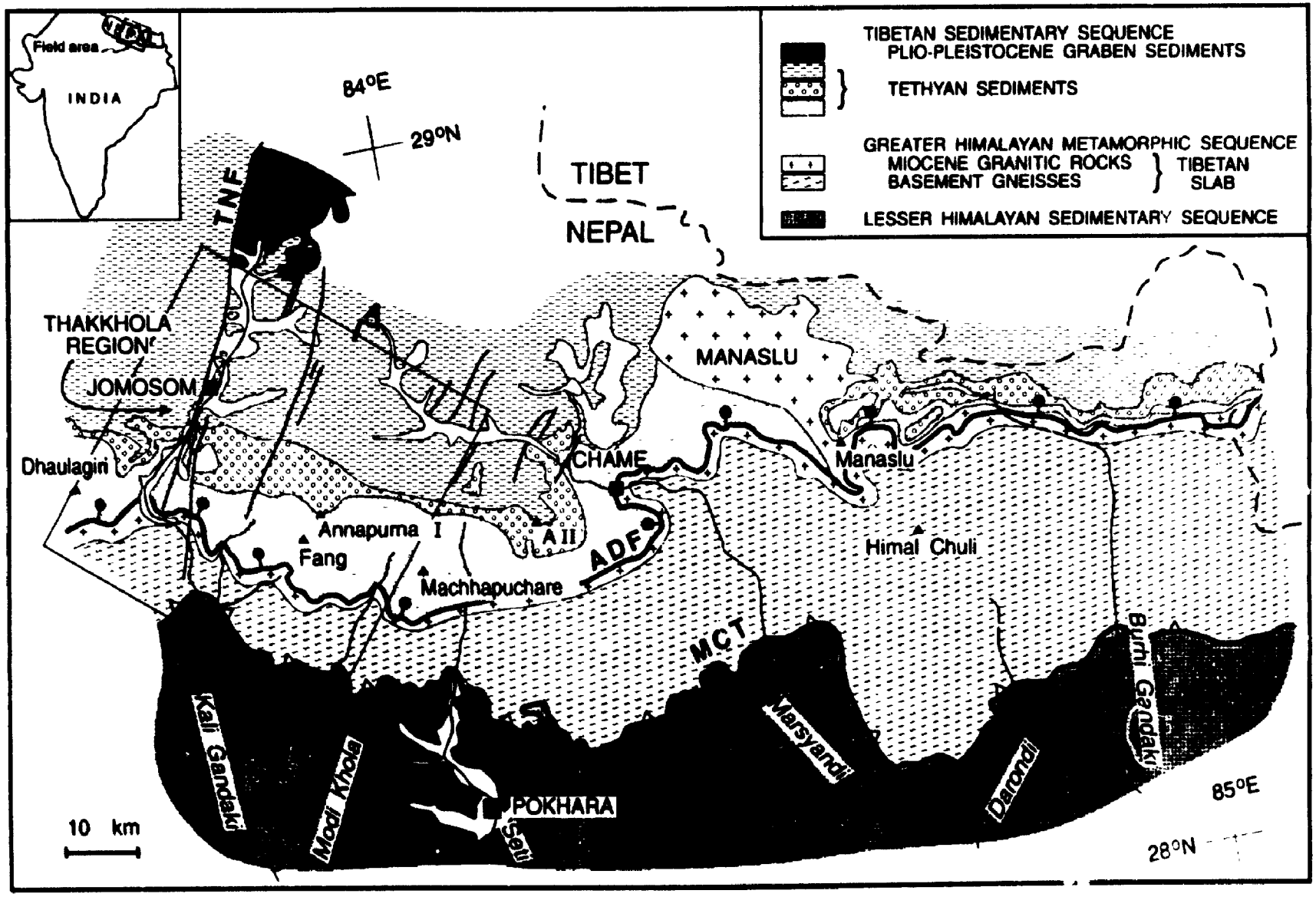
Field area
INDIA
84°E
29°N
TIBET
NEPAL
TNF
THAKKHOLA REGION
JOMOSOM
Dhaulagiri
MANASLU
CHAME
Manaslu
Annapurna I
Fang
A II
ADF
Machhapuchare
Himal Chuli
MCT
Kali Gandaki
Modi Khola
POKHARA
Seti
Marsyandi
Darondi
Burhi Gandaki
85°E
28°N
10 km
TIBETAN SEDIMENTARY SEQUENCE
PLIO-PLEISTOCENE GRABEN SEDIMENTS
TETHYAN SEDIMENTS
GREATER HIMALAYAN METAMORPHIC SEQUENCE
MIOCENE GRANITIC ROCKS
BASEMENT GNEISSES
TIBETAN SLAB
LESSER HIMALAYAN SEDIMENTARY SEQUENCE

Figure 3.2. Detail of the field area: shaded dashed line follows route of traverses; A-A' locates line of cross section line in Figure 3.6; MCT = Main Central Thrust; ADF = Annapurna detachment fault; TNF = Thakkhola normal fault; stars and station numbers indicate locations of geochronology samples; see Figure 3.1 for legend.

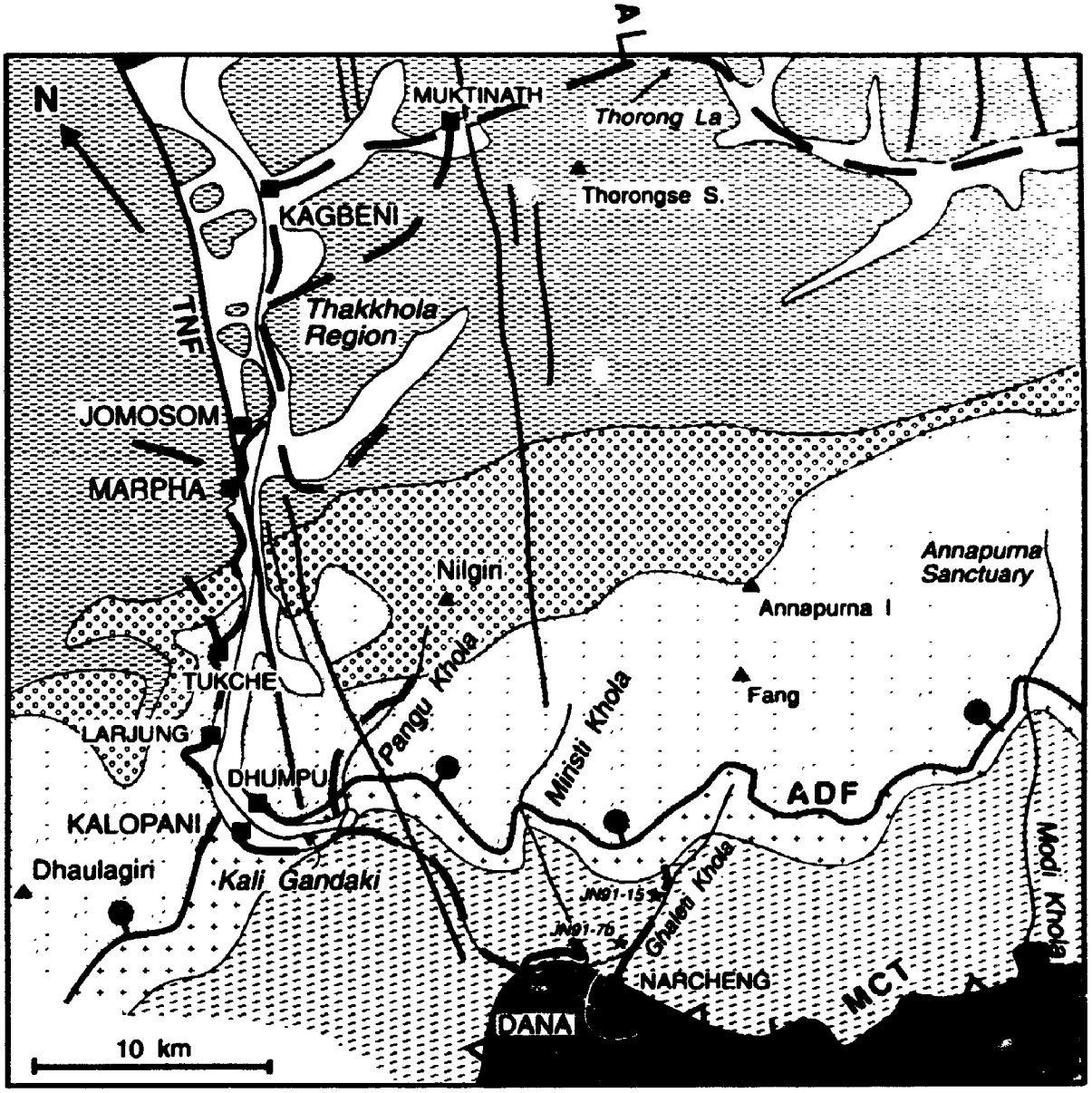
N
MUKTINATH
Thorong La
Thorongse S.
KAGBENI
Thakkhola Region
TNF
JOMOSOM
MARPHA
Nilgiri
Annapurna Sanctuary
Annapurna I
TUKCHE
Pangu Khola
Miristi Khola
Fang
LARJUNG
DHUMPU
ADF
KALOPANI
Dhaulagiri
Kali Gandaki
JN91-15
JN91-76
Ghaleri Khola
Modi Khola
NARCHENG
MCT
DANA
10 km

Figure 3.3. Sequence of idealized cross sections from the initial collision of India and Eurasia to present (from Lyon-Caen and Molnar, 1983). a) Formation of the Main Central Thrust (MCT) after an assumed 100 km of subduction of part of the northern margin of India. b) Formation of the Main Boundary Fault (MBF; also known as the Main Boundary Thrust) after an assumed 125 km of underthrusting of India along the MCT. Note the marked uplift of material over the MCT. c) Underthrusting of an assumed 125 km of India along the MBF. Note that again pronounced uplift occurs where the MBF changes dip. d) Same as (c) but eroded to present level.

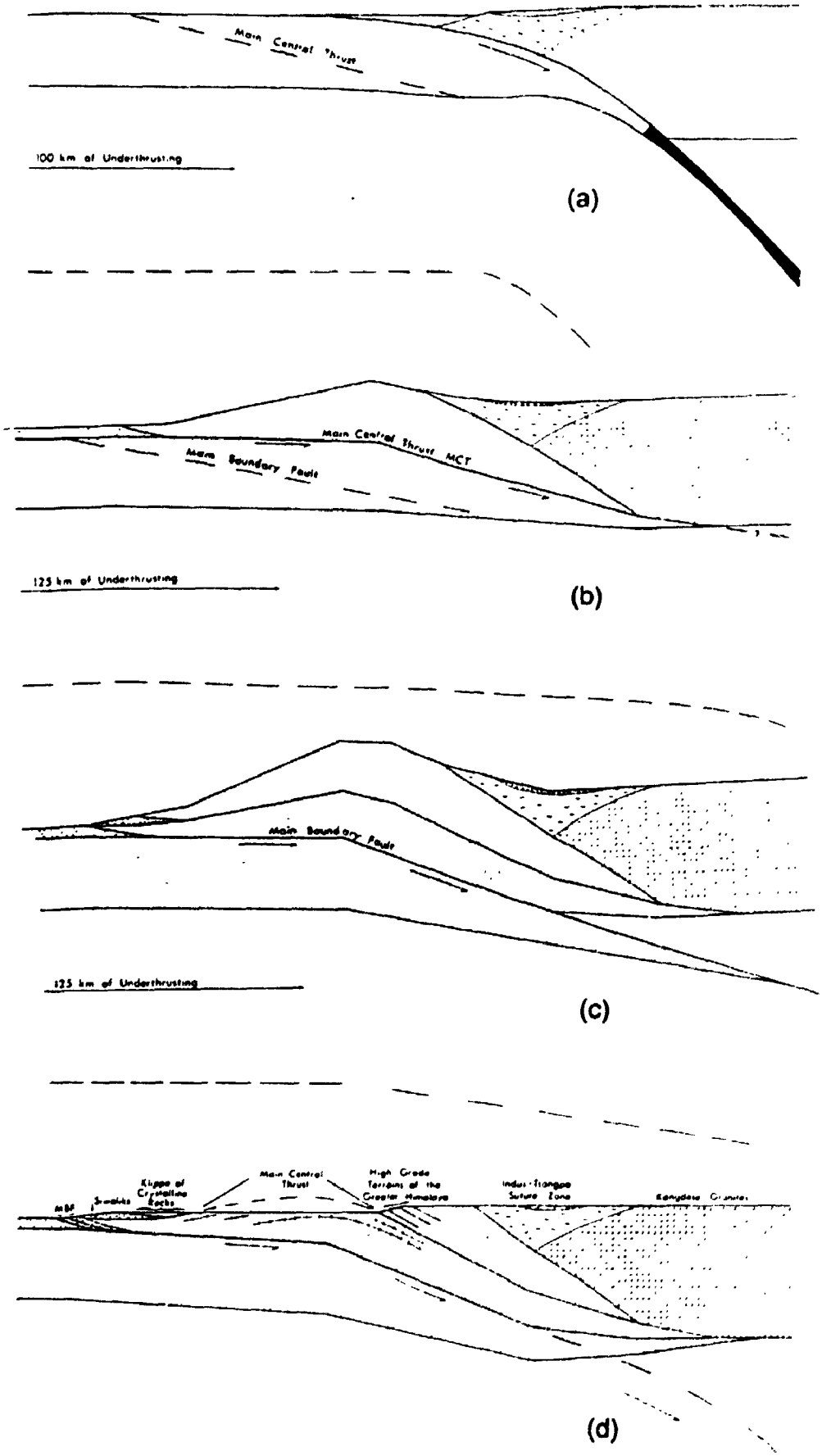
Main Central Thrust
100 km of Underthrusting
(a)
Main Central Thrust MCT
Main Boundary Fault
125 km of Underthrusting
(b)
Main Boundary Fault
125 km of Underthrusting
(c)
Klippe of Crystalline Rocks
Main Central Thrust
High Grade Terrains of the Greater Himalaya
Indus-Tsangpo Suture Zone
MBF
Siwaliks
(d)

Figure 3.4. Map of the main structural subdivisions in the Himalaya - Transhimalaya (after Le Fort, 1975). Arrows and names indicate the regions where Greater Himalayan leucogranites have been dated using the U-Pb system. See Table 3.4 for the ages of leucogranites in these regions. Small letters are abbreviations for: e, Everest; K, Kathmandu; Kg, Kargil; L, Lhasa; Lh, Leh; m, Manaslu; P, Peshawar; T, Thimpu; X, Xigaze. The following superscripts indicate other commonly used names: (1) Indus-Tsangpo suture zone; (2) Tibetan Sedimentary sequence, Tethys Himalaya; (3) Greater Himalayan leucogranites; (4) Greater Himalayan metamorphic sequence, Tibetan Slab, Annapurna Gneiss complex, Vaikrita group, Central Crystalline, Himalayan gneiss zone, Takhtstang gneiss; (5) Lesser Himalayan sedimentary Sequence, Midland formations; (6) Sub-Himalaya, Ganges Plain, Siwalik lowlands.

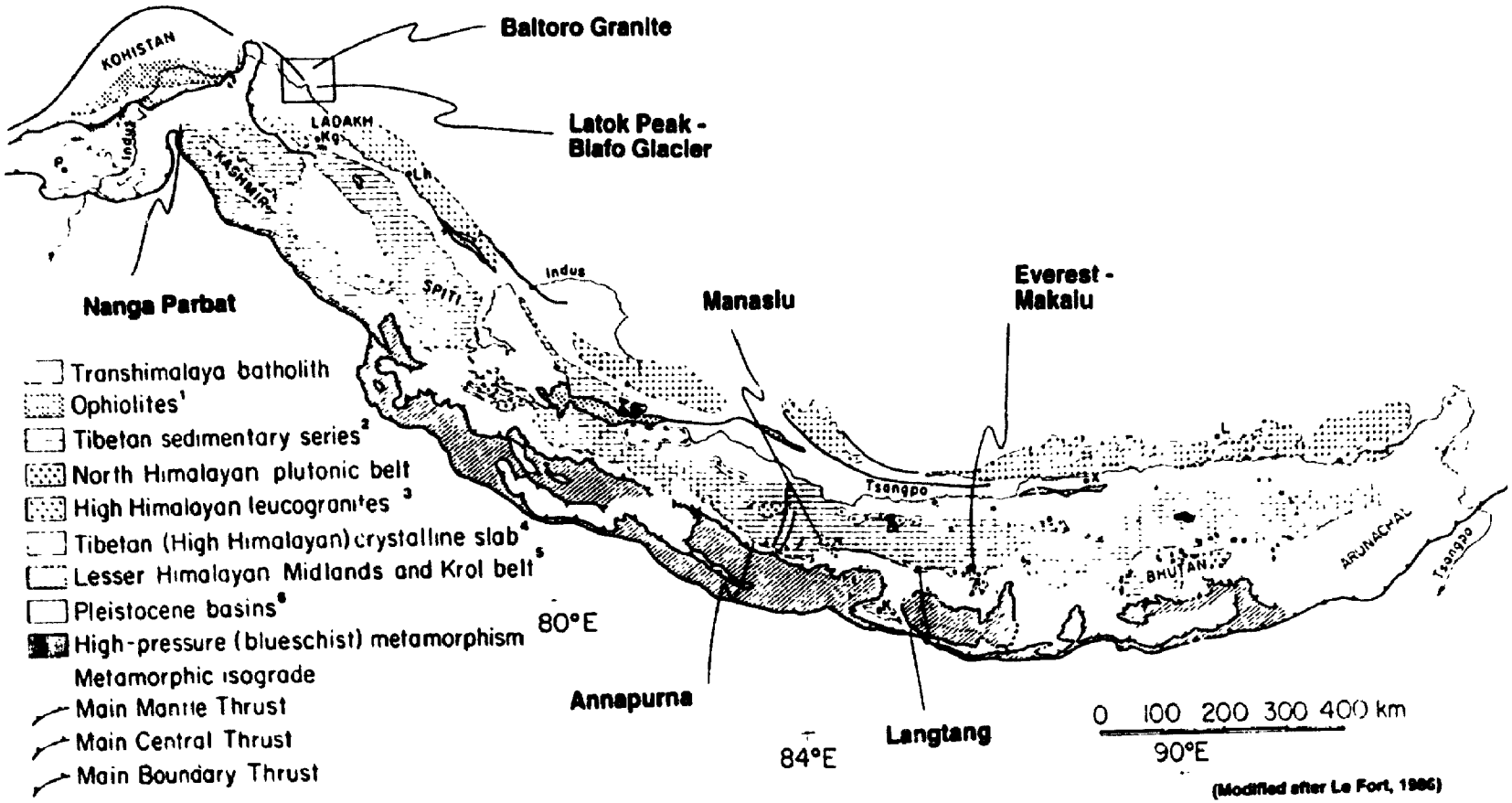

(Modified after Le Fort, 1986)

Figure 3.5. (a) Balanced and (b) restored cross sections of the eastern Nepal Himalaya through the Greater Himalaya north of Melung-Tse and the Ganges Plain south of Sindhuli Bazaar (from Schelling, 1992). Rocks above the MCT belong to the Greater Himalaya. Only the Lesser and Sub-Himalaya beneath and south of the MCT have been restored. Main Central Thrust, MCT; Sun Kosi Thrust, SKT; Main Boundary Thrust, MBT; Main Detachment Fault, MDF; Kamala Thrust, KT; Main Frontal Thrust, MFT.

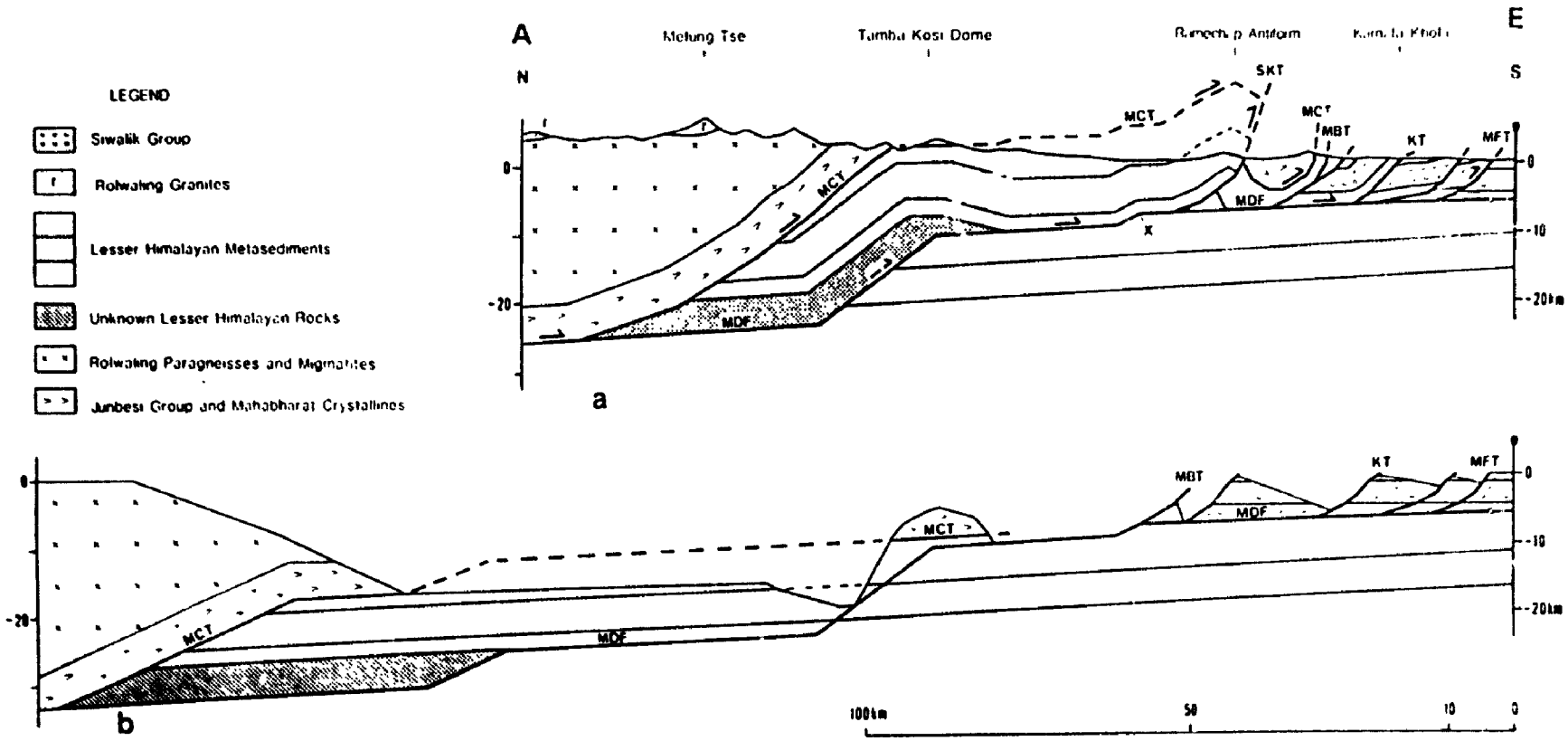
LEGEND
Siwalik Group
Rolwaling Granites
Lesser Himalayan Metasediments
Unknown Lesser Himalayan Rocks
Rolwaling Paragneisses and Migmatites
Junbesi Group and Mahabharat Crystallines
A
N
E
S
Melung Tse
Tamba Kosi Dome
SKT
MCT
MBT
KT
MFT
MDF
X
0
-10
-20km
a
b
-20
100km
50
10
0

Figure 3.6. Cross section modified after Colchen et al. (1986). MCT = Main Central Thrust; ADF = Annapurna detachment fault (located as per Caby et al., 1983).

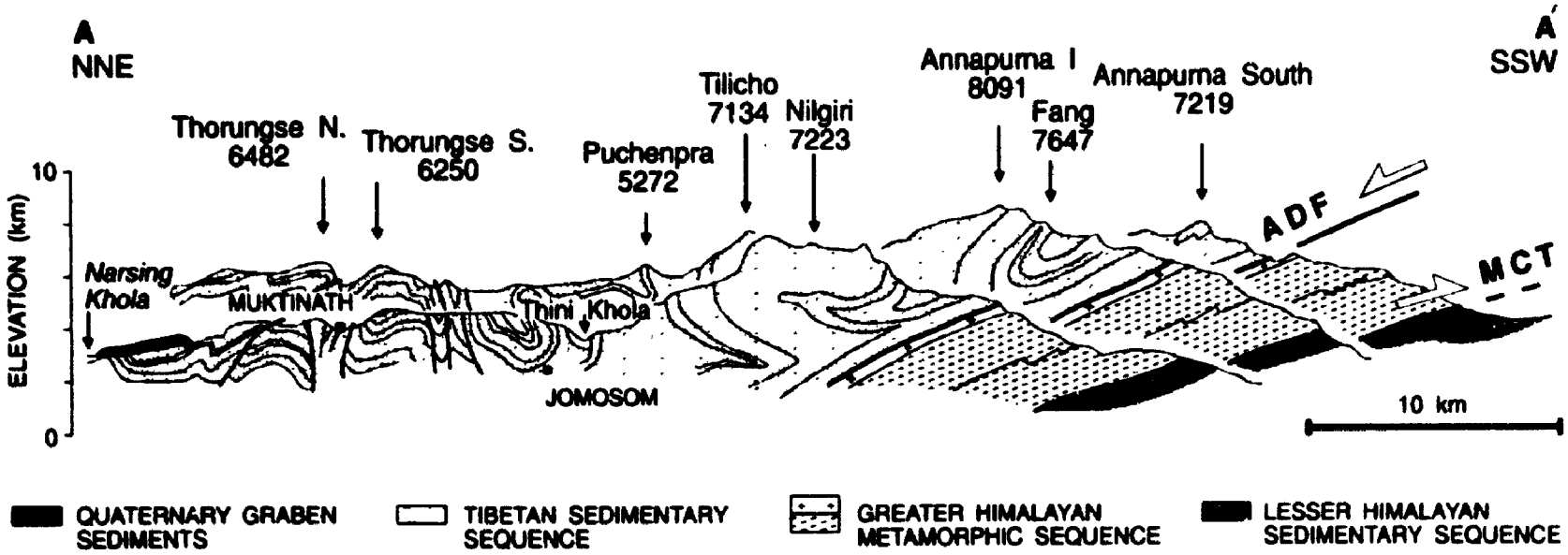
A
NNE
A'
SSW
Thorungse N.
6482
Thorungse S.
6250
Puchenpra
5272
Tilicho
7134
Nilgiri
7223
Annapurna I
8091
Fang
7647
Annapurna South
7219
ELEVATION (km)
10
0
Narsing
Khola
MUKTINATH
Thini Khola
JOMOSOM
ADF
MCT
10 km
QUATERNARY GRABEN SEDIMENTS
TIBETAN SEDIMENTARY SEQUENCE
GREATER HIMALAYAN METAMORPHIC SEQUENCE
LESSER HIMALAYAN SEDIMENTARY SEQUENCE

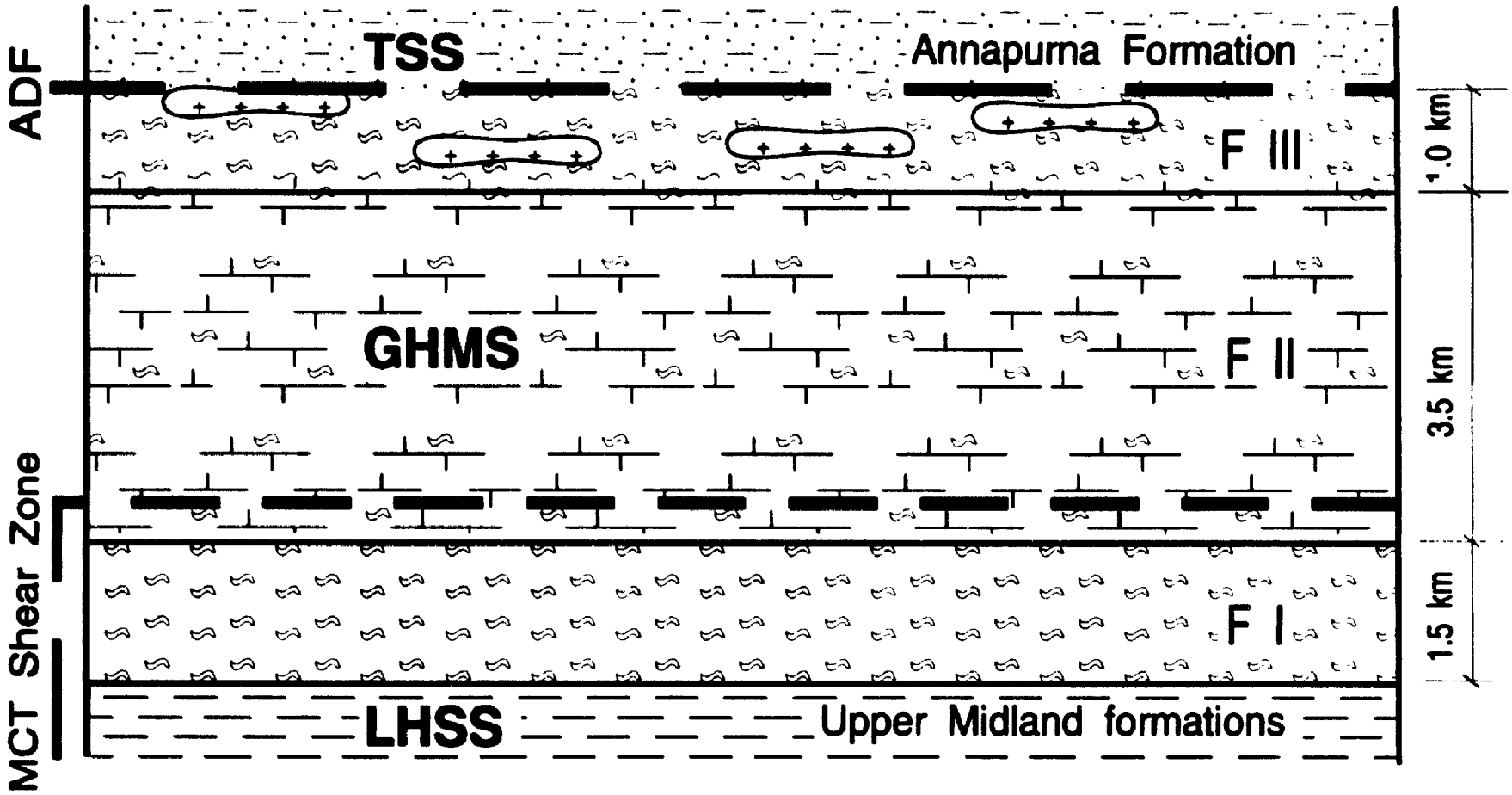

Figure 3.7. Schematic tectonostratigraphic section through the Kali Gandaki region. MCT (Main Central Thrust); ADF (Annapurna detachment fault); TSS (Tibetan sedimentary sequence); GHMS (Greater Himalayan metamorphic sequence); LHSS (Lesser Himalayan sedimentary sequence). See Table 3.1 for description of units.

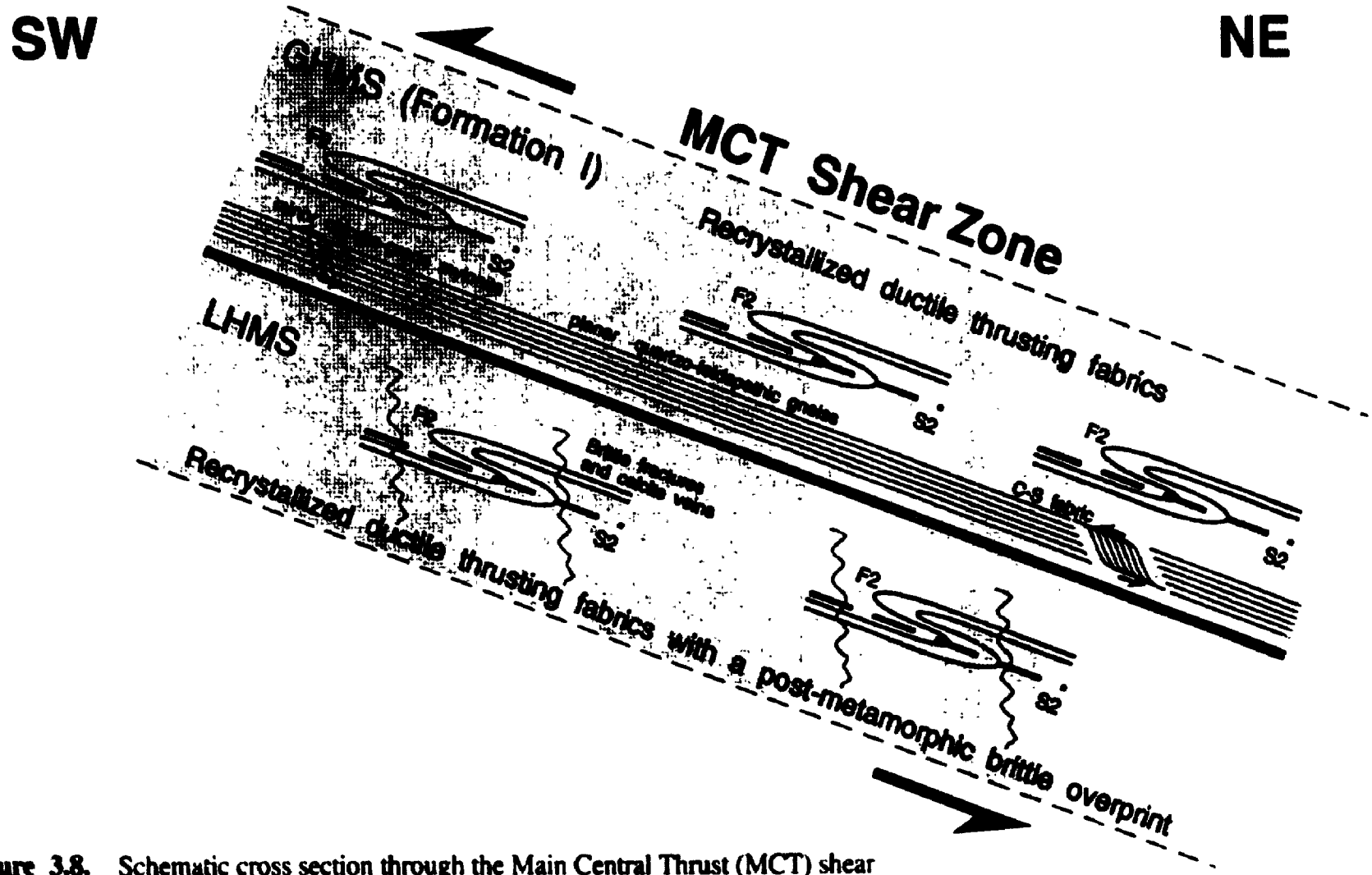

Figure 3.8. Schematic cross section through the Main Central Thrust (MCT) shear zone in the Kali Gandaki region. View is to the northwest, perpendicular to the stretching lineation. GHMS (Greater Himalayan metamorphic sequence); LHSS (Lesser Himalayan sedimentary sequence). See Figure 3.9 for a schematic cross section perpendicular to this view.

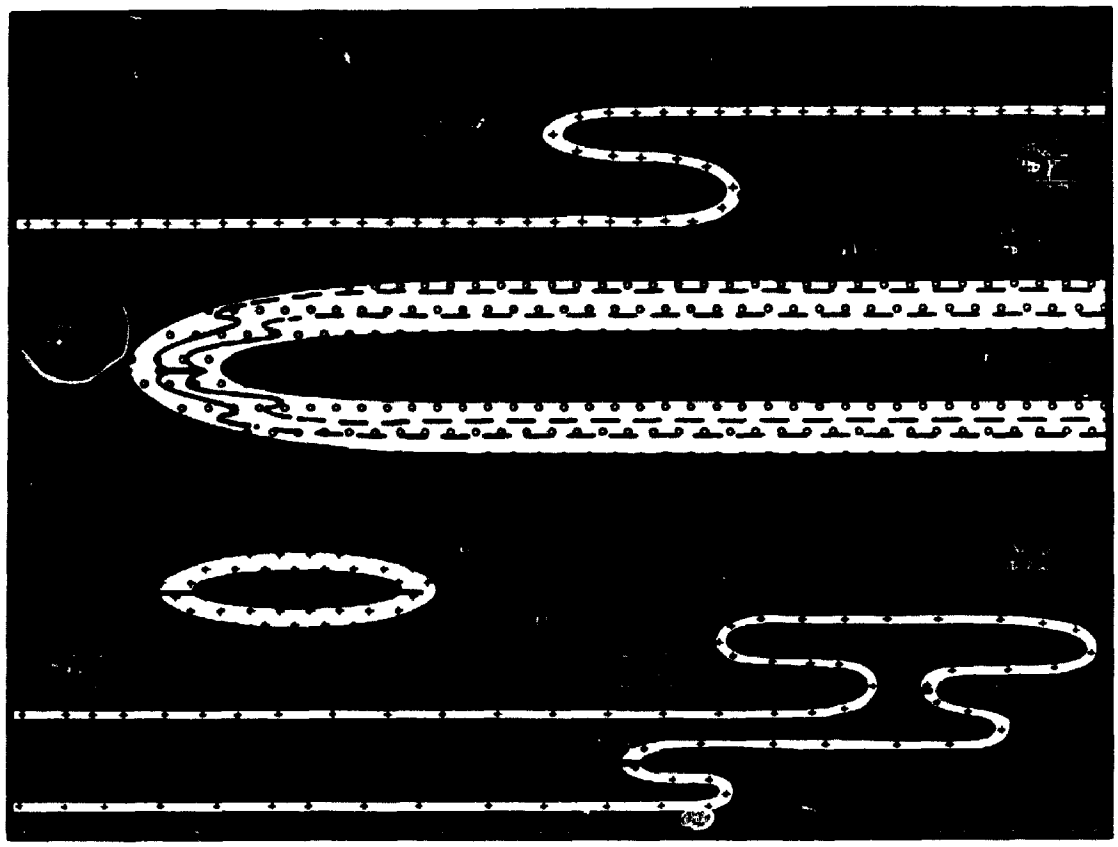

LEGEND

leucosome

Quartzofeldspathic gneiss

Pelitic gneiss

S0 - Compositional layering

S1 - First-phase foliation

S2 - Second-phase foliation

F1 - First-phase fold

F2 - Second-phase fold

Figure 3.9. Schematic cartoon of the lithologic and fabric relationships observed in Formation I gneisses within the Main Central Thrust shear zone. View is towards the northeast down the dip of the S2 foliation, parallel to the stretching lineation.

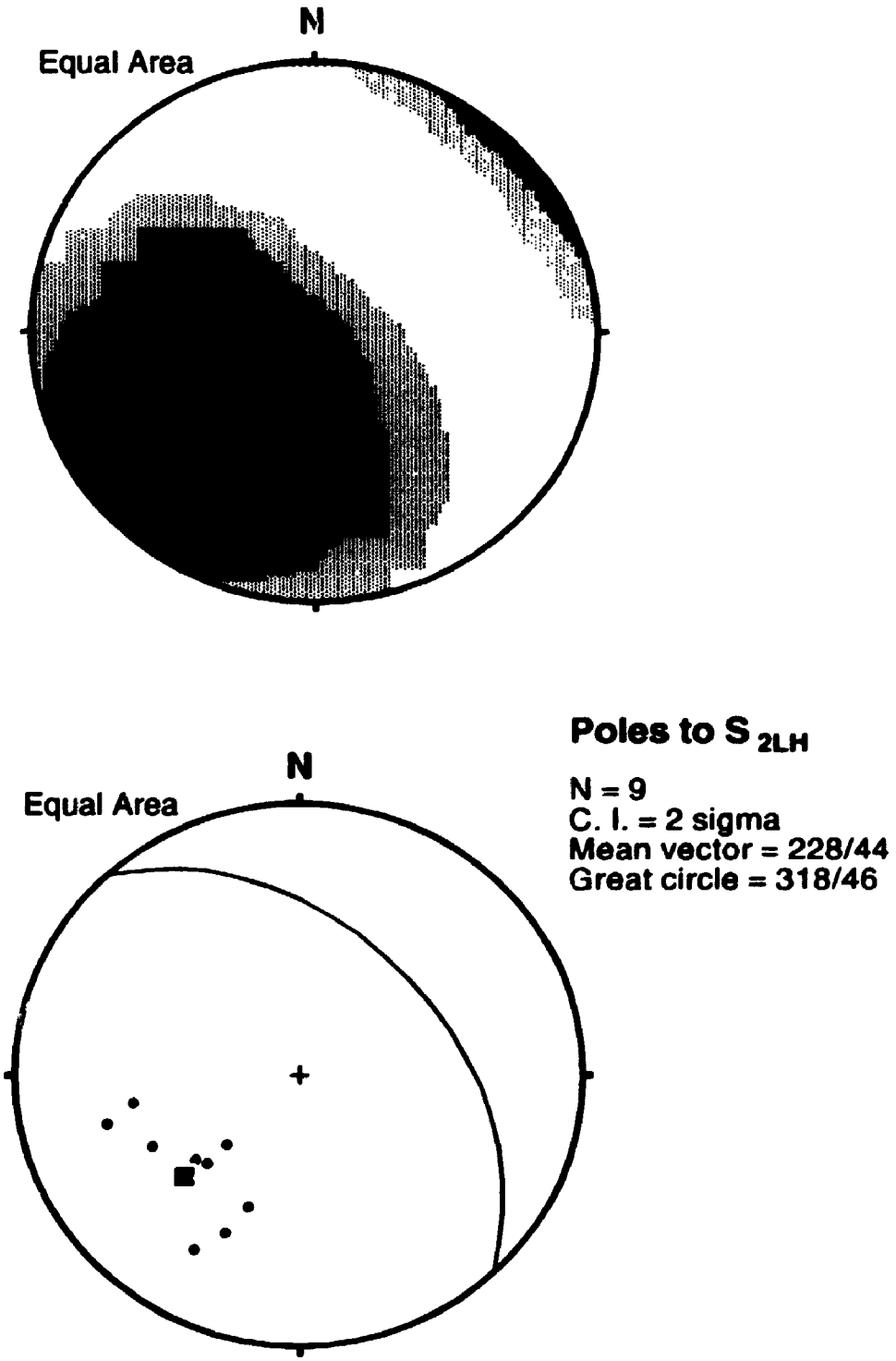

Figure 3.10. Scatter plot and contour of poles to S2 foliations in the Lesser Himalayan sedimentary sequence. N, number of points; C. I., contour interval; square indicates mean vector.

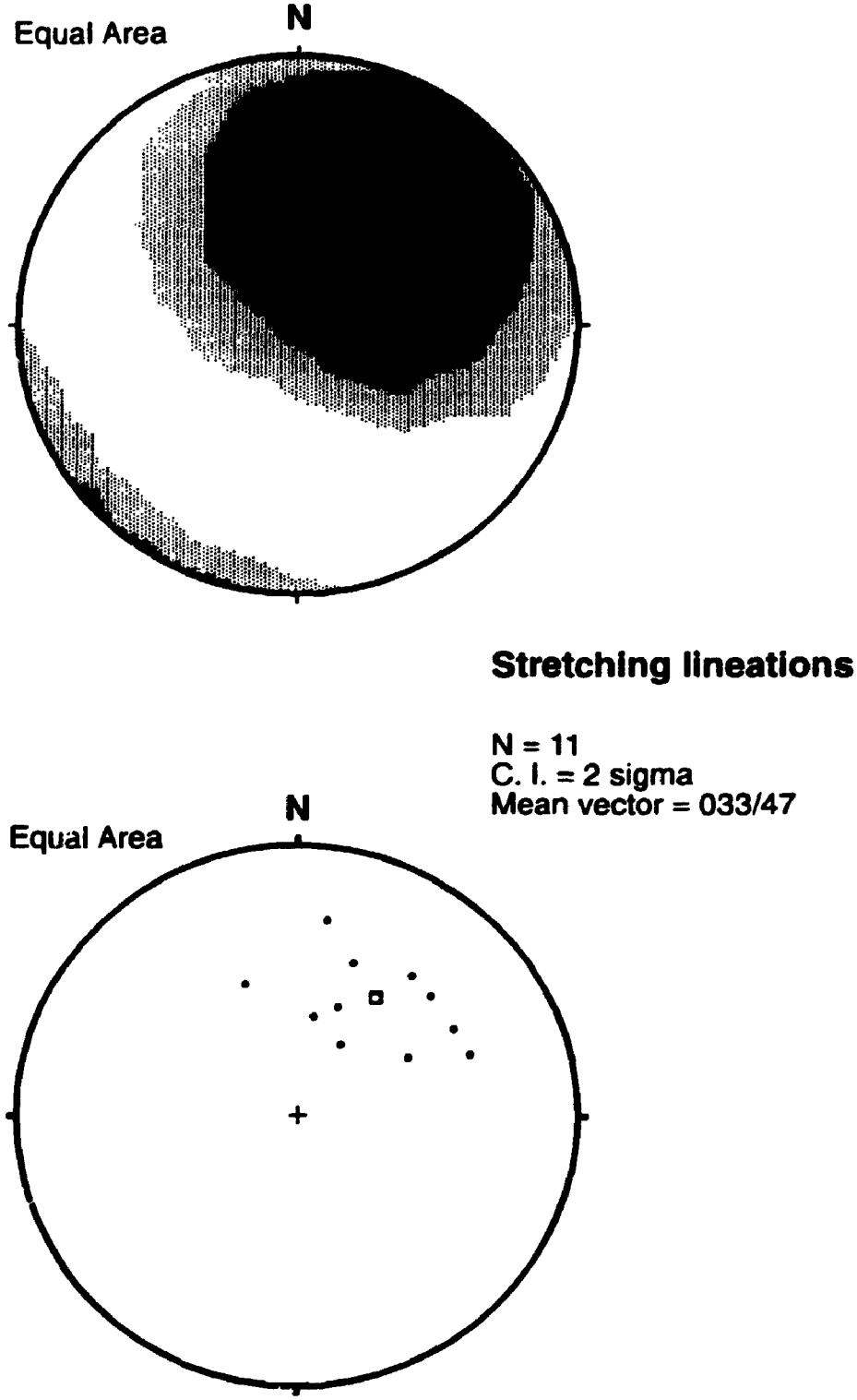

Figure 3.11. Scatter plot and contour of stretching lineations in the Greater Himalayan metamorphic sequence and the Lesser Himalayan sedmentary sequence. N, number of points; C. I., contour interval; square indicates mean vector.

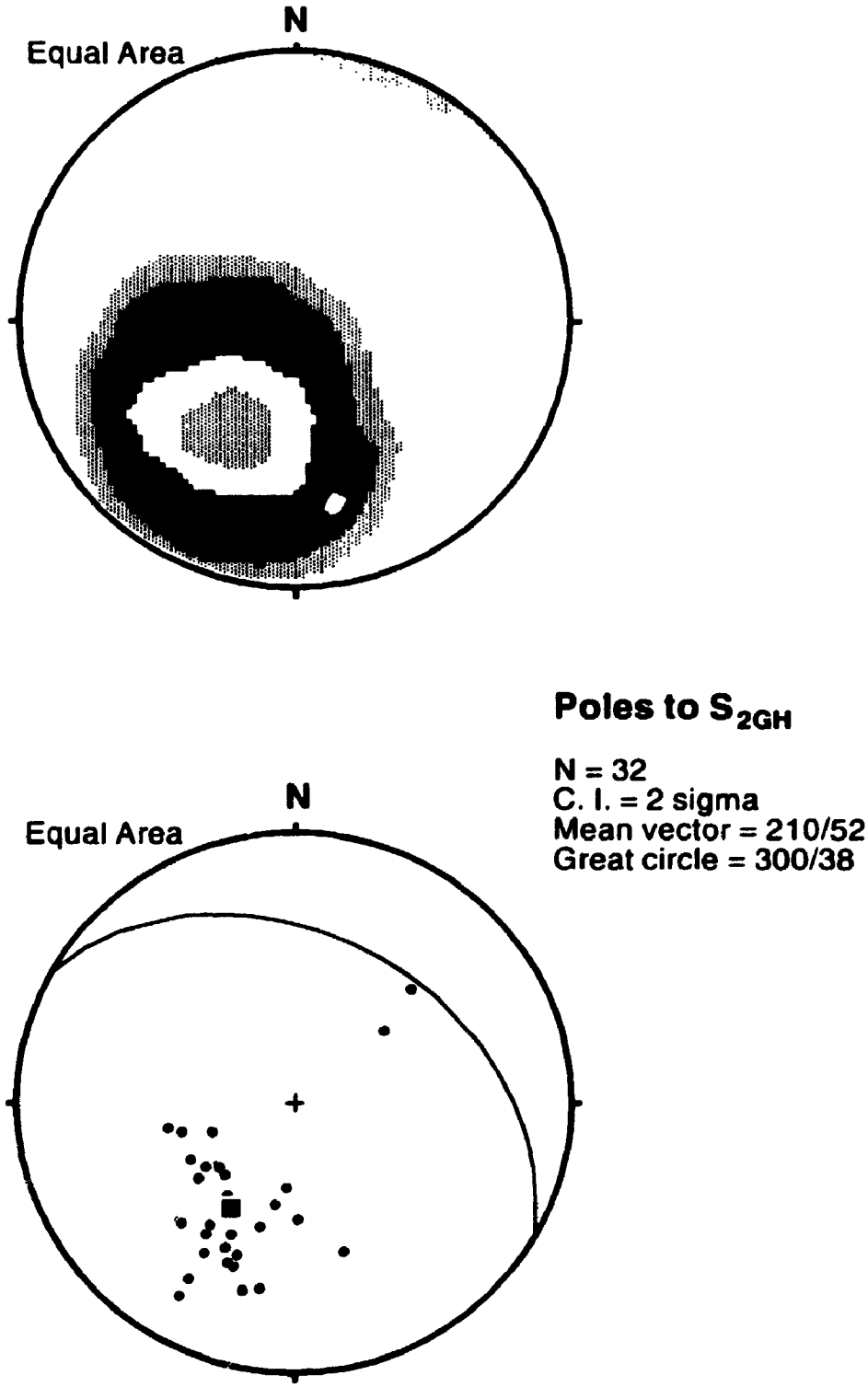

Figure 3.12. Scatter plot and contour of poles to S2 foliations in the Greater Himalayan metamorphic sequence. N, number of points; C. I., contour interval; square indicates mean vector.

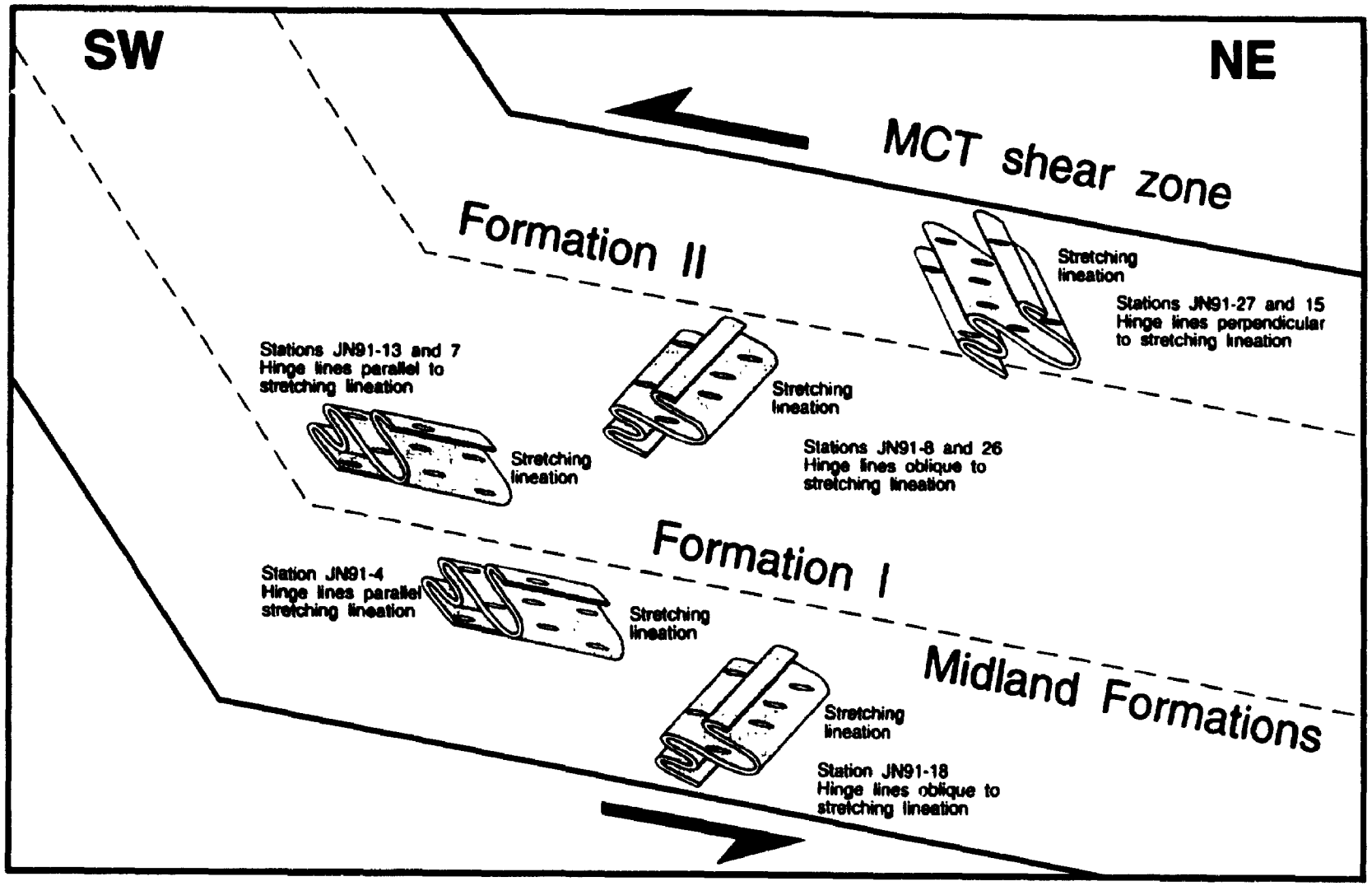

Figure 3.13. Composite cartoon of the strain gradient associated with ductile shearing on the Main Central Thrust (MCT). In the highest strain zones F2 hinge lines are parallel to stretching lineations. Structurally above and below the high strain zones, hinge lines progressively become perpendicular to stretching lineations. See text for details.

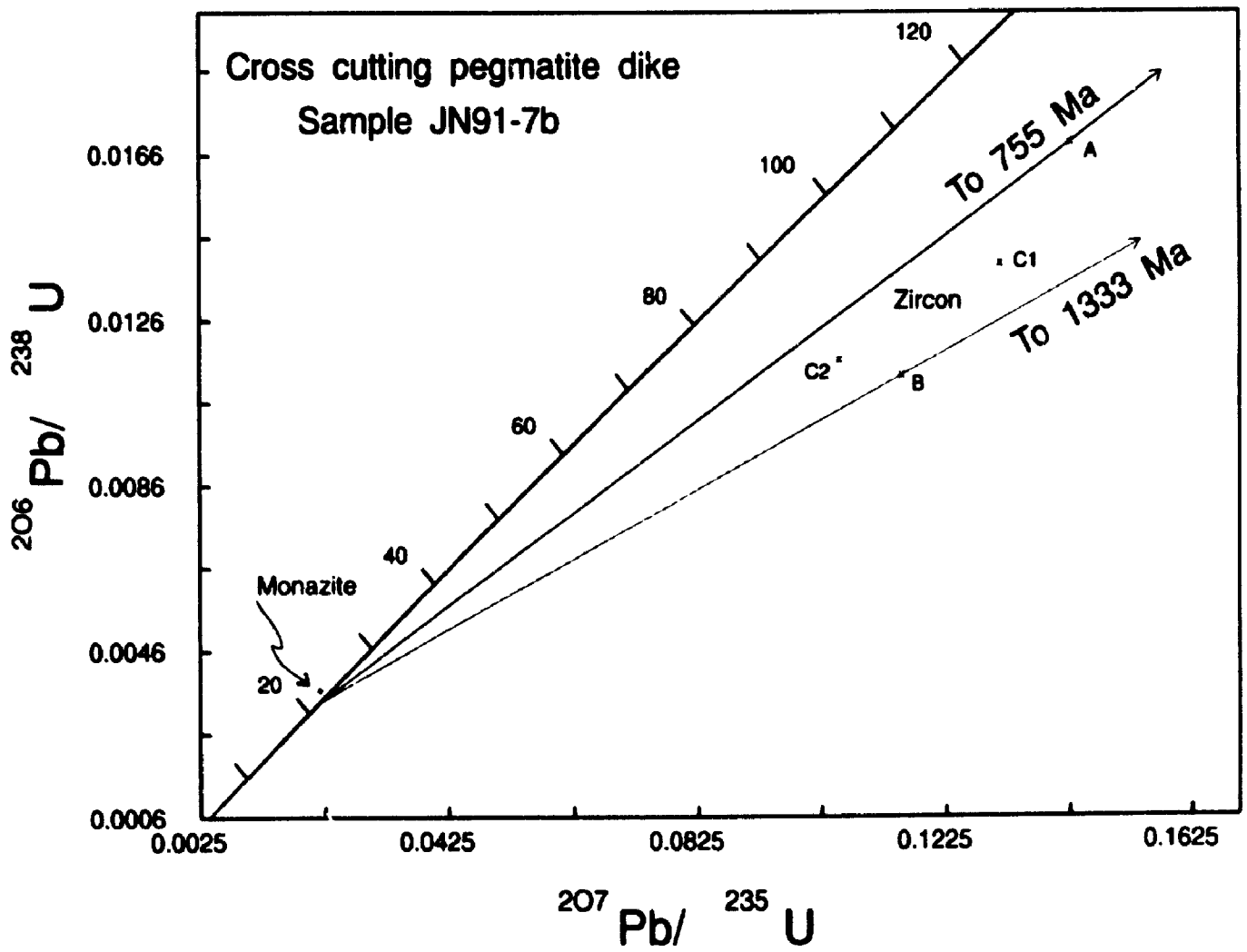

Figure 3.14. Concordia plot for sample JN91-7b with York regression lines through the discordant zircon data. The lower intercepts of the lines pass through the interpreted crystallization age of 21.8 Ma and have upper intercepts at 755 and 1033 Ma. Zircons are shown as an "x" and the corresponding letter refers to the fraction in Table 3.3; monazites are shown as tiny ellipses. See Figure 3.16 for a detail of the monazite data.

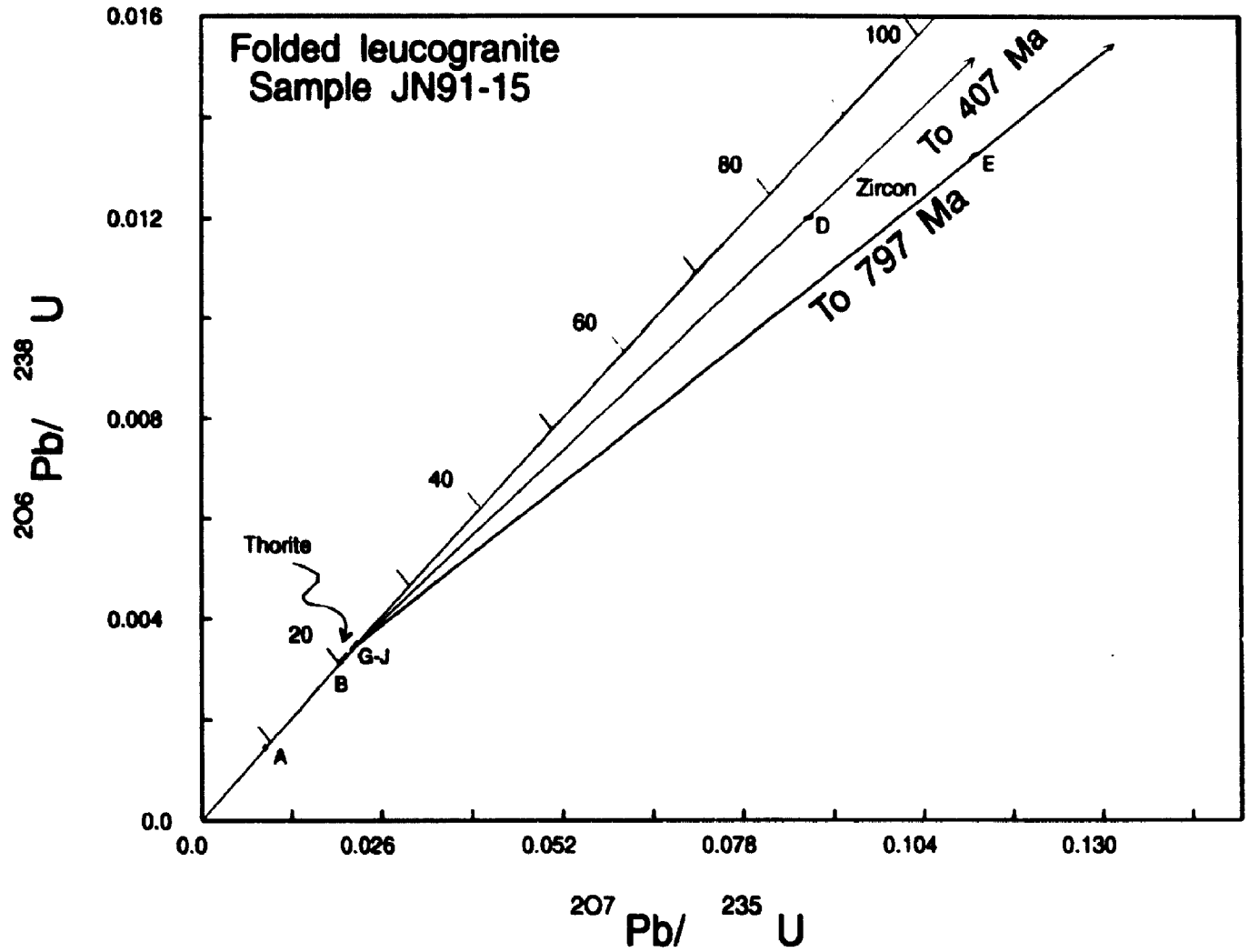

Figure 3.15. Concordia plot for sample JN91-15 with York regression lines through the discordant zircon data. The lower intercepts of the lines pass through the interpreted crystallization age of 22.5 Ma and have upper intercepts of 407 and 797 Ma. Zircons are represented by a small ellipse, and thorites are shown as an "x"; corresponding letters refer to the fraction in Table 3.3. See Figure 3.16 for a detail of the thorite data.

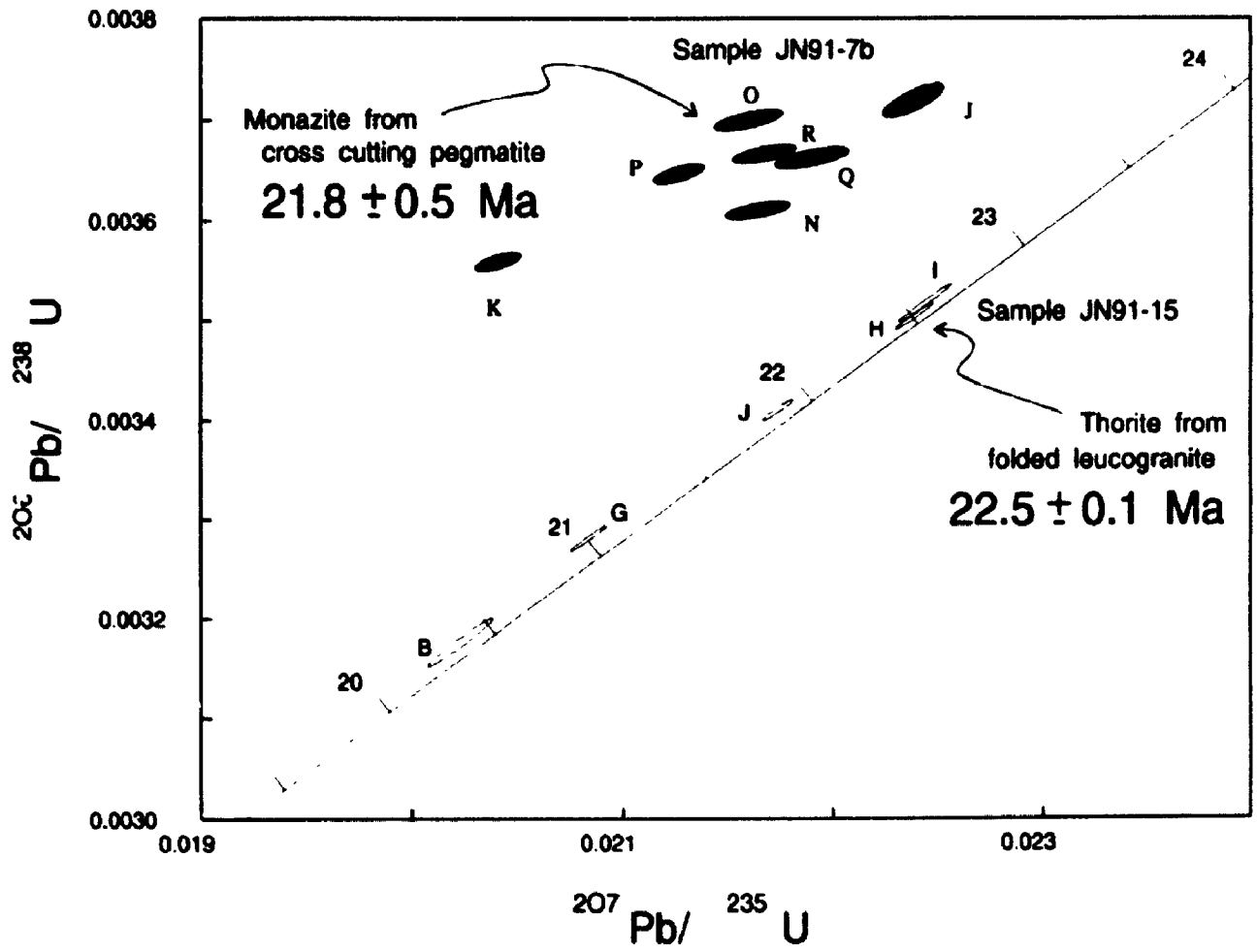

Figure 3.16. Concordia plot and interpreted crystallization ages for samples JN91-7b and JN91-15. Monazite and thorite are shown as shaded and open ellipses, respectively; corresponding letters refer to fractions in Table 3.3.

Map 1. Geologic map of the Kali Gandaki - Annapurna region

Map 2. Station location map

Table 3.1. Summary of rock types and mineralogy in the Kali Gandaki region

Tectonic Unit		Formation	Lithologies	Mineralogy
ADF	TSS	Annapurna Formation	Calcareous psammite to semi-pelitic schist and phyllite	Qtz+Cal+Bt+Ms+Chl+Ep ± Ap ± Tur ± Ab ± Mrg
	GHMS	Formation III	Migmatitic quartzofeldspathic gneiss	Qtz+Pl+Bt+Ms ± Tur
			Pelitic layers	Qtz+Pl+Bt+Ms+Grt+Ky
			Leucogranite	Qtz+Pl+Kfs+Ms+Bt ± Grt ± Tur ± Zm ± Th
		Formation II	Calc-silicate gneiss	Cal+Qtz+Pl+Ms+Bt+Ap ± Hbl ± Di ± Grt ± Tur ± Spn
MCT Shear Zone		Formation I	Pelitic and quartzo-feldspathic gneiss	Qtz+Pl+Bt+Ms+Grt+Ky ± St ± Chl ± Ap ± Ep ± Zo ± Rt ± Tur ± Mnz ± Zm
	LHSS	Midland formations	Pelitic schist and phyllite	Bt+Ms+Qtz
			Micaceous metadolomite	Dol+cal+Ms+Bt ± Ep ± Tur ± Grt
			Clean quartzite	Qtz+Ms+Cal+Bt ± Tur ± Ep ± Pl ± Zo
			Quartz-rich micaceous carbonates	Cal+Dol+Qtz+Ms+Bt ± Grt ± Pl

Notes:

MCT (Main Central Thrust); ADF (Annapurna detachment fault); LHSS (Lesser Himalayan sedimentary sequence); GHMS (Greater Himalayan metamorphic sequence); TSS (Tibetan sedimentary sequence). See Appendix A for mineral abbreviations, Appendix B for a complete list of samples and mineralogy and Appendix C for sample descriptions.

Table 3.2. Characteristic deformation and metamorphism within the Lesser and Greater Himalaya

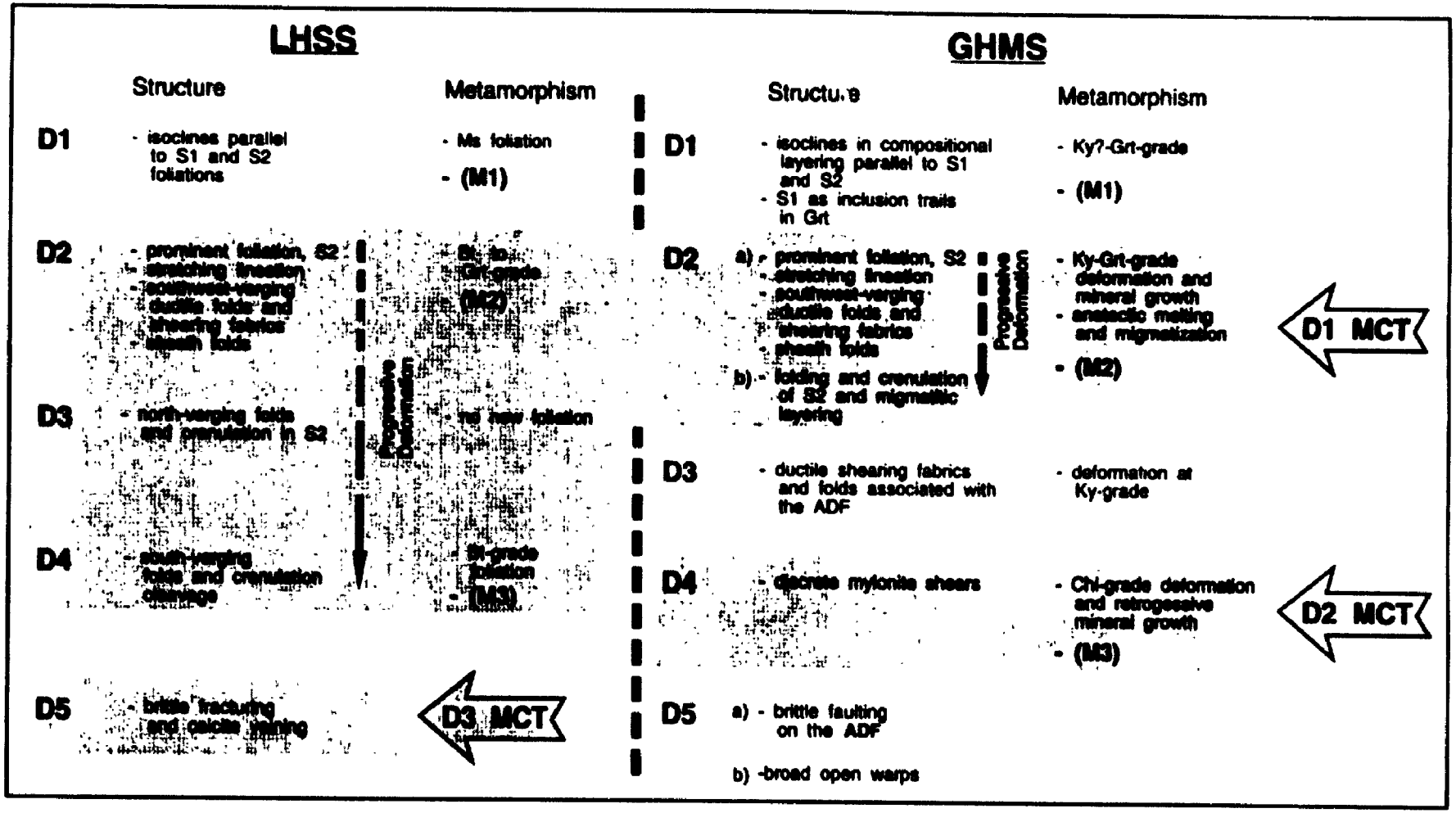

LHSS; Lesser Himalayan sedimentary sequence; GHMS, Greater Himalayan metamorphic sequence; MCT, Main Central Thrust; ADF, Annapurna detachment fault.
D(1-n), deformation events; S(1-n), surfaces; M(1-n), metamorphic events.
Shaded portions indicate which events have been correlated between the LHSS and the GHMS and/or interpreted as a phase of MCT movement. See text for details.

Table 3.3 U-Pb isotopic data

Fraction[a]	Wt.[b] (μg)	U (ppm)	Pb[c] (ppm)	$^{206}Pb/^{204}Pb$[d]	Pb[c] (pg)	^{208}Pb (%)	$^{206}Pb/^{238}U$[f] (%)	$^{206}Pb/^{238}U$[f] (Ma)	$^{207}Pb/^{235}U$[f] (%)	$^{207}Pb/^{235}U$[f] (Ma)	Corr.[g] Coeff.	$^{207}Pb/^{206}Pb$[f] (%)	$^{207}Pb/^{206}Pb$[h] (Ma)
JN91- 7b; crosscutting pegmatite													
B- 3Zr, 350	48	1616	19	3426	16	12.2	0.011264±0.11	72.2±0.2	0.11558±0.13	111.1±0.3	0.86	0.07442±0.07	1052.8±2.6
A- 3Zr, 300	40	1460	24	2743	22	5.6	0.016913±0.12	108.1±0.2	0.14279±0.16	135.5±0.4	0.75	0.06123±0.11	647.3±4.5
J- 4Mon, 275, na	140	5689	79	644	293	75.9	0.003719±0.22	23.9±0.1	0.02239±0.32	22.5±0.1	0.79	0.04365±0.20	-130.2±9.9
K- 9Mon, 150, na	36	9918	87	819	101	63.3	0.003559±0.13	22.9±0.1	0.02041±0.27	20.5±0.1	0.67	0.04159±0.21	-251.2±10.4
N- 1Mon, 300	22	5379	69	533	53	74.4	0.003611±0.12	23.2±0.1	0.02164±0.36	21.7±0.2	0.63	0.04347±0.29	-140.6±14.6
O- 1Mon, 300	34	6100	78	501	103	73.7	0.003700±0.15	23.8±0.1	0.02160±0.38	21.7±0.2	0.67	0.04233±0.30	-206.7±14.9
P- 1Mon, 300	45	6740	79	695	104	72.0	0.003647±0.14	23.5±0.1	0.02127±0.29	21.4±0.1	0.68	0.04229±0.22	-209.0±10.9
Q- 1Mon, 300	30	5662	77	447	94	75.8	0.003663±0.14	23.6±0.1	0.02190±0.41	22.0±0.2	0.67	0.04336±0.33	-146.7±16.3
R- 3Mon, 120	26	5776	78	546	68	75.4	0.003657±0.12	23.6±0.1	0.02167±0.35	21.8±0.2	0.64	0.04287±0.29	-175.1±14.2
C1- 2Zr, 250	15	1752	25	2428	10	10.4	0.013990±0.10	89.5±0.2	0.13135±0.15	125.3±0.4	0.73	0.06809±0.10	871.4±4.2
C2- 2Zr, 250	14	1558	18	1412	12	7.1	0.011651±0.11	74.7±0.2	0.10553±0.20	101.9±0.4	0.67	0.06570±0.15	796.7±6.1

Table 3.3 U-Pb isotopic data (Concluded)

Fraction[a]	Wt.[b] (μg)	U (ppm)	Pb[c] (ppm)	$^{206}Pb/^{204}Pb$[d]	Pb[e] (pg)	^{208}Pb (%)	$^{206}Pb/^{238}U$[f] (%)	$^{206}Pb/^{238}U$[f] (Ma)	$^{207}Pb/^{235}U$[f] (%)	$^{207}Pb/^{235}U$[f] (Ma)	Corr.[g] Coeff.	$^{207}Pb/^{206}Pb$[f] (%)	$^{207}Pb/^{206}Pb$[h] (Ma)
JN91- 15; folded leucogranite													
D- 17Zr, 120, na	26	1101	12	610	36	2.3	0.012011±0.14	77.0±0.2	0.08743±0.34	85.1±0.6	0.64	0.05279±0.27	319.8±12.3
E- 22Zr, 100, na	28	4386	54	1473	69	1.3	0.013219±0.16	84.7±0.3	0.11126±0.19	107.1±0.4	0.77	0.06104±0.12	640.6±5.2
A- 3Th, 110, na	8	300714	502	1321	164	22.6	0.001433±0.22	9.2±0.0	0.00909±0.30	9.1±0.0	0.78	0.04599±0.18	-2.7±8.8
B- 3Th, 100, na	3	564562	2085	3689	93	22.5	0.003177±0.39	20.4±0.1	0.02023±0.39	20.3±0.1	0.98	0.04618±0.08	7.0±3.7
G- 1Th, 150, na	2	260015	988	13893	7	22.2	0.003281±0.20	21.1±0.1	0.02084±0.20	20.9±0.1	0.98	0.04606±0.03	0.8±1.7
H- 1Th, 100, na	2	275422	1140	14685	8	23.7	0.003504±0.19	22.5±0.1	0.02239±0.20	22.5±0.1	0.98	0.04634±0.04	15.4±1.7
I- 1Th, 100, na	2	358802	1476	12111	12	23.0	0.003517±0.27	22.6±0.1	0.02244±0.28	22.5±0.1	0.98	0.04627±0.04	11.9±2.0
J- 2Th, 75, na	1	345802	1386	9413	9	23.3	0.003410±0.16	21.9±0.1	0.02174±0.17	21.8±0.1	0.97	0.04623±0.04	9.7±2.0

Notes

[a] First letter is fraction; # is number of grains, Mon = monazite, Th = thorite, Zr = zircon; # is crystal length in microns; na = not abraded (all other fractions are abraded.

[b] Sample weight error of ± 0.001 mg in concentration uncertainty.

[c] Radiogenic Pb.

[d] Corrected for fractionation and spike Pb.

[e] Total common Pb in analysis in picograms.

[f] Corrected for blank U and Pb, and common Pb; errors are 1 std. error of the mean in % for ratios and 2 std. errors of the mean in Ma.

[g] Correlation Coefficient of errors in $^{206}Pb/^{238}U$ and $^{207}Pb/^{235}U$.

[h] Corrected for blank and common Pb; errors are 2 std. errors of the mean in Ma.

Table 3.4. U-Pb leucogranite ages for the regions shown in Figure 3.4

Location	Minerals Analyzed	Crystallization Age (Ma)	Reference
Baltoro	Zr, Mon, Th	21.5 ± 0.5	Parrish and Tirrul, 1989
Karakorum	Zr, Mon	25.5 ± 0.3/0.8 and 21.4 ± 0.3/0.6	Scharer et al., 1990
Nanga Parbat	Zr	<10 and >35	Zeitler and Chamberlain, 1991
Annapurna	Mon	21.8 ± 0.5	This study
	Th	[a]22.5 ± 0.1	This study
Manaslu	Mon	25.5 ± 0.5	Deniel et al., 1987
	Mon	~ 20	Copeland et al., 1990
Langtang	Mon, Xen	[b]20.4 to 20.7	Parrish et al., 1992
Everest	Zr, Mon	14.3 ± 0.6	Scharer et al., 1986
	Zr, Mon	[c]20 ± 1	Copeland et al., 1988
Makalu	Mon	[d]21.9 ± 0.2 and [d]24.0 ± 0.4	Scharer, 1984

Notes.

- a, multiply deformed; b, sheared and metamorphosed; c, foliated; d, local low-grade shearing; otherwise undeformed and not metamorphosed.

Zr - zircon
Mon - monazite
Th - thorite
Xen - xenotime

Plate 3.1

A) Oriented photomicrograph of recrystallized quartzite from the Lesser Himalaya near Dana (left is to the southwest; shear plane is parallel to the top and bottom of the photograph). "S"-fold in thicker quartz layer and the obliquity of the preferred orientation of quartz and mica with the shear plane indicate top-to-the southwest thrusting.

B) View to the east of folded dolomite layers along the Kali Gandaki, south of Dana (top is to the right). Southwest-verging F_4 folds and crenulations refold the prominent S_2 foliation.

C) View down the dip of the S_2 foliation in semi-pelitic migmatite of Formation I. Thin leucosome layer is folded by F_1 folds that plunge down dip and is refolded by an F_2 sheath fold.

D) View to the north of compositionally layered, planar quartzo-feldspathic and pelitic gneiss of Formation I along the Ghaleti Khola north of Narcheng. Pelitic layer (p); arenaceous layer (a); and transposed leucosome (l). Camera case near (a) and hammer in foreground for scale.

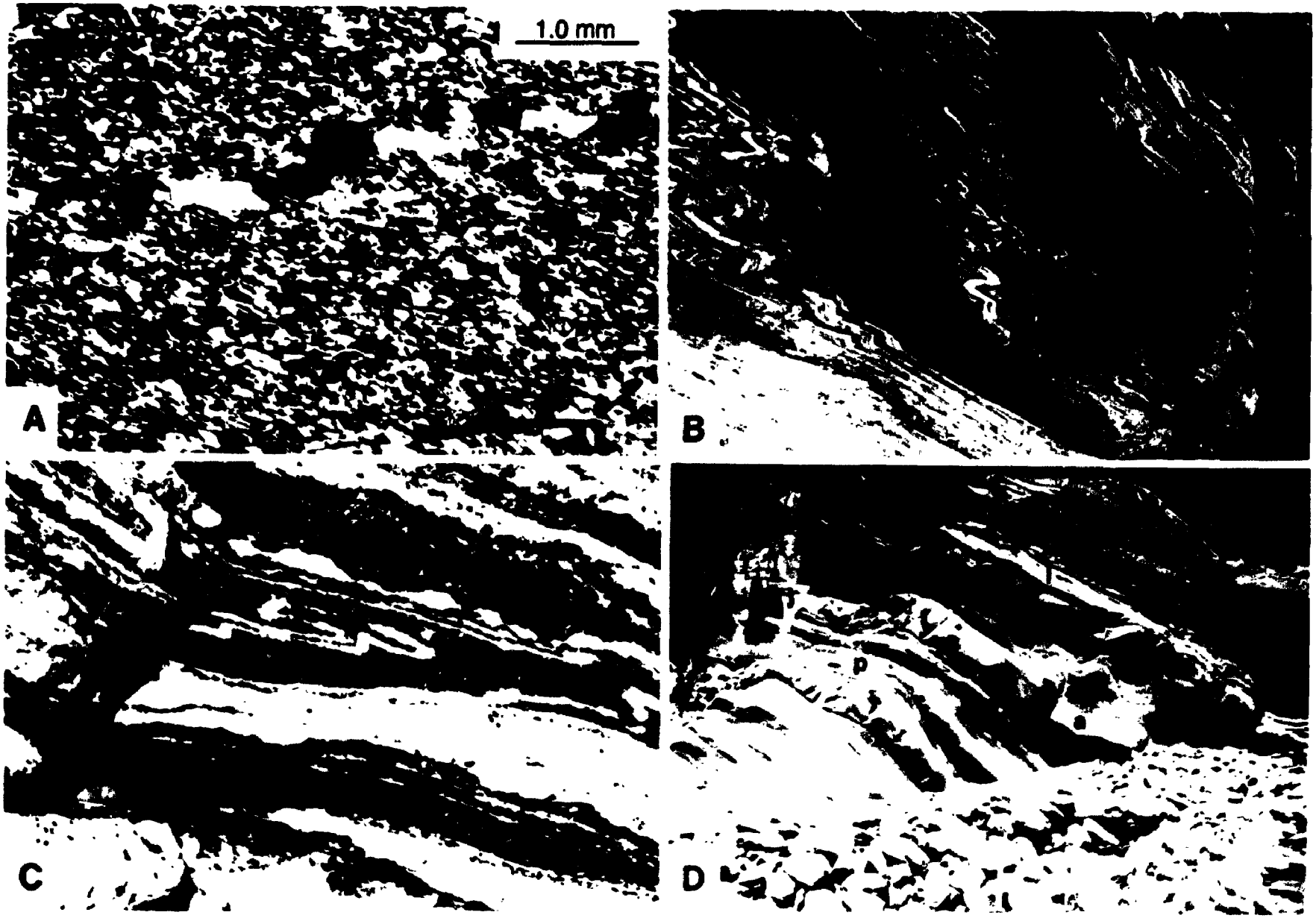
1.0 mm
A
B
C
D
p

Plate 3.2

a) Coarse-grained migmatite layer in calc-silicate gneiss of Formation II (top is to the right). Core of the the large porphyroblast (mineral clot) is diopside (d) which is rimmed by hornblende (h) and garnet (g); tourmaline (t) is abundant in the leucosome.

b) Leucogranitic material intruded into calc-silicate gneiss of Formation II.

c) Photomicrograph of calcareous schist from the Lesser Himalaya. Crenulatations in the lower right hand corner are remnants of the S_1 foliation, which is transposed into the prominent S_2 foliation.

d) Photomicrograph of the S_4 crenulation cleavage in dolomite south of Dana. Sample is from the outcrop in Plate 3.1b.

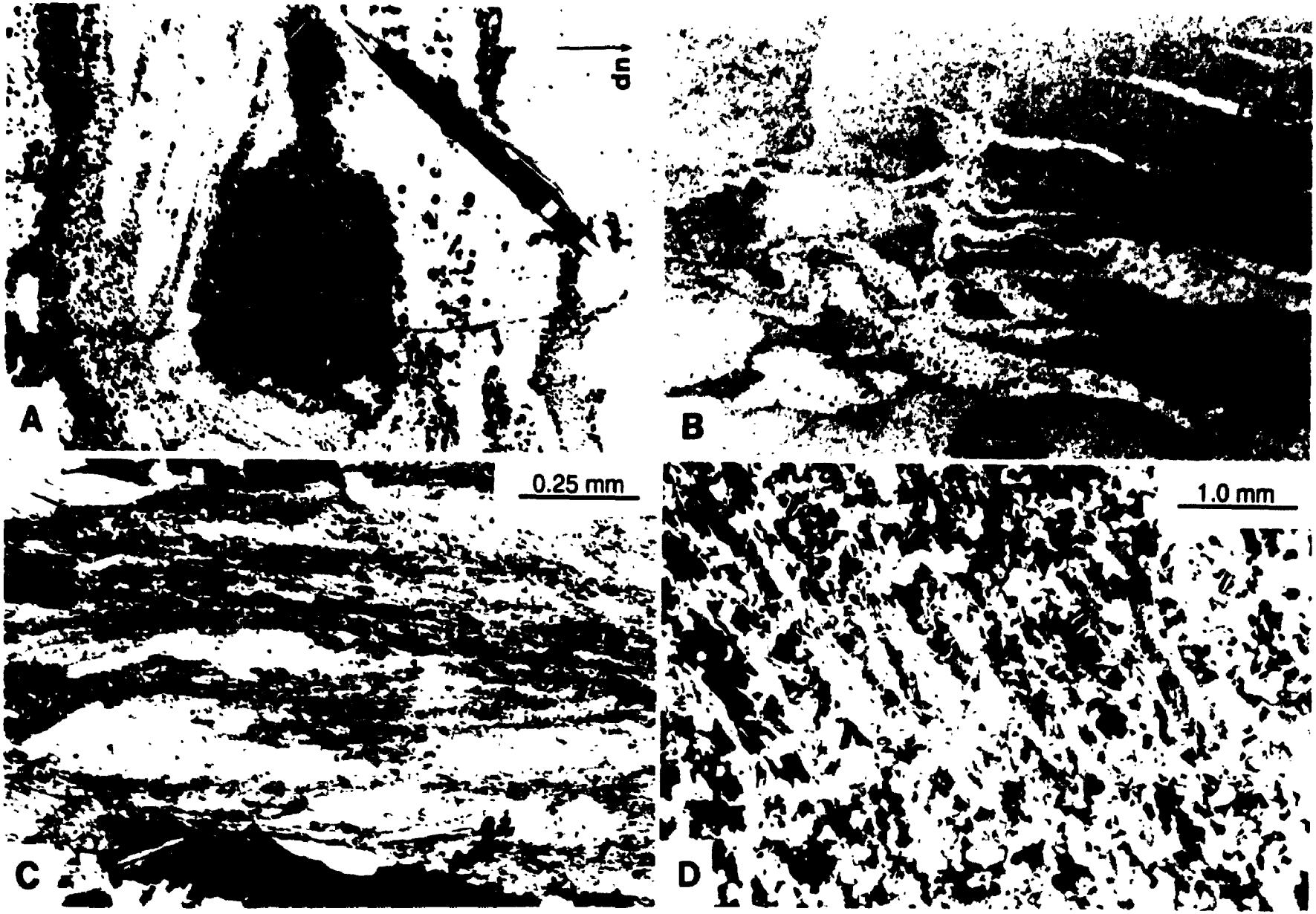
up
A
B
0.25 mm
C
1.0 mm
D

Plate 3.3

A) View to the southeast of interlayered quartzite and pelitic rocks of the Lesser Himalaya near Dana. C-S fabrics defined by the obliquity of the flattening foliation in pelite with the shear plane (taken to be compositional layering) indicate top-to-the-southwest thrusting.

B) An F_1 isocline defined by compositional layering in Formation I gneiss along the Ghaleti Khola (closure above the hammer head).

C) Photomicrograph of an M_1 garnet in migmatitic gneiss of Formation I along the Kali Gandaki. The opaque inclusion trail defines an S_1 foliation.

D) View to the southeast of migmatitc gneiss of Formation I along the Ghaleti Khola (up is to the right; water in the foreground). Outcrop displays planar layers (bottom right), a shallow plunging F_2 "Z"-fold indicating top-to-the-southwest thrusting and steeply plunging F_2 folds (a).

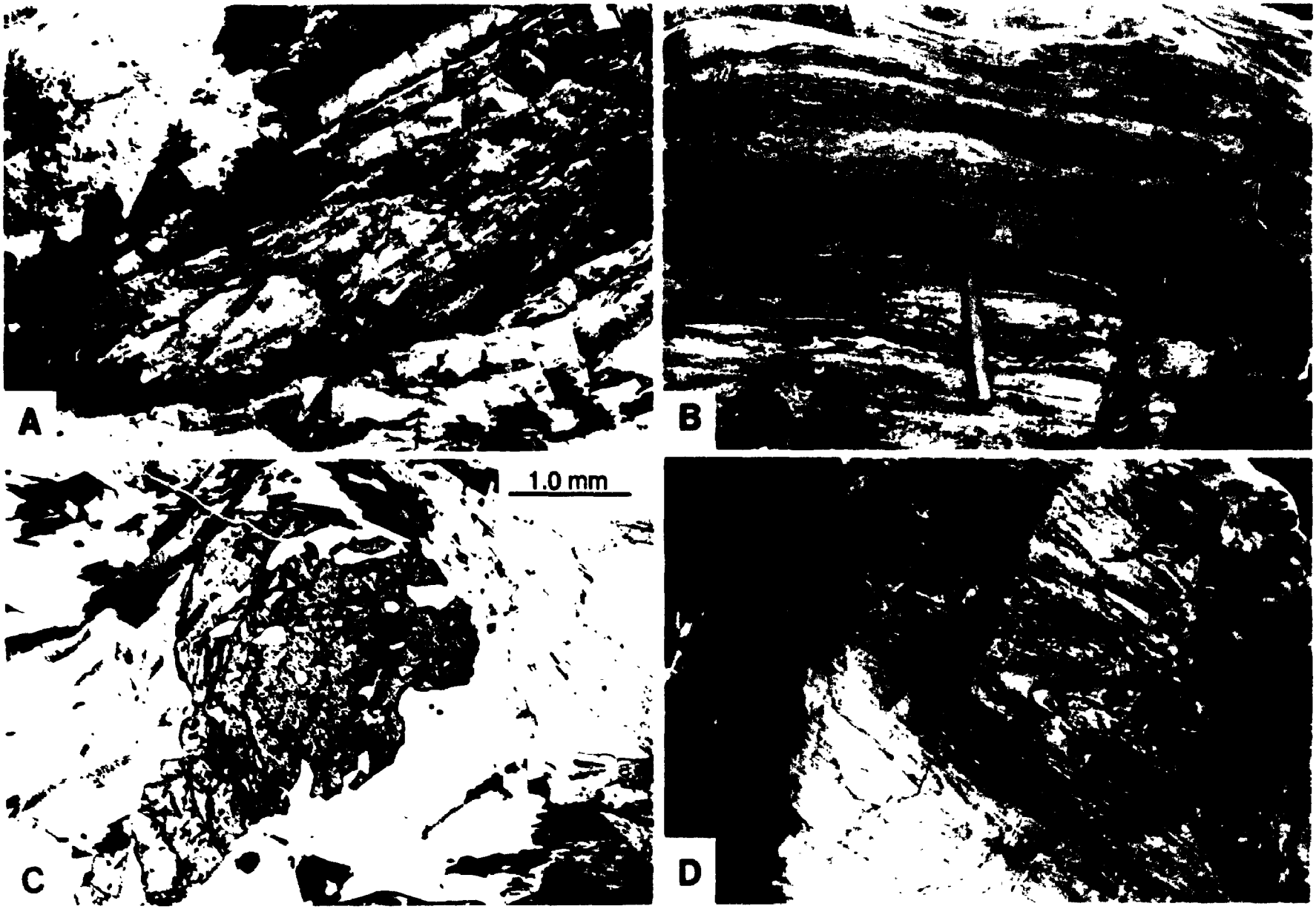
A
B
C
D
1.0 mm

Plate 3.4

A) Medium-grained kyanite-garnet-bearing semi-pelitic gneiss from the high-strain portion of the MCT shear zone. The garnets (g) are related to M_2 and are ~1 mm in size.

B) Crenulated, kyanite(k)-garnet(g)-bearing semi-pelitic gneiss from within the MCT shear zone.

C) Coarse-grained kyanite-garnet-bearing migmatite from the top-most portion of Formation I. Large porphyroblasts are M_1 garnets.

D) Photomicrograph of an oriented gneiss from Formation I (left is to the southwest; shear plane is parallel with the top and bottom of the photograph). A syn-tectonic M_2 garnet with asymmetric, out-of-plane biotite tails indicates top-to-the-southwest thrusting.

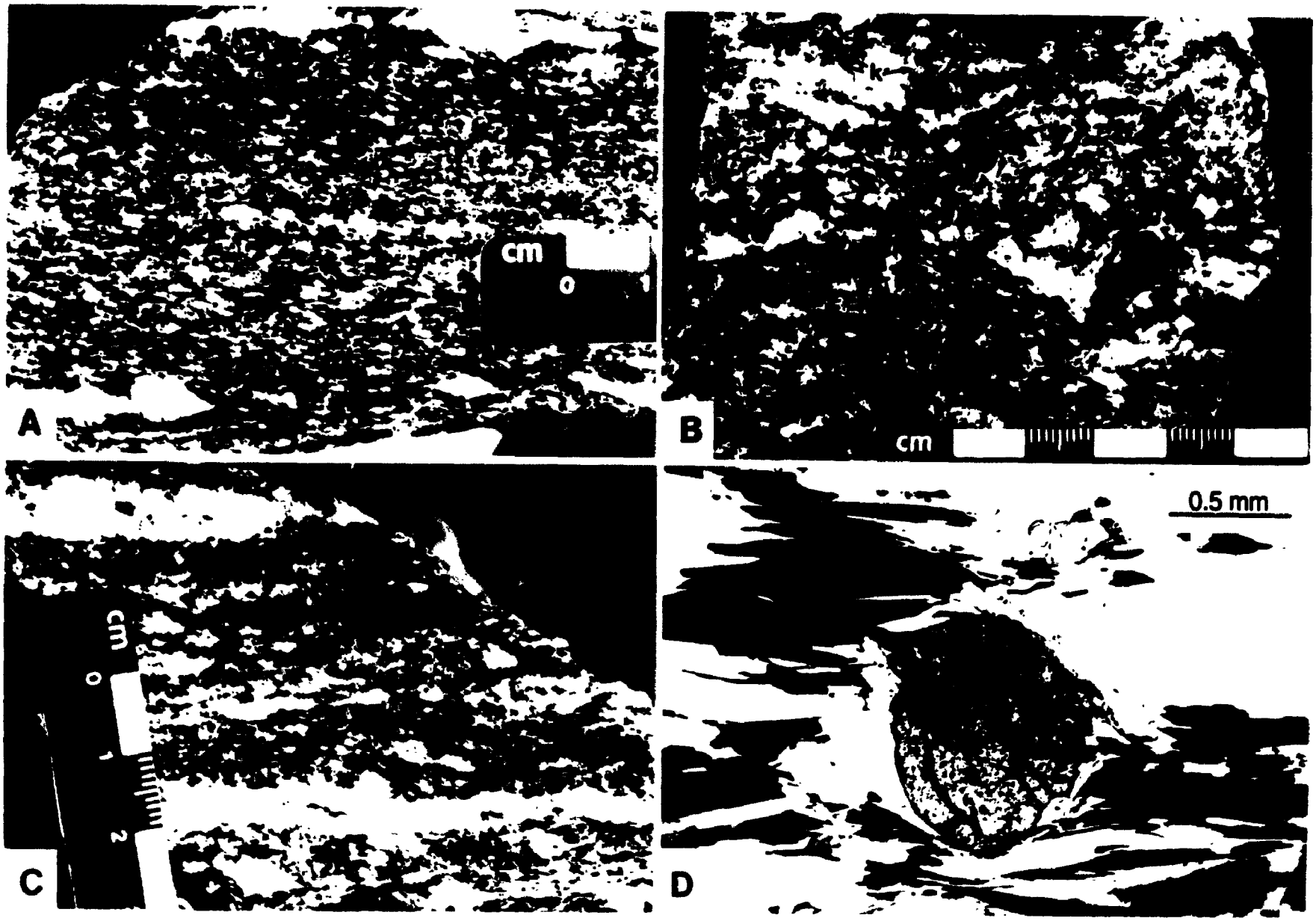
A
cm
0
1
B
k
cm
C
cm
0
1
2
D
0.5 mm

Plate 3.5

A) View to the northwest, perpendicular to the stretching lineation of migmatitic gneiss in the high strain portion of the MCT shear zone. The leucosome originally dipped less steeply than the the shear plane (prominent S_2 foliation) and is now folded and compressed indicating top-to-the-southwest thrusting.

B) Photomicrograph of oriented D_3 chlorite-grade mylonite from Formation I near the contact with the Lesser Himalaya (right is to the southwest; shear plane is parallel with the top and bottom of the photograph). C-S fabric indicates top-to-the-southwest thrusting. At the bottom of the photograph, S_2 biotite is replaced by chlorite (c).

C) Photomicrograph of E-lamellae in previously recrystallized quartz from a gneiss in Formation I.

D) Photomicrograph of a ductilely deformed M_1 garnet from Formation I.

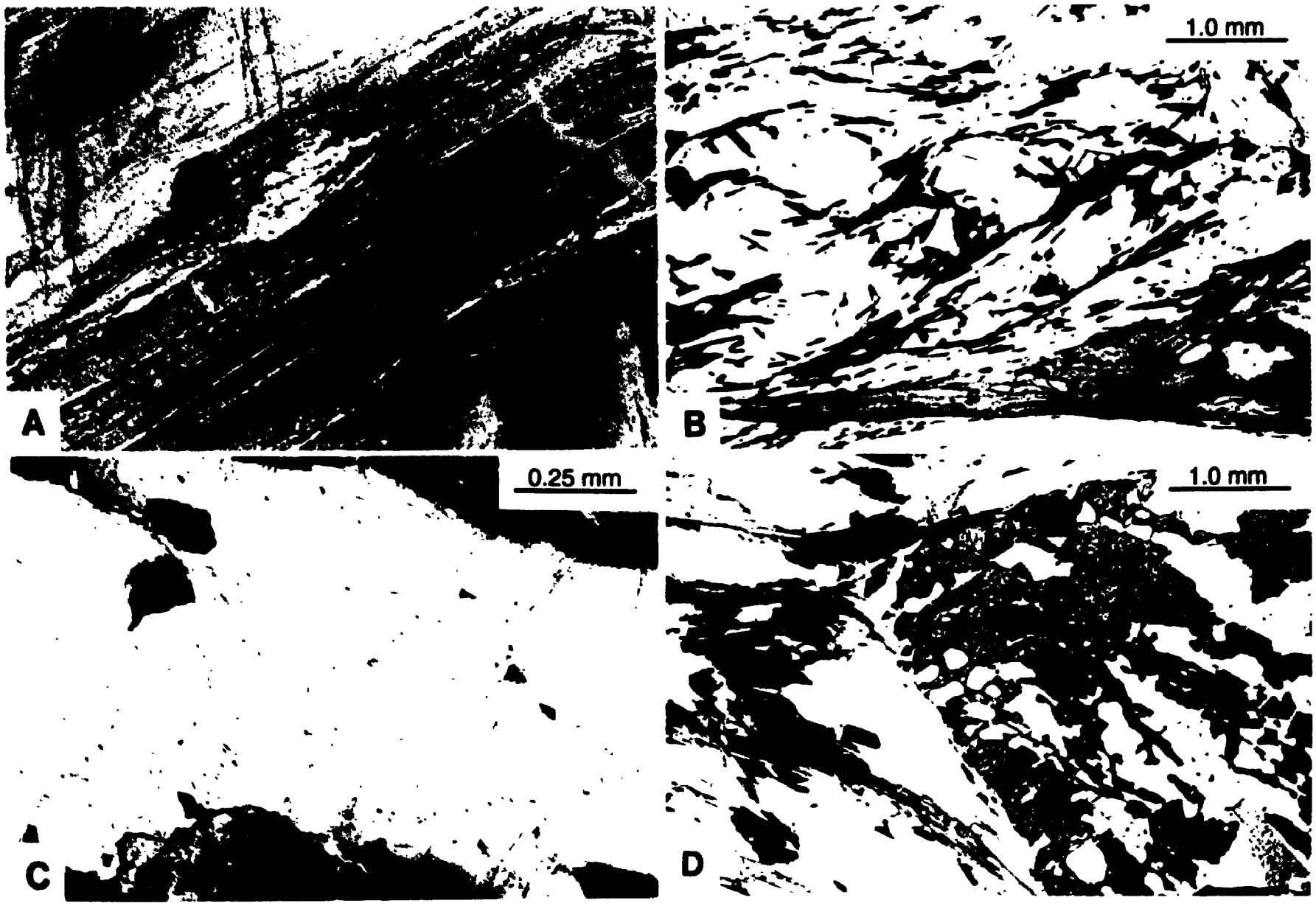
A
B
1.0 mm
C
0.25 mm
D
1.0 mm

Plate 3.6

A) Photomicrograph of twinned M_2 kyanite from a quartz-feldspar sweat in the high-strain portion of the MCT shear zone. Fractures in kyanite are filled with white mica.

B) Photomicrograph of pristine syn- to post-tectonic M_2 garnets from the high-strain portion of the MCT shear zone.

C) Photomicrograph of blocky, randomly oriented, post-tectonic M_2 muscovite overprinting the S_2 foliation in Formation I gneiss.

D) Photomicrograph of M_3 chlorite replacing biotite along the rim of a kyanite. Pleochroic halos in biotite are probably the result of M_2 monazite radioactive decay.

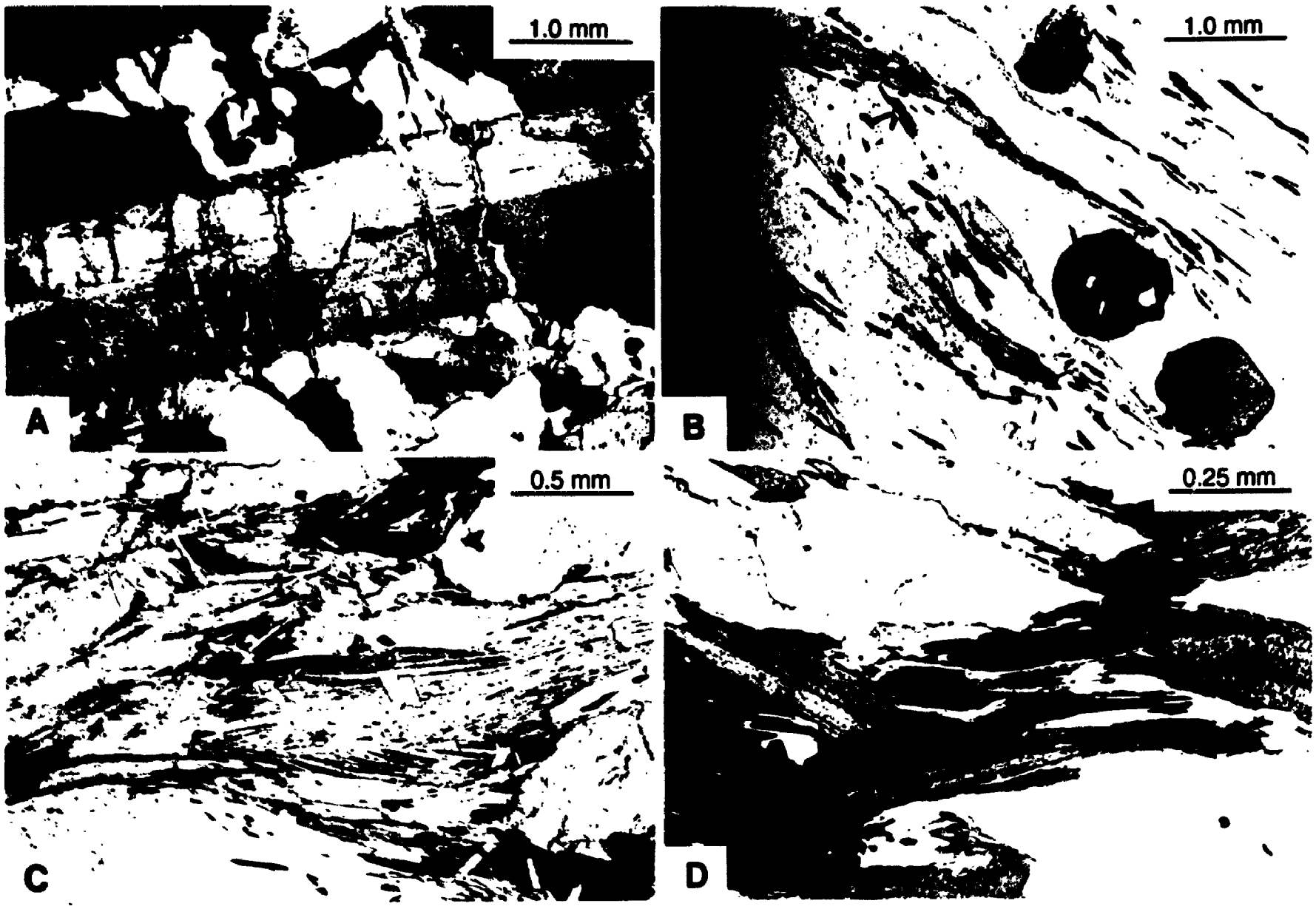
1.0 mm
A
1.0 mm
B
0.5 mm
C
0.25 mm
D

Plate 3.7

A) Photomicrograph of M_3 chlorite replacing garnet. Apatite in the lower right corner.

B) View to the southeast of a folded leucogranite in Formation III calc-silicate gneiss along the Ghaleti Khola. Leucogranite (white) contains the S_2 foliation and outlines a shallow plunging F_2 fold. A sample from this intrusion (JN91-15) has been dated using the U-Pb system.

C) Close-up of 3.7b. The hook on the "Z"-fold under the hammer head and mushroom shape of the adjacent leucosome indicate that F_2 is interfering with an earlier phase of folding (F_1).

D) A coarse-grained, post-tectonic plagioclase-quartz pegmatite that cuts the S_2 foliation in Formation I. A sample from this dike (JN91-7b) has been dated using the U-Pb system.

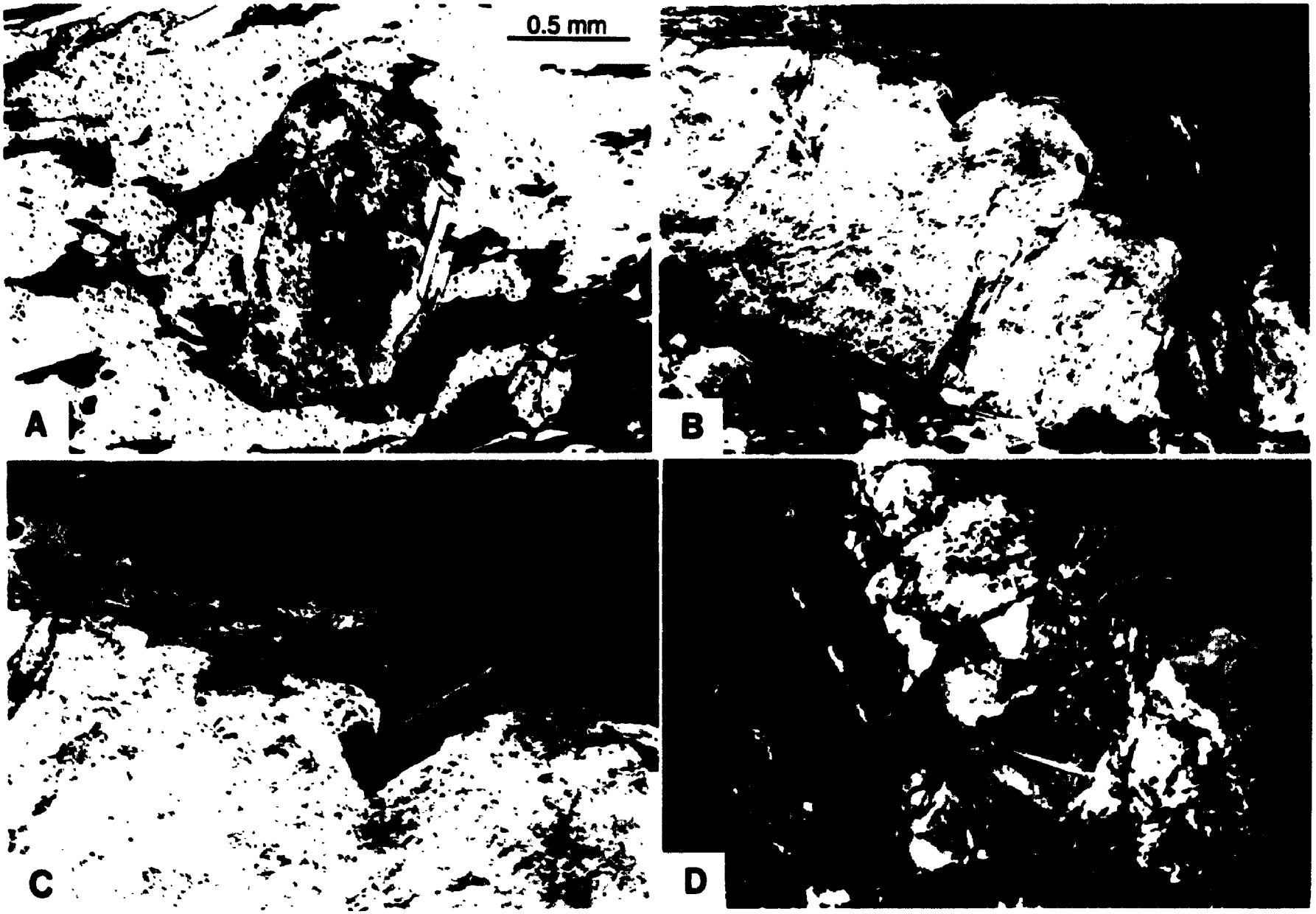
0.5 mm
A
B
C
D

Plate 3.8

A) Photomicrograph of unstrained plagioclase and quartz from sample JN91-7b.

B) Clear, euhedral, unfractured zircons recovered from sample JN91-7b.

C) Euhedral, whole crystals of monazite and fragments of larger monazite recovered from sample JN91-7b.

D) Euhedral, clear thorite crystals recovered from sample JN91-15.

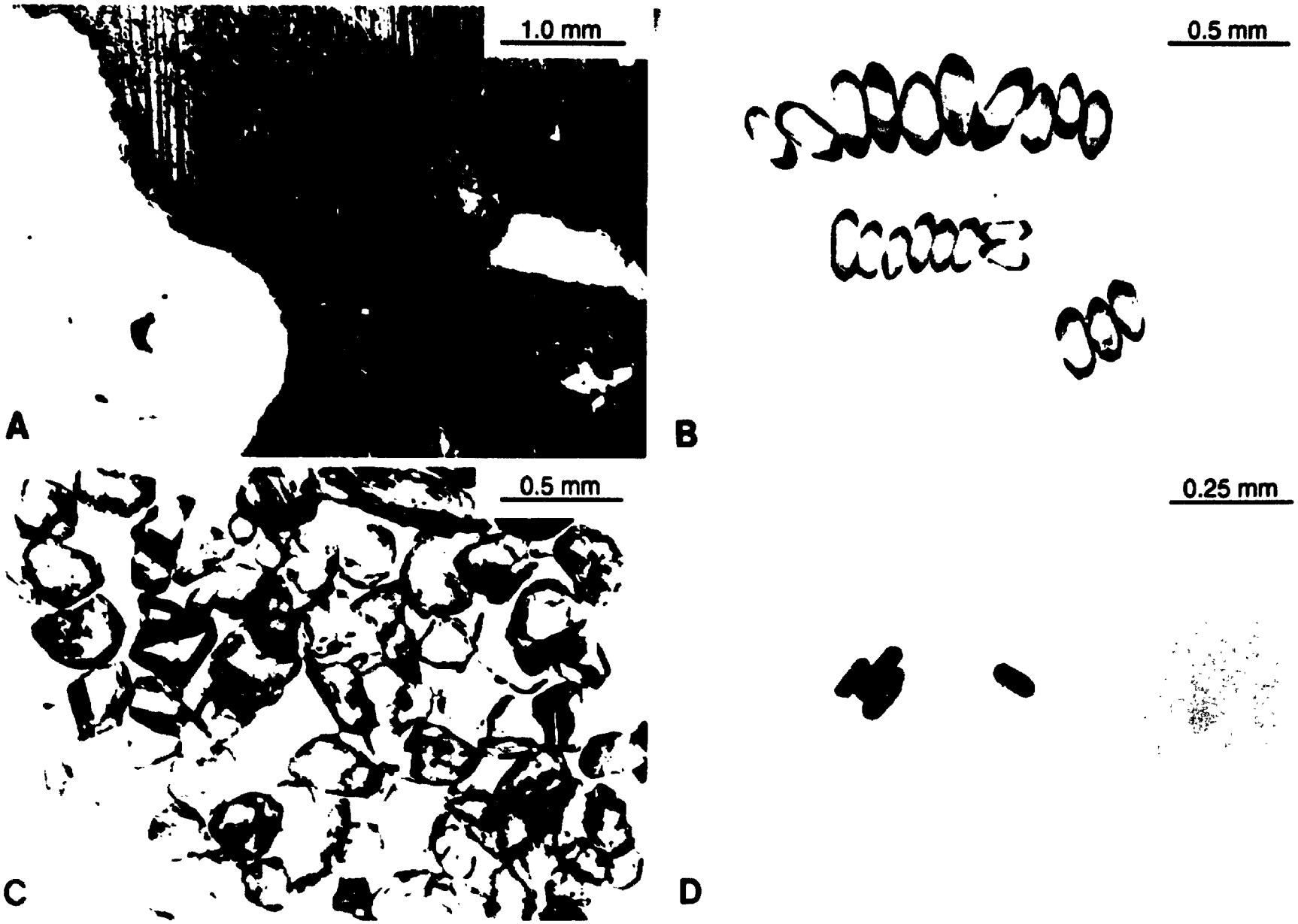
1.0 mm
A
0.5 mm
B
0.5 mm
C
0.25 mm
D

REFERENCES

Amano, K. and Taira, A., 1992. Two-phase uplift of Higher Himalayas since 17 Ma. Geology, 20: 391-394.

Amano, K. and Taira, A., 1993a. Two-phase uplift of Higher Himalayas since 17 Ma: Comment and Reply. Geology, 21: 189.

Amano, K. and Taira, A., 1993b. Two-phase uplift of Higher Himalayas since 17 Ma: Comment and Reply. Geology, 21: 379.

Arita, K., 1983. Origin of the inverted metamorphism of the Lower Himalayas, central Nepal. Tectonophysics, 95: 43-60.

Armstrong, R. L., 1972. Low-angle (denudation) faults, hinterland of the Sevier orogenic belt, eastern Nevada and western Utah. Geological Society of America Bulletin, 83: 1729-1754.

Barker, A. J., 1990. Introduction to metamorphic textures and microstructures. Chapman and Hall, New York, 161 p.

Beaumont, C., Fullsack, P. and Hamilton, J., 1992. Erosional control of active compressional orogens. In Thrust tectonics. Edited by K. R. McClay, p. 1-18. Chapman and Hall, London.

Besse, J., Courtillot, V., Pozzi, J. P., Westphal, M. and Zhou, Y., 1984. Paleomagnetic estimates of crustal shortening in the Himalayan thrusts and Zangpbo suture. Nature, 311: 621-626.

Bordet, P., Colchen, M., Krummenacher, D., Le Fort, P., Mouterde, R. and Remy, M., 1968. Esquisse geologiques de la Thakkhola (Nepal Central). Editions du Centre National de la Recherche Scientifique, Paris, France, 1/75 000.

Bordet, P., Colchen, M., Krummenacher, D., Le Fort, P., Mouterde, R. and Remy, M., 1971. Recherches geologiques dans L'Himalaya du Nepal, region de la Thakkhola. Editions du Centre National de la Recherche Scientifique, Paris, France, 279 p.

Brown, R. L. and Nazarchuk, J. H., 1993. Annapurna detachment fault in the Greater Himalaya of central Nepal. In Himalayan Tectonics. Edited by P. J. Treloar and M. P. Searle, Geological Society Special Publication, in press.

Brunel, M. and Kienast, J. R., 1986. Etude petro-structurale des chevauchements ductiles himalayens sur la transversale de l'Everest-Makulu (Nepal oriental).

Canadian Journal of Earth Sciences, 23: 1117-1137.

Burchfiel, B. C. and Royden, L. H., 1985. North-south extension within the convergent Himalayan region. Geology, 13: 679-682.

Burchfiel, B. C., Chen, Z., Hodges, K. V., Liu, Y., Royden, L. H., Deng, C. and Xu, J., 1992. The South Tibetan detachment system, Himalayan orogen: extension contemporaneous with and parallel to shortening in a collisional mountain belt. Geological Society of America, Special Paper 269, 41 p.

Caby, R., Pecher, A. and Le Fort, P., 1983. Le grand chevauchement central himalayen: nouvelles données sur le métamorphisme inverse à la base de la Dalle du Tibet. Revue de géologie dynamique et de géographie physique, 24: 89-100.

Chen, W. P. and Molnar, P., 1981. Constraints on the seismic wave velocity structure beneath the Tibetan plateau and their tectonic implications. Journal of Geophysical Research, 86: 5937-5962.

Colchen, M., Le Fort, P., and Pecher, A., 1986. Geological researches in the Nepal's Himalaya: Annapurna - Manaslu - Ganesh Himal. Editions du Centre National de la Recherche Scientifique, Paris, France, 136 p., 1 geologic map, 1:200,000 scale.

Coney, P. J., 1980. Cordilleran metamorphic core complexes: An overview. In Cordilleran metamorphic core complexes. Edited by M. D. Crittenden, Geological Survey of America, Memoir 153, p. 7-31.

Copeland, P., 1993. Two-phase uplift of Higher Himalayas since 17 Ma: Comment and Reply. Geology, 21: 188.

Copeland, P., and Harrison, T. M., 1987. Constraints on the age of normal faulting, north face of Mt. Everest: Implications for Oligo-Miocene uplift. EOS (Transactions, American Geophysical Union) 68(44): 1444.

Copeland, P. and Harrison, T. M., 1990. Episodic rapid uplift in the Himalaya revealed by $^{40}Ar/^{39}Ar$ analysis of detrital K-feldspar and muscovite, Bengal fan. Geology, 18: 354-357.

Copeland, P., Parrish, R. and Harrison, T. M., 1988. Identification of inherited radiogenic Pb in monazite and its implications for U-Pb systematics. Nature, 333: 760-763.

Copeland, P., Harrison, T. M. and Le Fort, P., 1990. Age and cooling history of the Manaslu granite: implications for Himalayan tectonics. Journal of Volcanology and Geothermal Research, 44: 33-50.

Corrigan J. and Crowley, K. D., 1990. Fission-track analysis of detrital apatites from sites 717 and 718, ODP Leg 116, central Indian Ocean. In Proceedings of the Ocean Drilling Program, 16: 75-92.

Dahlen, F. A., 1990. Critical taper model of fold-and-thrust belts and accretionary wedges. Annual Reviews of Earth and Planetary Science, 18: 55-99.

Deniel, C., Vidal, P., Fernandez, A., Le Fort, P. and Peucat, J. J., 1987. Isotopic study of the Manaslu granite (Himalaya, Nepal): inferences on the age and source of Himalayan leucogranites. Contributions to Mineralogy and Petrology, 96: 78-92.

Dodson, M. H., 1973. Closure temperature in cooling geochronological and petrological systems. Contributions to Mineralogy and Petrology. 40: 259-274.

Ferrara, G., Lombardo, B. and Tonarini, S., 1983. Rb/Sr geochronology of granites and gneisses from the Mount Everest region, Nepal Himalaya. Geologishe Rundschau, 72: 119-136.

Frondel, C., 1958. Systematic mineralogy of uranium and thorium. U. S. Geological Survey Bulletin 1064, U. S. government print office, 400 p.

Gansser, A., 1964. Geology of the Himalayas. Interscience Publishers, London, England, 289 p.

Gansser, A., 1980. The significance of the Himalayan suture zone. Tectonophysics, 62: 37-52.

Gariepy, C., Allegre, C. J. and Xu, R. H., 1985. The Pb-isotope geochemistry of granitoids from the Himalaya-Tibet collision zone: implications for crustal evolution. Earth and Planetary Science Letters, 74: 220-234.

Gradstein, F. M., von Rad, U., Gibling, M. R., Jansa, L. F., Kaminski, M. A., Kristiansen, I. L., Ogg, J. G., Rohl, U., Sarti, M., Thurow, J. W., Westerman, G. E. G. and Weidmann, J., 1992. Stratigraphy and depositional history of the Mesozoic continental margin of central Nepal. Geologisches Jahrbuch, Bundesanstalt fur Geowissenschaften und Rohstoffe, Reihe B, Heft 77, 140 p.

Hanes, J. A., 1991. K-Ar and 40Ar/39Ar geochronology: Methods and applications.

In Short course handbook on applications of radiogenic isotope systems to problems in geology. Edited by L. Heaman and J. N. Ludden. Mineralogical Association of Canada, p. 27-57.

Harrison, T. M., 1981. Diffusion of ^{40}Ar in hornblende. Contributions to Mineralogy and Petrology, 78: 324-331.

Harrison, T. M., Duncan, I. and McDougall, I., 1985. Diffusion of ^{40}Ar in biotite: temperature, pressure and compositional effects. Geochimica et Cosmochimica Acta, 50: 247-253.

Hashimoto, S., Ohta, Y. and Akiba, C., 1973. Geology of the Nepal Himalayas. Saikon, Tokyo, 286 p.

Hodges, K. V., and Silverberg, D. S., 1988. Thermal evolution of the Greater Himalaya, Garhwal, India. Tectonics, 7: 583-600.

Hodges, K. V., Hubbard, M. S. and Silverberg, D. S., 1988. Metamorphic constraints on the thermal evolution of the central Himalayan Orogen. Philosophical Transactions of the Royal Society of London, A326: 257-280.

Hodges, K. V., Lux, D., Burchfiel, B. C., Royden, L. H., Chen, Z., Deng, C., Liu, Y. and Xu, J., 1989. Tectonic denudation and the unroofing history of the central Himalayan. Geological Society of America Abstracts with Programs, 21: A182.

Hollister, L. S. and Crawford M. L., 1986. Melt-enhanced deformation: a major tectonic process. Geology, 14: 558-561.

Honegger, K., Dietrich, V., Frank, W., Gansser, A., Thoni, M. and Trommsdorf, V., 1982. Magmatism and metamorphism in the Ladakh Himalayas (the Indus-Tsangpo suture zone). Earth and Planetary Science Letters, 60: 253-292.

Hubbard, M. S., 1989. Thermobarometric constraints on the thermal history of the Main Central Thrust Zone and Tibetan Slab, eastern Nepal Himalaya. Journal of Metamorphic Geology, 7: 19-30.

Hubbard, M. S. and Harrison, T M., 1989. $^{40}Ar/^{39}Ar$ age constraints on deformation and metamorphism in the Main Central Thrust and Tibetan slab, eastern Nepal Himalaya. Tectonics, 8: 865-880.

Hyndman, D. W., 1985. Petrology of igneous and metamorphic rocks, second edition. McGraw-Hill, 767 p.

Johnson, M. R. W. and Oliver, G. J. H., 1990. Precollisional and postcollisional events in the Himalaya. Geology, 18: 753-756.

Kretz, R., 1983. Symbols for rock forming minerals. American Mineralogist, 68: 277-279.

Krogh, T. E., 1982. Improved accuracy of U-Pb zircon ages by the creation of more concordant systems using an air abrasion technique. Geochimica et Cosmochimica Acta, 46: 637-649.

Le Fort, P., 1975. Himalayas: the collided range. Present knowledge of the continental arc. American Journal of Science, 275-A: 1-44.

Le Fort, P., 1981. Manaslu leucogranite: a collision signature of the Himalaya - a model for its genesis and emplacement. Journal of Geophysical Research, 86(B11): 10 545-10 568.

Le Fort, P., 1986. Metamorphism and magmatism during the Himalayan collision. In Collision tectonics. Edited by M. P. Coward and A. C. Ries. Geological Society Special Publication 19, p. 159-172.

Le Fort, P., Pecher, P. and Upreti, B. N., 1987a. A section through the Tibetan Slab (Kali Gandaki valley): mineral chemistry and thermobarometry of the Main Central Thrust zone. In: Orogenic Evolution of Southern Asia (from Turkey to Indonesia). Edited by P. Le Fort, M. Colchen and C. Montenat. Sciences de le Terre, p. 211-228.

Le Fort, P., Cuney, M., Deniel, C., France-Lanord, C., Sheppard, S. M. F., Upreti, B. N. and Vidal, P., 1987b. Crustal generation of Himalayan leucogranites. Tectonophysics, 134: 39-57.

Lyon-Caen, H. and Molnar, P., 1983. Constraints on the structure of the Himalaya from an analysis of gravity anomalies and a flexural model of the lithosphere. Journal of Geophysical Research, 88: 8171-8191.

Macfarlane, A. M., Hodges, K. V. and Lux, D., 1992. A structural analysis of the Main Central thrust zone, Langtang National Park, central Nepal Himalaya. Geological Society of America Bulletin, 104: 1389-1402.

Maluski, H., Matte, P. and Brunel, M., 1988. Argon 39 - Argon 40 dating of metamorphic and plutonic events in the North and High Himalayan belts (southern Tibet - China). Tectonics, 7: 299-326.

Mattauer, M., 1986. Intracontinental subduction, crust-mantle decollement and

crustal-stacking wedge in the Himalayas and other collision belts. In Collision tectonics. Edited by M. P. Coward and A. C. Ries. Geological Society Special Publication 19, p. 37-50.

Minster, B. and Jordan, T., 1978. The present-day plate motions. Journal of Geophysical Research, 83: 5331-5354.

Molnar, P., 1984. Structure and tectonics of the Himalaya: constraints and implications of geophysical data. Annual Review of Earth and Planetary Science, 12: 489-518.

Molnar, P., 1988. A review of geophysical constraints on the deep structure of the Tibetan Plateau, the Himalayas and Karakoram, and their tectonic implications. Philosophical Transactions of the Royal Society of London, Series A, 326: 33-88.

Molnar, P. and Tapponnier, P., 1975. Cenozoic tectonics of Asia: Effects of a continental collision. Science, 189: 419-426.

Parrish, R. R., 1990. U-Pb dating of monazite and its application to geological problems. Canadian Journal of Earth Sciences, 27: 1413-1450.

Parrish, R. R., Roddick, J. C., Loveridge, W. D. and Sullivan, R. W., 1987. Uranium-lead analytical techniques at the geochronology laboratory, Geological Survey of Canada; In Radiogenic age and isotopic studies: Report 1; Geological Survey of Canada, Paper 87-2, p. 3-7.

Parrish R. and Tirrul, R., 1989. U-Pb age of the Baltoro granite, northwest Himalaya, and its implications for monazite U-Pb systematics. Geology, 17: 1076-1079.

Parrish, R. R., Hodges, K. V. and Macfarlane, A. M., 1992. U-Pb geochronology of igneous and metamorphic rocks near the Main Central Thrust in the Langtang area, central Nepal Himalaya (abs). Himalaya-Karakorum-Tibet Workshop, 7th, Oxford, England, April 1992.

Pecher, A., 1977. Geology of the Nepal Himalaya: deformation and petrography in the Main Central Thrust zone. In Himalaya - sciences de la terre. Colloques internationaux du CNRS, No. 268, Vol. 2, p. 301-318.

Pecher, A., 1989. The metamorphism in the Central Himalaya. Journal of Metamorphic Geology, 7: 31-41.

Pecher, A. and Le Fort, P., 1977. Origin and significance of the Lesser Himalaya

augen gneisses. In Himalaya - sciences de la terre. Colloques internationaux du CNRS, No. 268, Vol. 2, p. 319-329.

Platt, J. P., 1986. Dynamics of orogenic wedges and the uplift of high-pressure metamorphic rocks. Geological Society of America Bulletin, 97: 1037-1053.

Purdy, J. W. and Jager, E., 1976. K-Ar ages on rock-forming minerals from the central Alps. Memoirs, Institute of Geology and Mineralogy, University of Podova, 30: 1-31.

Ramsay, J. G., 1967. Folding and fracturing of rocks. McGraw-HillBook Company, New York, 568 p.

Sahni, A. and Kumar, V., 1974. Palaeogene palaeobiogeography of the Indian sub-continent. Palaeogeography Palaeoclimatology Palaeoecology, 15: 209-226.

Scharer, U., 1984. The effect of initial 230Th disequilibrium on young U-Pb ages: The Makalu case, Himalaya. Earth and Planetary Science Letters, 76: 191-204.

Scharer, U. and Allegre, C. J., 1983. The Palung granite (Himalaya); high-resolution U-Pb systematics in zircon and monazite. Earth and Planetary Sciences Letters, 63: 423-432.

Scharer, U., Xu, R. H. and Allegre, C. J., 1984. U-Pb geochronology of Gandese (Transhimalayan) plutonism in the Lhasa-Xigaze region, Tibet. Earth and Planetary Science Letters, 69: 311-320.

Scharer, U., Xu, R. H. and Allegre, C. J., 1986. U-(Th)-Pb systematics and the ages of Himalayan leucogranites, South Tibet. Earth and Planetary Science Letters, 77: 35-48.

Scharer, U., Copeland, P., Harrison, M. T. and Searle, M. P., 1990. Age, cooling history, and origin of post-collisional leucogranites in the Karakorum Batholith: a multi-system isotope study. Journal of Geology, 98: 233-251.

Schelling, D., 1992. The tectonostratigraphy and structure of the eastern Nepal Himalaya. Tectonics, 11: 925-943.

Scholtz, C. H., 1980. Shear heating and the state of stress on faults. Journal of Geophysical Research, 85: 6174-6184.

Searle, M. P. and Fryer, B. J., 1986. Garnet, tourmaline and muscovite-bearing leucogranites, gneisses and migmatites of the Higher Himalayas from Zanskar, Kulu, Lahoul and Kashmir. In Collision Tectonics. Edited by M. P. Coward

and A. C. Ries. Geological Society Special Publication no. 19, p. 185-201.

Searle, M. P. and Rex, A. J., 1989. Thermal model for the Zanskar Himalaya. Journal of Metamorphic Geology, 7: 127-134.

Searle, M. P., Rex, A. J., Tirrul, R., Rex, D. C., Barnicoat, A. and Windley, B. F., 1989. Metamorphic, magmatic and tectonic evolution of the central Karakorum in the Biafo-Baltoro-Hushe regions of northern Pakistan. In Tectonics of the Western Himalayas. Geological Society of America Special Paper no. 232, p. 47-73.

Shirey, S. B., 1991. The Rb-Sr, Sm-Nd and Re-Os isotopic systems: A summary and comparison of their applications to cosmochronology and geochronology of igneous rocks. In Short course handbook on applications of radiogenic isotope systems to problems in geology. Edited by L. Heaman and J. N. Ludden. Mineralogical Association of Canada, p. 103-162.

Stern, C. R., Kligfield, R. and Schelling, D., 1989. The Bhagirathi leucogranite of the High Himalaya (Garhwal, India): Age, petrogenesis and tectonic implications. In Tectonics of the Western Himalayas. Geological Society of America Special Paper no. 232, p. 33-45.

Stocklin, 1980. Geology of Nepal and its regional frame. Journal of the Geological Society of London, 137: 1-34.

Swapp, S. M. and Hollister, L. S., 1991. Inverted metamorphism within the Tibetan Slab of Bhutan: Evidence for a tectonically transported heat source. Canadian Mineralogist, 29: 1019-1041.

Treloar, P. J and Rex, D. C., 1990. Cooling and uplift histories of the crystalline thrust stack of the Indian plate internal zones west of Nanga Parbat, Pakistan Himalaya. Tectonophysics, 180: 323-349.

Vidal, P., Cocherie, A. and Le Fort, P., 1982. Geochemical investigations of the origin of the Manaslu leucogranite (Himalaya, Nepal). Geochimica et Cosmochimica Acta, 46: 2279-2292.

Xu, R. H., Scharer, U and Alkgre, C. J., 1985. Magmatism and metamorphism in the Lhasa block (Tibet): a geochronological study. Journal of Geology, 93: 41-57.

APPENDIX A

MINERAL ABBREVIATIONS

Ab	albite	Mrg	margarite
Ap	apatite	Mnz	monazite
Bt	biotite	Ms	muscovite
Cal	calcite	Pl	plagioclase
Chl	chlorite	Qtz	quartz
Di	diopside	Sil	sillimanite
Dol	dolomite	Spn	sphene
Ep	epidote	St	staurolite
Grt	garnet	Th	thorite
Hbl	hornblende	Tur	tourmaline
Kfs	K-feldspar	Zr	zircon
Ky	kyanite	Zo	zoisite

(Abbreviations after Kretz, 1983; see Chapter 3 references)

Appendix B.. List of samples and mineralogy

Thin section and hand sample #	Ab	Ap	Bt	Cal	Chl	Di	Dol	Ep	Grt	Hbl	Kfs	Ky	Mrg	Mnz	Ms	Pl	Qtz	Sil	Spn	St	Tur	Zm	Zo
Lesser Himalayan sedimentary sequence																							
JN91-2a [a]								x							x		x				x		
JN91-2b			x					x		x						x							
JN91-18 [a]			x	x			x	x							x		x				x		
RB92-1		x	x								x				x	x	x						
RB92-3			x	x					✓						x		x				x		
RB92-5 [a]			x	x											x		x				x		
RB92-6 [a]			x	x				x							x	x	x						
RB92-9a [a]			x	x											x		x						
RB92-9b			x												x		x						
RB92-9c [a]			x	x											x		x						
RB92-34			x	[illegible]			x								x		x						
Greater Himalayan metamorphic sequence																							
Formation I																							
JN91-4a		x		[illegible]											x		x				x		x
JN91-4b [a]			x		x			x	x			x		?		x	x				x		
JN91-5 [a]		x	x		x										x	x	x		x		x	x	?
JN91-6a,b [a]			x		x							x			x	x	x						
JN91-7a [a]		x	x		x				x						x	x	x				x		
JN91-7b *			x											x	x	x	x				x		
JN91-8			x						x			x			x	x	x				x		
JN91-16			x		x				x			x			x	x	x				x		

(cont'd)

Appendix B. List of samples and mineralogy (cont'd)

Thin section and hand sample #	Ab	Ap	Bt	Cal	Chl	Di	Dol	Ep	Grt	Hbl	Kfs	Ky	Mrg	Mnz	Ms	Pl	Qtz	Sil	Spn	St	Th	Tur	Zm	Zo
JN91-19a			✓									✓			✓		✓							
JN91-19b		x	x		x			x	x			?			x	x	x		x					
JN91-21		x	x						x			x			x	x	x		x				x	
JN91-23			x						x			x			x	x	x		x					
JN91-40 [a]		x	x						x		x	x					x	x				x		
JN91-41 [a]		x	x		x				x			x			x	x	x	x						
RB92-4 [a]		x	x		x			x	x						x	x	x			?		x	x	x
Formation II																								
JN91-11a			x	x		x				x							x		x			x		
JN91-12 [a]		x	x	x		x				x						x	x		x			x		
JN91-14 [a]		x	x	x		x				x	x					x	x		x			x		x
JN91-15 [a]		x	x		x										x	x	x				x		x	
JN91-26			x	x		x		x								x	x		x			x		x
Formation III																								
JN91-28b		x	x								x				x	x	x		x			x	x	
JN91-29		x	x						x		x			?	x	x	x					x	x	
JN91-31b [a]		x	x								x				x	x	x					?		
JN91-31c [a]		x	x								x			?	x	x	x					x		
JN91-31d [a]		x	x						x		x			?	x	x	x		x			x	x	
JN91-31e			✓									✓				✓	✓							
RB91-15			x						x		x				x	x	x					x		

Appendix B. List of samples and mineralogy (concluded)

Thin section and hand sample #	Ab	Ap	Bt	Cal	Chl	Di	Dol	Ep	Grt	Hbl	Kfs	Ky	Mrg	Mnz	Ms	Pl	Qtz	Sil	Spn	St	Tur	Zm	Zo
Tibetan sedimentary sequence																							
JN91-30a,b[a]		x	x	x	x			x							x		x		?				
JN91-31a			✓												✓	✓	✓						
JN91-31f [a]		x	x	x				x							x		x						
JN91-31g																✓	✓				✓		
JN91-32 [a]			x	x	x			x							x		x						
JN91-34			x					x							x		x						
JN91-35			✓	✓											✓								
JN91-35b [a]			x	x	x										x		x						
JN91-37 [a]					x			x							x		x				x		
JN91-39				x				x							x		x				x		
RB92-12			x	x											x		x						
RB92-21	x		x	x	x			x					x		x		x				x		

Notes:
- see appendix A for mineral abbreviations and appendix C for sample descriptions
- sample numbers correspond to station locations (see Map 2)

x - present in thin section
✓ - present in hand specimen
? - non positive petrographic identification
• - geochronolgy sample
a - oriented sample

APPENDIX C.

SAMPLE DESCRIPTIONS

Lesser Himalayan sedimentary sequence

JN91-2a

Hand sample - Fine-grained, white, Ms-bearing quartzite with a weak stretching lineation; weakly bedded with right-way-up cross-beds.

Thin section - Qtz is elongate but recrystallized.

Oriented: 265/25

JN91-2b

Hand sample - Medium grained, green, Bt-bearing gabbro.

Thin section - Ep is coarse grained and zoned; Pl has abundant inclusions of Bt and Hbl; has been strained and lacks a good igneous texture.

JN91- 18

Hand sample - Cream coloured, dolomitic schist with a strong Bt crenulation cleavage.

Thin section - dominantly dolomite; Ms foliation and layering are crenulated by Bt foliation.

Oriented: 135/65

RB92-1

Hand Sample - Highly strained, Bt-Ms gneiss with mm- to cm-scale Kfs augen (Ulleri augen gneiss).

Thin section - Possible Grt; Kfs contain abundant Pl and Ms inclusions; Qtz rich layers are recrystallized.

RB92-3

Hand sample - Calcareous schist with clots of Bt (green) and Ms.

Thin section - Shear bands and C-S fabrics outlined by micas; Qtz is recrystallized; Cal has a preferred orientation.

RB92-5

Hand sample - Clean, fine grained, white quartzite with a good stretching

lineation.

Thin section - Minor Ms outlining foliation; most Qtz is recrystallized; minor Cal with a preferred orientation.

Oriented: 325/40

RB92-6

Hand sample - Fine-grained quartzite with micaceous layers.

Thin section - Good C-S fabric defined by layering and preferred orientations of Qtz and Bt.

Oriented; 330/50

RB92-9a

Hand sample - Silver-blue, Qtz-mica schist with C-S fabrics and down-dip hinge lines.

Thin section - Recrystallized Qtz.

Oriented: 060/65

RB92-9b

Hand sample - Rusty pelitic schist with a strong crenulation.

Thin section - crenulated Bt-Ms foliation.

RB92-9c

Hand sample - Silver-blue quartzite.

Thin section - Cal and Qtz have a preferred orientation.

Oriented: 295/20

RB92-34

Hand sample - White micaceous carbonate.

Thin section - Dol and Cal.

Greater Himalayan metamorphic sequence

Formation I

JN91-4a

Hand sample - Medium grained, black, siliceous schist with a micaceous foliation.

Thin section - Abundant opaque mineral in Ms foliation; recrystallized but some undulatory extinction.

JN91-4b

Hand sample - Highly sheared, medium grained, Ky-Grt-bearing semi-pelitic schist with a strong Ky-stretching lineation.

Thin section - M_2 Grt's with in-plane Bt tails indicating top-to-the-southwest shear sense; minor Chl after Bt and Grt; Mnz halos in Bt.

Oriented: 290/55

JN91-5

Hand sample - Medium grained, flaggy, quartzo-feldspathic gneiss.

Thin section - Abundant sericitic Pl; minor Chl after Bt; Qtz is elongate with undulose extinction.

Oriented: 308/45

JN91-6

Hand sample - Coarse-grained quartzo-feldspathic sweat with cm-scale Ky.

Thin section - Twinned Ky with undulose extinction and pull-aparts filled with sericite and minor Chl.

Oriented: 307/77

JN91-7a

Hand sample - Highly sheared, medium grained, Grt-bearing semi-pelitic schist.

Thin section - M_2 Grt's are 1 mm in size with Bt tails indicating a top-to-the-southwest sense of shear; minor Chl after Grt.

Oriented: 303/49

JN91-7b

Hand sample - Coarse grained, Pl-Qtz pegmatite (geochronology sample).

Thin section - Mostly large Pl; no Kfs in section; minor Bt, Ms and Qtz; Pl are unstrained but some Qtz has undulatory extinction; abundant Zrn and Mnz were recovered for dating although they are not present in view of the thin section.

JN91-8

Hand sample - Crenulated, medium grained, Ky-Grt-bearing semi-pelitic gneiss.

Thin section - folded opaque inclusion trails in M_1 Grt; Ky are folded and broken; blocky Ms overprints Bt.

JN91-16

Hand sample - Ky-Grt-bearing semi-pelitic schist-gneiss.

Thin section - Minor Chl after Bt; sericite after Pl; C-S fabrics and shear bands; highly recrystallized.

JN91-19a

Hand sample - Small blades of pale blue Ky in Bt-Ms schist.

JN91-19b

Hand sample - Crenulated, medium grained, Bt-Grt semi-pelitic schist.

Thin section - No new cleavage associated with the crenulation; M_2 Grt's are 1 mm in size; tiny Ky?; Chl after Grt.

JN91-21

Hand sample - Coarse grained, Ky rich, semi-pelitic migmatite.

Thin section - Minor Chl and Ms after Bt and Ky; highly recrystallized.

JN91-23

Hand sample - Coarse grained, Ky-Grt-bearing migmatitic gneiss.

Thin section - Ky and Bt wrap M_1 Grt's; Grt's are up to 10 mm in size and have inclusion trails (inclusions are coarser grained in the matrix) and are ductilely deformed; sericite after Ky and Pl.

JN91-40

Hand sample - Coarse grained, highly sheared, Grt-Sil-bearing quartzo-feldspathic gneiss from the Marsyandi River valley.

Thin section - Abundant fibrolite; some prismatic Sil; no Ms; abundant Kfs.

Oriented: 315/30

JN91-41

Hand sample - Coarse grained, Grt-Ky-Sil-bearing pelitic migmatite from the Marsyandi.

Thin section - Ms present; fibrolitic Sil.

Oriented: 248/35

RB92-4

Hand sample - Coarse grained, Chl altered, Grt-Bt-bearing quartzo-feldspathic mylonite with C-S fabrics.

Thin section - Ms random over Bt; Chl after Bt; C-S fabric outlined by Chl and Bt indicates top-to-the-southwest shear sense; Bt is folded into isoclines.

Oriented: 048/49

Formation II

JN91-11a

Hand sample - Weakly layered, coarse grained, Di-Hbl-Bt-bearing calc-silicate gneiss.

Thin section - Granoblastic texture; abundant sphene; Qtz is large and irregular with undulose extinction.

JN91-12

Hand sample - Medium grained, mm- to cm-scale layered, planer calc-silicate gneiss.

Thin section - Recrystallized; Qtz has undulose extinction; anomalous blue Zo present.

JN91-14

Hand sample - Coarse grained, weakly layered, Bt-bearing quartzo-feldspathic gneiss (possible igneous origin).

Thin section - Isoclinal migmatitic layers; granoblastic; minor Cal present.

Oriented: 269/21

JN91-15

Hand sample - Coarse grained, foliated, Tur-bearing, 2-mica leucogranite (geochronology sample).

Thin section - granoblastic texture with minor Chl after Bt; sericite after Pl; no Mnz but abundant Ap.

JN91-26

Hand sample - Medium grained, dark, well layered, planar, semi-pelitic to calc-silicate gneiss.

Thin section - Anomalous blue Zo; recrystallized with even extinction.

Formation III

JN91-28b

Hand sample - Foliated 2-mica leucogranite.

Thin section - granoblastic; abundant Ap and Zrn with cores.

JN91-29

Hand sample - Coarse grained, Grt-Tur-bearing quartzo-feldspathic gneiss.

Thin section - Zrn and Mnz present; perthitic Kfs; Bt-Ms foliation and Qtz-feldspar segregations.

JN91-31b

Hand sample - Highly sheared, planar, 2-mica leucogranite.

Thin section - Bt-Ms foliation; broken angular Kfs; many Qtz inclusions in Kfs.

Oriented: 012/29

JN91-31c

Hand sample - Highly sheared, planar, Tur-bearing, 2-mica leucogranite.

Thin section - Bt-Ms foliation; Ms is coarse and blocky.

Oriented: 345/35

JN91-31d

Hand sample - Highly sheared, planar, Grt-Tur-bearing, 2-mica leucogranite with attenuated felsic layers.

Thin section - More sheared than other samples; Bt-Ms foliation wraps Grt; Mnz and Zrn present.

Oriented: 324/39

JN91-31e

Hand sample - Blue Ky in Qtz-feldspar segregation.

RB92-25

Hand sample - Highly sheared, planar, Grt-Tur-bearing migmatitc quartzo-feldspathic gneiss; Tur is lineated.

Thin section - pristine M_2 Grt in felsic segregations; Ms is coarse and blocky; recrystallized.

Tibetan sedimentary sequence

JN91-30

Hand sample - Highly sheared, fine grained, tan, mm-scale layered psammite with pods of Qtz.

Thin section - recrystallized with even extinction; zircon in Bt (detrital?).

Oriented: 320/35

JN91-31a

Hand sample - Planar Bt-Ms schist with very coarse Ms in a fracture.

JN91-31f

Hand sample - Very planar, flaggy, mm- to cm-scale layered Bt psammite.

Thin section - Ms is coarse, blocky and post-tectonic; monazite?.

Oriented: 318/30

JN91-31g

Hand sample - Coarse grained, Pl-Qtz-Tur pegmatite. A sample of this pegmatite was crushed but no Mnz or Zrn was recovered for U-Pb dating.

JN91-32

Hand sample - Fine grained, white, calcareous schist with random, blocky Bt porphyroblasts.

Thin section - Foliation is mostly Ms with a preferred orientation of Cal; Bt is post-tectonic; Chl after Bt.

Oriented: 065/90

JN91-34

Hand sample - Thinly laminated, black phyllite with weathered out pyrite.

Thin section - S_0 visible; blocky Bt.

JN91-35

Hand sample - Tan phyllite with S_0 visible.

JN91-35b

Hand sample - Fine grained, light coloured, Qtz-carbonate schist with visible S_0 and Bt porphyroblasts.

Thin section - Bt are blocky and random, some completely psuedomorphed by Chl.

Oriented: 228/15

JN91-37

Hand sample - Fine grained, black, phyllitic pelite with obvious layering and a well developed foliation.

Thin section - Qtz-Ms-Tur layers; crenulation offsets layering; Chl porphyroblasts.

Oriented: 085/15

JN91-39

Hand sample - Dark, fine grained, phyllitic quartzite with visible layering.

RB92-12

Hand sample - Grey, micaceous limestone with mm-scale pelitic layers.

Thin section - Mostly Cal; Bt layers outline asymmetric and isoclinal folds with and axial plane cleavage; Ms is random and blocky (post-tectonic); S_1 and S_2 visible.

RB92-21

Hand sample - Siliceous phyllite with a good crenulation and fine grained, weathered porphyroblasts.

Thin section - Mostly Qtz, Cal and Ms; medium-grained porphyroblasts of Bt, Chl and Ab are random and clearly overprint the foliation; good greenschist facies; Mrg needles are present.

END

18-07-94

FIN